CERTIFICATO DI FIRMA DIGITALE

Si certifica che questo documento informatico

phd_unisi_086955.pdf

composto da n°94pagine

È stato firmato digitalmente in data odierna con Firma Elettronica Qualificata (FEQ), avente l'efficacia e gli effetti giuridici equivalenti a quelli di una firma autografa, ai sensi dell'art. 2702 del Codice Civile e dell'art. 25 del Regolamento UE n. 910/2014 eIDAS (electronic IDentification Authentication and Signature).

PROCESSI INFORMATICI COMPLETATI

- **Apposizione di Firma Elettronica Qualificata Remota** emessa da Intesi Group S.p.A. in qualità di prestatore di servizi fiduciari qualificati autorizzato da AgID, per garantire con certezza l'autenticità, l'integrità, il non ripudio e l'immodificabilità del documento informatico e la sua riconducibilità in maniera manifesta e inequivoca all'autore, ai sensi dell'art. 20 comma 2 del CAD - D.lgs 82/2005.

- **Apposizione di Marca Temporale Qualificata** emessa da Intesi Group S.p.A. in qualità di prestatore di servizi fiduciari qualificati autorizzato da AgID, per attribuire una data e un orario opponibile a terzi, ai sensi dell'art. 20 comma 3 del CAD - D.lgs 82/2005 e per far sì che la Firma Elettronica Qualificata apposta su questo documento informatico, risulti comunque valida per i prossimi 20 anni a partire dalla data odierna, anche nel caso in cui il relativo certificato risultasse scaduto, sospeso o revocato.

- **Apposizione di Contrassegno Elettronico**, l'unica soluzione tecnologica che permette di prorogare la validità giuridica di un documento informatico sottoscritto con firma digitale e/o marcato temporalmente, rendendolo inalterabile, certo e non falsificabile, una volta stampato su supporto cartaceo, ai sensi dell'art. 23 del CAD - D.lgs 82/2005.

  Per risalire all'originale informatico è necessario scansionare il Contrassegno Elettronico, utilizzando l'applicazione HONOS, disponibile per dispositivi Android e iOS.

UNIVERSITÀ DI SIENA 1240

DIPARTIMENTO DI MEDICINA MOLECOLARE E DELLO

SVILUPPO

DOTTORATO DI RICERCA IN MEDICINA MOLECOLARE

CICLO XXXIV

Coordinatore: Prof. Vincenzo Sorrentino

Study of the molecular characteristics of spastic paraplegia type 11: its impact on oxidative metabolism and response to drugs treatments

Settore scientifico disciplinare: BIO/18

Dottorando:

Serena Mero

Serena Mero

<table>
<tr><td>**Tutor:**</td><td>**Co-tutor:**</td></tr>
<tr><td>*Federica Gemignani*</td><td>*Santorelli*</td></tr>
<tr><td>Prof.ssa Federica Gemignani</td><td>Prof. Filippo M. Santorelli</td></tr>
</table>

Anni 2018/2021

List of original publications

- Moro F, Rubegni A, Pochiero F, **Mero S**, Procopio E, Baldacci J, Donati MA, Santorelli FM. Autophagic Vacuolar Myopathy caused by a CLN3 mutation. A Case Report. Neuromuscolar Disorders. 2019 Jan; 29(1):67-69.

- Marranci A, D'Aurizio R, Vencken S, **Mero S**, Guzzolino E, Rizzo M, Pitto L, Pellegrini M, Chiorino G, Greene CM, Poliseno L. Systematic evaluation of the microRNAome through miR-CATCHv2.0 identifies positive and negative regulators of BRAF-X1 mRNA. RNA Biology. 2019 Mar; 30:1-14.

- Naef V*, **Mero S***, Fichi G*, D'Amore A, Ogi A, Gemignani F, Santorelli FM, Marchese M. Swimming in Deep Water: Zebrafish Modeling of Complicated Forms of Hereditary Spastic Paraplegia and Spastic Ataxia. Frontiers Neuroscience. 2019 Dec 10;13:1311.

- Pellacani S, Dosi C, Valvo G, Moro F, **Mero S**, Sicca F, Santorelli FM. Customized multigene panels in epilepsy: the best things come in small packages. Neurogenetics. 2020 Jan; 21(1):1-18.

- D'Amore A, Tessa A, Naef V, Bassi MT, Citterio A, Romaniello R, Fichi G, Galatolo D, **Mero S**, Battini R, Bertocci G, Baldacci J, Sicca F, Gemignani F, Ricca I, Rubegni A, Hirst J, Marchese M, Sahin M, Ebrahimi-Fakhari D, Santorelli FM. Loss of ap4s1 in zebrafish leads to neurodevelopmental defects resembling spastic paraplegia 52. Annals Clinical and Translational Neurology. 2020 Apr; 7(4):584-589.

- Brogi L, Marchese M, Cellerino A, Licitra R, Naef V, **Mero S**, Bibbiani C, Fronte B. β-Glucans as Dietary Supplement to Improve Locomotion and Mitochondrial Respiration in a Model of Duchenne Muscular Dystrophy. Nutrients. 2021 May; 12;13(5):1619.

- **Mero S**, Salviati L, Leuzzi V, Rubegni A, Calderan C, Nardecchia F, Galatolo D, Desbats MA, Naef V, Gemignani F, Novelli M, Tessa A, Battini R, Santorelli FM, Marchese M. New pathogenic variants in COQ4 cause ataxia and neurodevelopmental disorder without detectable CoQ $_{10}$ deficiency in muscle or skin fibroblasts. Journal of Neurology. 2021 Sep; 268(9):3381-3389.

- Runfola M, Perni M, Yang X, Marchese M, Bacci A, **Mero S**, Santorelli FM, Polini B, Chiellini G, Giuliani D, Vilella A, Bodria M, Daini E, Vandini E, Rudge S, Gul S, Wakelam MJO, Vendruscolo M, Rapposelli S. Identification of a thyroid hormone derivative as a pleiotropic agent for the treatment of Alzheimer's disease. Pharmaceuticals. 2021 Dec; 14(12):1330.

ABSTRACT

The Hereditary Spastic Paraplegias (HSPs) are inherited neurological disorders characterized by progressive spasticity and pyramidal weakness, predominantly in the lower limbs. Collectively, HSPs are rare conditions affecting any age, and cause important health problems due to gradual functional deterioration, sometimes leading to premature death. Over 80 genes are currently associated with HSPs and the number is still increasing, as well as the clinical features associated with the disease. We focused our study on SPG11-HSP, the most frequent form of autosomal recessive HSP. This is a neurodegenerative disease with no cure requiring new insights on the mechanisms to find new opportunity to therapy. We tested SPG11 patients' biological material and engineered SPG11 knock-out neuroblastoma cell line. *SPG11* encodes SPATACSIN, a large protein without a clear specific function associated to the disease. We demonstrated a loss-of-function mechanism with an involvement of mitochondria with consequences on oxidative metabolism. Then, with a multi-omics approach on SPG11 patients' fibroblasts, we extended the knowledge of the putative pathway involved in SPG11 disease thanks to proteomic analysis and we defined putative disease biomarkers with lipidomic analysis. Lastly, the pharmacological approach with the two FDA approved drugs, *ataluren* and *miglustat* highlighted that the former did not appear to impact on SPG11 cells whereas the latter evidenced a slight modulatory effect on the new pathways identified through proteomic in patients' fibroblasts.

Altogether, studies performed during this doctoral work further underlined the usefulness of *in vivo* and *in vitro* studies on patients and their biological material as a tool for future investigations to dissect pathogenesis and to hypothesize effective therapies. Nonetheless further studies remain imperative to challenge SPG11-HSP disease progression with the ambition to modify tomorrow clinical practice in the large number of young children with spasticity. This increases the need of a more precise diagnosis at the pre-symptomatic stage, and potentiality to undergo safe and efficacious pharmacological treatments.

INDEX

1. INTRODUCTION

1.1 Hereditary spastic paraplegias

The Hereditary Spastic Paraplegias (HSPs) are a group of neurodegenerative diseases presenting with clinical and genetic heterogeneity. The prevalence ranges from 0.5 to 12 individuals per 100.000 (Braschinsky et al. 2009). HSPs are characterized by progressive spasticity and weakness in the lower limbs, due to the distal axonal degeneration of the longest axons of the corticospinal tract (**Figure 1**).
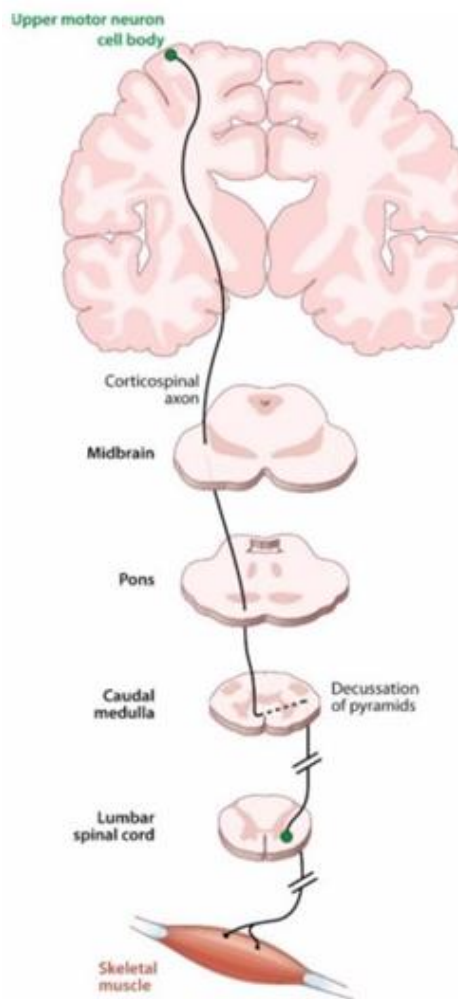
Figure 1. Schematic diagram of corticospinal tract, its descendent way from central nervous system to skeletal muscle (Blackstone 2012).

The degeneration involves mainly the axons of the upper motor neurons. These nerve cells are located in the motor cortex of the brain, and they carry messages to the brainstem and the spinal cord. They synapse to the lower motor neurons connected to the muscles, controlling the voluntary movements. Upper motor neurons require elevated energy metabolism, efficient

transport system through the axons and highly regulated communication mechanisms. Dysregulations in these processes can be attributed to multiple cellular mechanisms including perturbation of mitochondrial function, fatty acid and lipid metabolisms, autophagocytosis, axonal transport, myelin formation, endosome membrane trafficking and vesicle formation, reticulum endoplasmic function and morphology maintenance (Lo Giudice et al. 2014) (**Figure 2**).
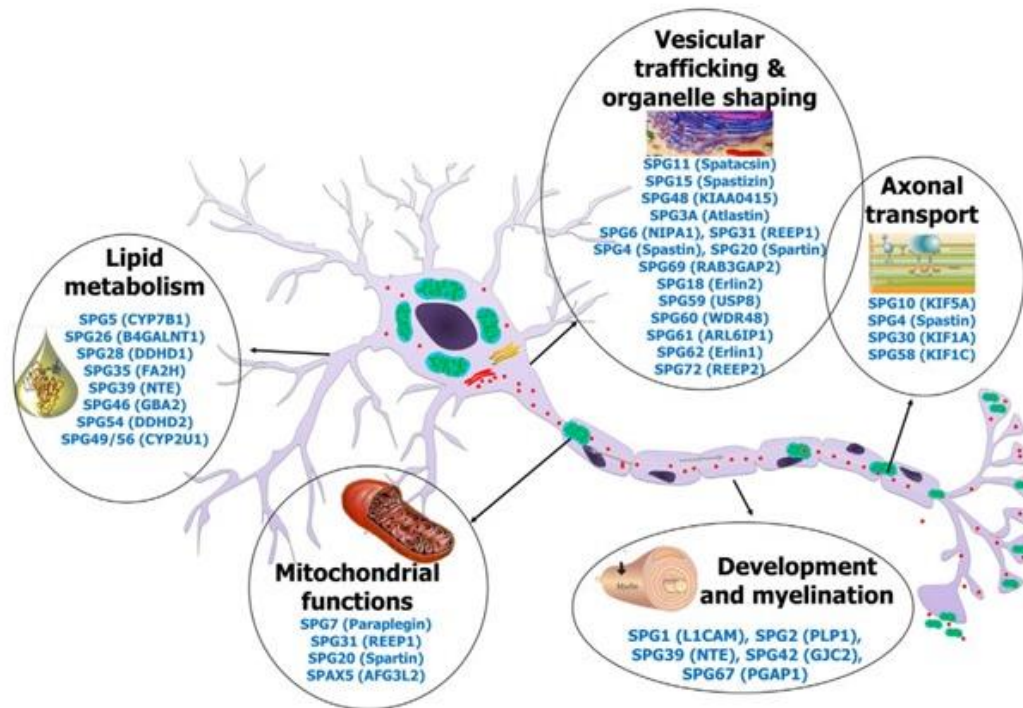
Figure 2. Overview of the main pathophysiological mechanisms involved in HSPs (Klebe, Stevanin, and Depienne 2015).

In the pre-genetic era, HSPs were classified upon age of onset, degree of spasticity and rate of progression (Harding 1983). In the post-genomic era, HSPs classification is focused upon genetic, whereby the phenotypic heterogeneity of HSPs has been associated to the same genetic defect. The genetic loci related to HSPs are termed *SPG* (for SPastic Gait) and are numbered consequently from SPG1, to SPG80. To date, we know more than 80 genes associated with HSPs, and the number is still increasing, such as the clinical features associated with the disease (Murala, Nagarajan, and Bollu 2021). HSPs can manifest at any age and all pattern of inheritance have been described (autosomal dominant, autosomal recessive, X-linked, and also maternally-inherited mitochondrial forms) (Hedera 2000). On clinical grounds, HSPs are classified in "pure" and "complex" forms based on well-established criteria (McDermott 2000). More in detail, in the "pure" types, symptoms are restricted to the lower limbs and to sphincter disturbances (Schüle and Schöls 2011), whereas the complicated forms manifest when there are pyramidal tract signs combined with other neurological symptoms, such as cerebellar ataxia, peripheral neuropathy,

intellectual disabilities and retinal abnormalities (Salinas et al. 2008). Moreover, HSPs often genetically and clinically overlap with other diseases of the nervous system, such as Amyotrophic Lateral Sclerosis (ALS) and even cerebral palsy (CP) (Tesson, Koht, and Stevanin 2015; Morgan et al. 2021) making complexity even higher.

1.1.1 Autosomal recessive spastic paraplegias

The autosomal-recessive SPG11 form (AR-SPG11) is one of the most prevalent recessively inherited complicated subtypes of spastic paraplegia (Hedera 2000). The main phenotype of SPG11-HSP patients is progressive leg muscle stiffness, but the majority of individuals exhibit additional neurological symptoms such as cognitive decline, thin corpus callosum and peripheral neuropathy overlapping with other AR-HSPs including SPG15 and SPG48 (Pensato et al. 2014) and to other neurodegenerative diseases such as axonal Charcot-Marie-Tooth disease, type 2X (CMT2X), juvenile amyotrophic lateral sclerosis 5 (J-ALS5), Parkinsonism and Kjellin syndrome (Pozner et al. 2020) (**Figure 3**).
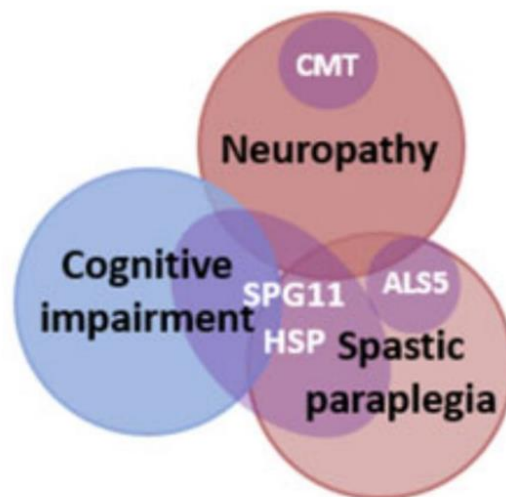
Figure 3. Clinical overlap of *SPG11* related disorders with other neurodegenerative diseases (Pozner et al. 2020).

A common and distinctive sign in patients with SPG11-HSP is the presence of thinning of the anterior corpus callosum (TCC) (Stevanin et al. 2007). More in detail, TCC cerebral MRI imaging of SPG11 patients is characterized by a specific hallmark named "ears of the lynx" (Pascual et al. 2019). This abnormal sign affects the region of the forceps minor of the corpus callosum, and it is useful to guide genetic testing in HSP diagnosis.

Genotypically, AR-SPG11 is associated with mutations in the *KIAA1840/SPG11* gene. The human *SPG11* gene is located on chromosome 15q21.1 and it is composed by 40 exons encoding SPATACSIN, a protein of 2443 amino acids (278KDa). SPATACSIN is ubiquitously expressed and in the nervous system is mainly expressed in the cerebral cortex, cerebellum, hippocampus

and pineal gland (Lo Giudice et al. 2014). Almost invariably, known mutations lead to the production of a truncated protein, which is consequently affected by a loss of function mechanism, but the exact role is largely unclear. However, SPATACSIN seems to be associated with neurite plasticity (Pérez-Branguli et al. 2014), lysosome recycling (Chang, Lee, and Blackstone 2014), clearance of gangliosides (Boutry et al. 2018), cholesterol trafficking and calcium homeostasis (Boutry et al. 2019a) and mitochondrial function and organization (Güner et al. 2021). Regarding neurite plasticity, it is essential to the maintaining cytoskeleton stability and regulating synaptic vesicle transport. SPG11 neurons showed a reduced neuronal complexity with a decreased number of neurites and an altered neuritis length (Pérez-Branguli et al. 2014). In addition, the GSK3β-signaling, the pathway that regulates proliferation and differentiation during brain development, was found to be dysregulated in SPG11-patients induced pluripotent stem cells (iPSCs) (Mishra et al. 2016). Concerning lysosomes recycling, indeed, SPATACSIN seems to have a pivotal role for the initiation of autophagic lysosome reformation (ALR), a pathway that generates new lysosomes, thanks to its interaction with SPASTIZIN (Chang, Lee, and Blackstone 2014), the protein encoded by the *ZFYVE26/SPG15* gene. SPATACSIN interacts also with the AP5 (Adaptor Protein 5) complex to mediate the retrieval of membrane proteins from late or terminal structures, such as endolysosomes, to Golgi complex for a correct autophagy process (Seaman 2019). Autophagy is a fundamental and conserved intracellular pathway that mediates the degradation of macromolecules and organelles in lysosomes. Proper autophagy function is important for central nervous system (CNS) development and neuronal function (Ebrahimi-Fakhari 2018). Recently, a role of SPATACSIN in mitochondrial function and organization has been described. In fact, they have been observed alteration of mitochondrial morphology in neurites, impaired mitochondrial membrane potential and axonal mitochondrial transport and neurites aggregates in alpha motor neurons derived from iPSCs of SPG11 patients (Güner et al. 2021). Lastly, in knockout mouse models, loss of SPATACSIN cause lysosomal accumulation of gangliosides (Branchu et al. 2017; Boutry et al. 2018), suggesting a link between lysosome membrane recycling and lipid metabolism. More in detail, lysosomal lipid accumulation is the result of an impaired formation of the membrane tubules in lysosomes resulting in an accumulation of cholesterol in this subcellular compartment and an altered calcium homeostasis (Boutry et al. 2019b). Hence, mice models (Varga et al. 2015; Branchu et al. 2017) that reproduce the motor phenotype of SPG11 patients show accumulation of autofluorescence material in degenerated neurons, defects of autophagy and lysosomal accumulation of lipids, and authorize to include SPG11 in the recently defined group of *Congenital Disorders of Autophagy* (CDA) (Ebrahimi-Fakhari et al. 2016). Other studies *in vivo* include two knock-down models in zebrafish using morpholino antisense oligonucleotide (Southgate et al. 2010; Martin et al. 2012). In both independent models, morphant embryos reproduce the developmental defects and CNS abnormalities with an altered neuronal differentiation and outgrowth, distinctive of SPG11-HSP.

1.2 Oxidative metabolism

The brain is one of the tissues with the highest energy demand of the human body. It amounts to 20% of the total body energy consumption. These enormous needs are because of the specialized functions of neurons, that are mainly dependent on glucose used for an efficient ATP production (Saxena 2012). Any disruption in ATP generation can easily turn into disease manifestation. Indeed, defects in mitochondrial dynamics and bioenergetic are typical of many neurodegenerative diseases like Alzheimer, Parkinson, Huntington (Swerdlow 2016) and HSPs (Lo Giudice et al. 2014). The main cause of oxidative stress in cells is the unbalance between pro-oxidants, such as the reactive of oxygen species (ROS) and antioxidants. The major source of ROS production is the electron transport chain in the mitochondria (Balaban, Nemoto, and Finkel 2005). The antioxidant response is fundamental to maintain cellular homeostasis and a protein involved in this process is the nuclear factor E2-related factor (NRF2), considered indeed, the master regulator of antioxidant response. In particular, the KEAP1-NRF2 pathway regulates both mitochondrial ad cytosolic ROS production (Kovac et al. 2015). In turn, NRF2 is regulated by the transcription factor EB (TFEB). TFEB highly enhances NRF2 activity through its stabilization and, together TFEB and NRF2 cooperate against cellular stress avoiding oxidative stress (Park et al. 2019). The study of the oxidative stress regards thus the bioenergetic of cells and the mitochondrial network. Moreover, the connection between mitochondrial dynamics and bioenergetics impacts in several fields of human biology as diverse as embryonic development, energy storage, cell motility, lipid and membrane biogenesis, intracellular trafficking and cell death (Benard, Bellance, and Jose 2011).

1.3 Pharmacological studies

The known mechanisms likely involved in SPG11-HSP have driven in the past few years to different pharmacological studies either *in vitro* or *in vivo*. Of relevance is the administration to SPG11 neuronal cells of the GK3 inhibitor, *tideglusib* to recover neurite plasticity and to promote cells survival (Pozner et al. 2018). To date, no specific drug treatment or cure exists for SPG11, and because of this testing FDA-approved drugs already authorized in the treatment of other diseases ("drug repositioning") could be promising. The two FDA-approved drugs *ataluren* and *miglustat* are attractive candidates for studies in SPG11.

1.3.1 Ataluren

Ataluren/PTC124/Translarna® is a drug able to read-through the premature termination codon (PTC) caused by nonsense mutations. It is already authorized in Italy and worldwide to treat boys presenting Duchenne Muscular Dystrophy (Bertoni and Namgoong 2016). Its mechanism of action is just under study, but some roles have been discovered (summarized in **Figure 4**). *Ataluren* seems to better correct UGA stop codon, followed by UAG and UAA (Rowe and Clancy

2009). In particular, studies showed that a more efficient stop codon readthrough was observed with the opal codon (UGA triplet) immediately followed by the amber codon (UAG, Loughran et al. 2014). Other researches have detected the potential of caffeine in the PTC read-through either alone or in combination with *ataluren* (Sarkar et al. 2019; Lentini et al. 2019). Even in animal model *ataluren* seems to work; for example, in a zebrafish model of choroideremia (CHM) harbouring a nonsense mutation in the zf-*chm* gene (*chm*[ru848] zebrafish line), it has been shown that PTC124 successful suppress the stop codon increasing *chm* mRNA levels compared to control wild-type fish (Moosajee et al. 2016).
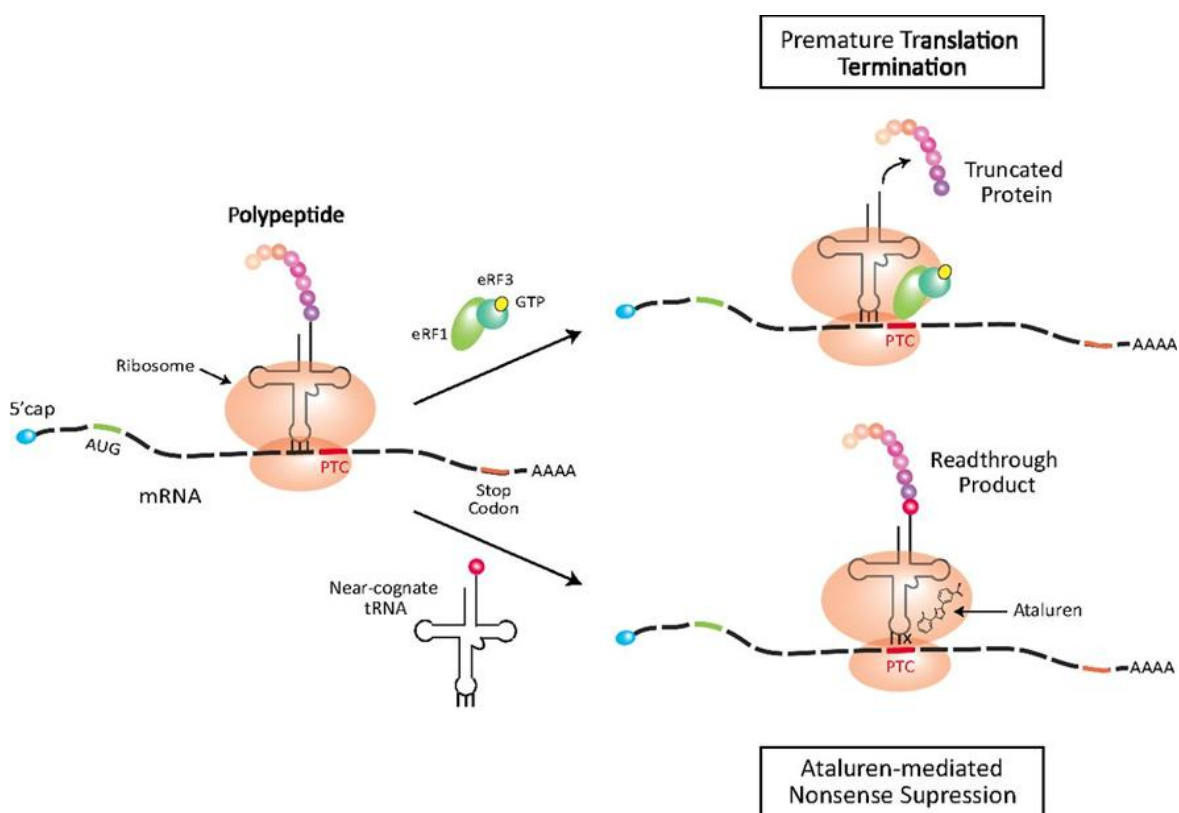
Figure 4. Mechanism of action of *ataluren* (Siddiqui and Sonenberg 2016)**.**

1.3.2 Miglustat

Miglustat/Zavesca® is a drug authorized in Italy and worldwide for the treatment of Gaucher (McCormack and Goa 2003) and Nieman-Pick type C1 (NPC1) diseases (Lyseng-Williamson 2014). *Miglustat* inhibits glucosyl-ceramide synthase, an enzyme that catalyzes the transfer of glucose to ceramide to form glucocerebroside, the first step in glycosphingolipid synthesis (**Figure 5**). The drug acts with the so called "substrate reduction therapy" (SRT), a mechanism adopted in few lysosomal storage disorders (LSDs) as opposed to the "enzyme replacement therapy" (ERT) approach. Both therapeutical strategies are used in clinical practice, though the infusion of wild-type enzyme (ERT) is more costly and impacts more on daily activities of patients than the SRT (Platt and Jeyakumar 2008).
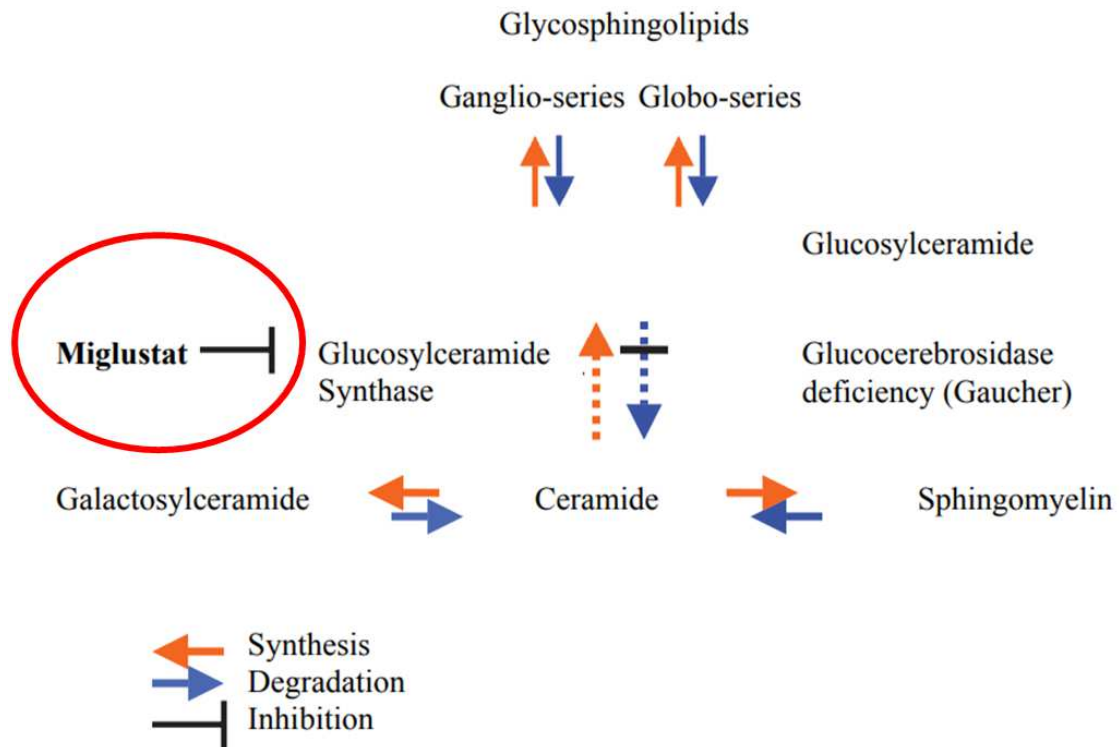
Figure 5. *Miglustat* inhibits gangliosides synthesis (Ficicioglu 2008).

It is known that *miglustat* decreases GM2 gangliosides levels in a cellular and murine model of Sandhoff disease (Jeyakumar et al. 1999), and represents the only drug registered to treat NPC1 patients (Sitarska, Tylki-Szymańska, and Ługowska 2021).

1.4 Multi-omics approaches

In the post-genomic era, medical research and many others fields have been revolutionized by high-throughput technologies (Lightbody et al. 2019) such as the "omics" strategies, the collective characterization and quantification of pools of biological molecules that translate into the structure, function, and dynamics of an organism (Hasin, Seldin, and Lusis 2017). Genomics was the first omics focused on identifying genetic variants associated with disease, response to treatment or for prognosis. Today exist many omics that study different aspects of biology, such as epigenomics, transcriptomics, proteomics, lipidomics, metabolomics, microbiomics, etc. The integration of multi omics data with clinical information is currently a very active field of medical research and it will led toward a more "precise" medicine (Ahmed 2020).

1.4.1 Proteomic

Proteomic refers to the analysis of the whole protein pattern of a cell, tissue or organism under defined conditions. The technology increasingly developed today to the analysis of the proteome is the mass spectrometry. Nowadays, proteomics has a huge impact in biological research, and the

fields with more benefits are the cancer (Huang et al. 2017; Peng et al. 2018) and the neurodegenerative diseases researches (Zhang et al. 2008; Puranik et al. 2020). The goal is to identify biomarkers that could facilitate the disease etiology and progression and to uncover the understanding pathological mechanisms, the alteration of expression patterns in response to various signals and the interpretation of functional protein pathways in different diseases (Aslam et al. 2017).

1.4.2 Lipidomic

Lipidomic refers to the large-scale analysis of lipids using mass spectrometry. Around 2005 there was the emergence of new generation lipidomic methods, therefore chemistry and biochemistry focus very strong on that. From 2015 onwards a large scale profiling became popular, the intention was to screen biomarkers for a hypothesis generating rather than hypothesis driven. Today the approach became a circle between biochemistry in biological systems and a quantitative procedure. Therefore, all the biochemistry knowledge accumulated over decades were integrated in the field of lipidomic. Lipid biochemistry is complex, diverse and dynamic. The definition of lipid is a molecule insoluble in water and soluble in organic solvents, so lipids were classified in LIPID MAPS® in 8 groups: fatty acids, glycerolipids, glycerophospholipids, sphingolipids, sterol lipids, prenol lipids, saccharolipids and polyketides (Fahy et al. 2009). Lipid composition of different cells, tissues is high variable. The brain is the second most abundant organ in terms of lipid concentration and diversity, thus lipid dysregulation has been linked to the progression and severity of many neurodegenerative diseases such as Alzheimer, Parkinson and Multiple Sclerosis (Castellanos et al. 2021). Alteration in lipid metabolism has emerged even in the group of HSPs where the heterogeneity of proteins involved have highlighted the following functional steps in disease status: impaired cholesterol hydroxylation, synthesis and trafficking; phospholipids synthesis and metabolism with consequences in cellular signaling; glycerophospholipids degradation; sphingolipids biosynthesis and degradation and fatty acid metabolism (Darios, Mochel, and Stevanin 2020).

1.5 Gene editing

Gene editing is a technique that revolutionized genetic research. It consists in genome manipulation in order to treat human disease. The principle concept of this technology is the use of nucleases to create double strand breaks (DSBs) in the DNA then repaired by homologous recombination (HR) or non-homologous end joining (NHEJ) mechanisms (Bak, Gomez-Ospina, and Porteus 2018). The early hybrid nucleases employed were zinc finger nucleases (ZFNs) and transcription activator-like effector nucleases (TALENs) (Gupta and Shukla 2017). The technique more frequently applied to edit genomes is the CRISPR/Cas9 system.

1.5.1 The CRISPR/Cas9 system

The Clustered Regularly Interspaced Palindromic Repeats (CRISPR) and CRISPR-associated protein (Cas) system is a worldwide mechanism, named CRISPR/Cas, used in genomic engineering "borrowed" from prokaryotes that use it as innate immunity system, to protect themselves by viral DNA infections (Marraffini 2015). Indeed, once the infection occurs, bacterial nucleases fragment viral DNA and incorporate it as short sequences (about 20 bp length) separated by short palindromic repeat, that will be used to recognize future invasions of the same type of "invader". In eukaryotic systems to manipulate genome are required only two elements: the Cas9 endonuclease, to direct gene editing and the single guide RNA (sgRNA) composed by the CRISPR RNA (crRNA) fused to trans-activating crRNA (tracrRNA) for a target-specificity (Razzaq and Masood 2018). Cas9 is an enzyme with helicases and polymerases properties whereas sgRNA have a specific sequence complementary to the target sequence. Briefly, Cas9 makes a complex with sgRNA and cleaves the DNA sequence upstream of a spacer named Protospacer Adjacent Motif (PAM). PAM sequence is usually NGG for *Streptococcus pyogenes* Cas9, the most common Cas used, and it is essential for DNA cleavage. The DSB generated by CRISPR/Cas9 system can activate two possible repair mechanisms: HR or NHEJ (**Figure 6**). On one hand HR is an error free method that joins only homologous templates and it is commonly used in plats for knock-in; on the other hand, NHEJ is an error-prone methods that rapidly repairs the DSB rejoining the ends, generating the insertion or the deletion (Indel) of nucleotides in the specific gene sequence. NHEJ is common used for gene knock-out (KO) (Tang et al. 2019). In the end, an assurance is that the CRISPR/Cas9 system is revolutionizing the study and the treatment of a lot of diseases and in the future it likely will help the understanding of many others.
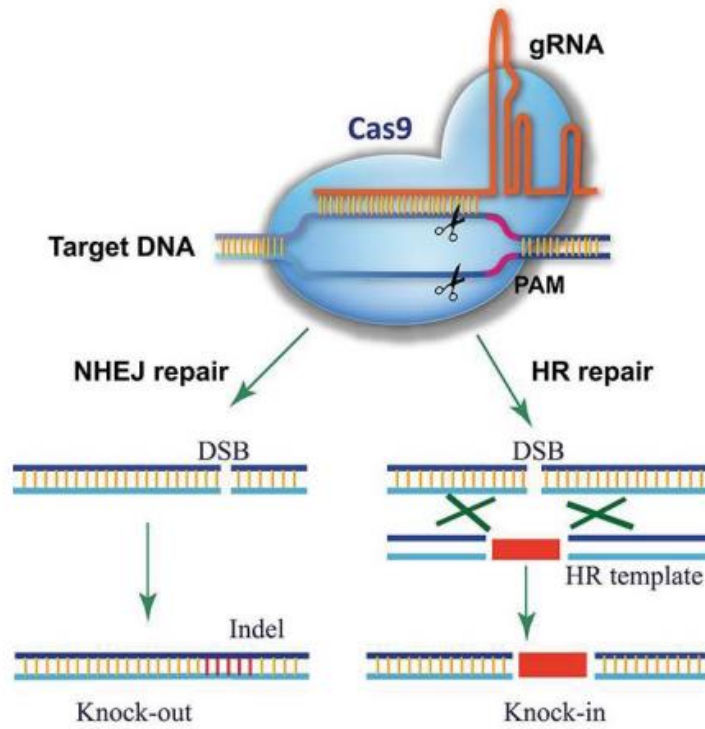
Figure 6. Schematic overview of the CRISPR/Cas9 technology (Razzaq and Masood 2018).

2. AIM

The aim of the work is to better characterize some of the molecular aspects of SPG11-HSP starting from patients derived materials obtained during the diagnostic procedures undertaken at the IRCCS Fondazione Stella Maris. To translate preclinical findings to the bedside, we complemented our investigations with the study *in vitro* ed *in vivo* with two FDA-approved drugs, *ataluren* and *miglustat* exploring new opportunities to therapy in SPG11-HSP. Finally, we complemented data from peripheral cells with a novel SPG11 knock-out neuroblastoma cell line.

Three principal goals were at the pillar of this PhD research project.

The **first** goal was to molecularly characterize peripheral cells from 22 SPG11-patients on the basis of their *SPG11* mutations. We collected patients' derived biological materials (cultured skin fibroblasts and blood samples for lymphocytes, protein and RNA extraction). We also tested the efficacy of *ataluren* in cases harboring nonsense variants attempting to recover *SPG11* mRNA expression.

The **second** objective was to investigate oxidative metabolism in SPG11 cells to ascertain in a "clinical setting" the relevance of this pathological mechanisms. Since *miglustat* also exerts a positive role in the lipid and protein oxidations seen in NPC1 (Ribas et al. 2012), we also explored the cellular consequences of a short-term treatment with SPG11 cell models.

The **third** goal is a multi-omics approach, through proteomic and lipidomic analysis in patients' cultured fibroblasts in order to seek putative biomarkers relative to SPG11-HSP disease. We also evaluated the modulatory effect of *miglustat* on proteome and lipidome of SPG11 patients' fibroblasts and plasma.

3. MATERIALS AND METHODS

3.1 Sample collection

Being a third-level center of the National Health Service (NHS) for the study of HSPs and other rare movement disorders, 22 SPG11 patients are regularly followed up at the Neurogenetic of IRCCS Fondazione Stella Maris, Pisa. Having obtain their written informed consent, patients' samples (skin fibroblasts and peripheral blood) were collected. It was not possible to collect all the samples from each patients because of the restrictions of the COVID-19 pandemia.

3.1.1 Skin biopsies

Skin biopsies were collected with a diagnostic, 3mm punch biopsy. The skin was then used to established a primary cell line according to standard diagnostic procedures (Geraghty et al. 2014).

3.1.2 Peripheral blood mononuclear cells isolation

Peripheral blood mononuclear cells (PBMCs) were isolated from whole blood using PBMC Spin Medium (PluriSelect, Leipzing DE, Germany). Five ml of whole blood were mixed with 5ml of PBS and the 10ml were layered on top of 3ml of PBMC Spin Medium. After 15minutes (min) at 800xg centrifuge with the brake off, the enriched cells from the density gradient medium and plasma interface were carefully collected and washed twice with PBS for 10min at 300xg at 4°C. The pellet of PBMC was collected and stored at -80°C until used.

3.1.3 Plasma and serum separation from whole blood

Five ml of whole blood were collected in BD Vacutainer serum or EDTA tube for serum and plasma separation respectively. For serum collection, the blood drawn was let in an upright position for 30 minutes (min), then it was centrifugated for 10 min at 2000xg at 4°C and the supernatant was divided in aliquots in 0.5mL polypropylene tubes. For plasma collection, the blood drawn was centrifugated for 10 min at 2000xg at 4°C and the supernatant was divided in 0.5mL aliquots. Serum and plasma aliquots were stored at -80°C until used.

3.1.4 RNA isolation from whole blood

Having collected 3 ml of peripheral blood in PAXgene Blood RNA Tube (Qiagen, Hilden, Germany), tubes were stored in upright position at room temperature for maximum of 72h before freezing at -20°C for 24h and then at -80°C for a long storage.

3.2 Studies in skin fibroblasts

3.2.1 Cell cultures

The cell lines used in this research program were:

- Primary cultures of human skin fibroblasts obtained from punch biopsies and

- SH-SY5Y neuroblastoma cells (kindly donated by Prof. Ciro Ippolito, University of Piemonte Orientale, Novara, Italy).

Both cell lines were growth in Dulbecco's modified Eagle's medium (DMEM) containing 4.5g/L glucose (Euroclone) and 1% antibiotics (Euroclone) supplemented with 10% fetal bovine serum (FBS, Euroclone), 0.5% uridine and 0.002% antimycotic for primary skin fibroblasts; and with 15% FBS and 1% non-essential amino acids for neuroblastoma cell line. Cells were maintained at 37°C with 5% CO_2.

3.2.1.1 Drugs administration

Patients skin fibroblasts were treated with two FDA-approved drugs: *miglustat* (N-Butyl-deoxynojirimycin·HCl, Santa Cruz Biotechnology, TX, USA) and *ataluren* (PTC124, PTC Therapeutics, NJ, USA). *Miglustat* was added to regular medium without uridine at 100µM for 72h. *Ataluren* was dissolved in complete medium without antibiotics at 40µM for 24h. Caffeine (Sigma-Aldrich, MO, USA) was also added to fibroblasts medium at 10mM concentrated alone or in combination with *ataluren*.

3.2.2 Molecular and biochemical studies

3.2.2.1 Quantitative real-time PCR (qPCR)

Total RNA was extracted from skin fibroblasts using High Pure RNA Isolation Kit (Roche), then 500ng of total RNA was retro-transcribed using PrimeScript™ RT Reagent Kit (Perfect Real Time) (Takara) following manufacturer's instructions. qPCR was performed using qPCRBIO SyGreen Mix Hi-ROX (PCR Biosystems, Wayne, PA.) and 7500 Fast Real-Time PCR Systems (Thermo Fisher Scientific). The ribosomal protein 18S was used as internal control. Gene expression levels were referred to the internal control, the relative quantification was carried out by means of the ΔCt method and the results were expressed as relative mRNA expression. Primers used are listed in supplemental material (**Table S1**).

3.2.2.2 Western blot

Cultured skin fibroblasts were collected at confluence, washed twice with PBS and then homogenized on ice using M-PER™ Mammalian Protein Extraction Reagent (Thermo Fisher Scientific) and Halt™ Protease Inhibitor Cocktail (100X) (Thermo Fisher Scientific). Homogenates were centrifuged for 10 min at 14,000 g at 4 °C, then supernatants were collected and stored at -80°C. 30 µg of proteins were loaded in Novex™ 4-12% Tris-Glycine Mini Gels, WedgeWell™ format (Thermo Fisher Scientific) using Novex™ Tris-Glycine SDS Sample Buffer (2X) (Thermo Fisher Scientific) and NuPAGE™ Sample Reducing Agent (10X) (Thermo Fisher Scientific). Blotting used Trans-Blot Turbo Transfer System (Bio-Rad Laboratories Inc,

Berkeley, CA) and Trans-Blot® Turbo™ RTA Mini PVDF Transfer Kit (Bio-Rad). Membranes were blocked with TBS/0.1% Tween20 (TTBS) containing 5% non-fat dry milk. Primary antibodies were incubated overnight at 4°C in TTBS with 2.5% non-fat dry milk, whereas secondary antibody peroxidase-conjugated anti-mouse and anti-rabbit were used (Cell Signaling Technology Inc., Danvers, MA) for 1 hour at room temperature in the same buffer used for the primary antibodies (2.5% non-fat dry milk in TTBS). Bands were revealed using Clarity Western ECL Substrate (Bio-Rad) and ChemiDoc™ Imaging System (Bio-Rad). ImageJ software (https://imagej.nih.gov/ij/) was used for densitometry analysis. Primary antibodies used were: anti-SPG11 (1:200, antibody 711811, Thermo Fisher Scientific), anti-ZFYVE26 (1:1000, antibody PA5-20685, Thermo Fisher Scientific), anti-SPG48 (1:500, antibody HPA035693, Sigma-Aldrich), anti-Nrf2 (1:1000, antibody ab62352, Abcam, Cambridge, UK) and as internal control anti-β-tubulin (1:1000, Cell Signaling Technology, Danvers, MA).

3.2.2.3 Micro-oxygraphy analysis

Oxygen consumption rate (OCR) was measured in skin fibroblasts and SH-SY5Y cells with a XFe24 Extracellular Flux Analyzer (Seahorse Bioscience, Agilent, CA, USA). Each cell line was plated in XF 24-well cell culture microplates at a density of 5E04 cells/well for fibroblasts, 6E04 cells/well for SH-SY5Y WT or transfected with px459 empty and 1,8E05 cells/well for Clone KO-SPG11, in 250 µL of normal culture media and incubated for 24h at 37°C in 5% CO_2 atmosphere. After replacing the growth medium with 500 µL of XF media (non-buffered DMEM medium, containing 10mM glucose, 2mM pyruvate, 2 mM glutamine; ph 7.4), pre-warmed at 37°C cells were preincubated for 30 min before starting the assay procedure. After baseline measurements, OCR was measured after sequentially adding to each well oligomycin and carbonyl cyanide 4-(trifluoromethoxy) phenylhy-drazone (FCCP) to reach a working concentration of 1µg/ml and 1.5 µM. We evaluated the fraction of non-mitochondrial oxygen consumption, by measuring OCR after complete inhibition of the mitochondrial respiratory chain by a mix of antimycin A and rotenone, both at a concentration 0.5 µM (all chemical from Sigma Aldrich) (Invernizzi et al., 2012) (**Figure 7**).
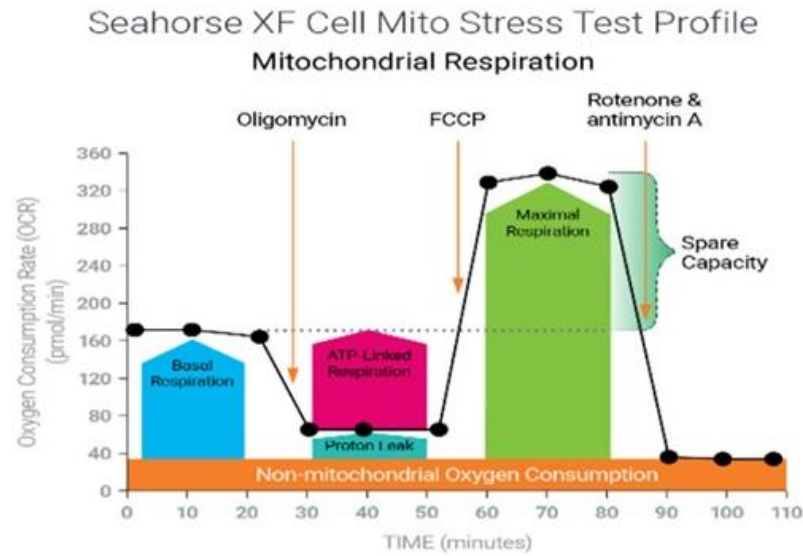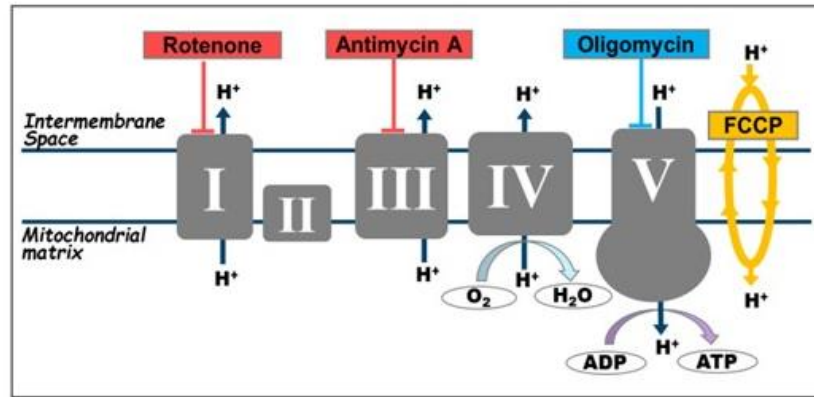
Figure 7. Schematic overview of the mitochondrial stress test using the extracellular flux analyzer. **A** Oxygen (O_2) consumption rate (OCR) measured during drugs administration. Basal respiration represents the energetic demand of cells under baseline condition. ATP-linked respiration represents the portion of basal respiration used to drive ATP production and, it is measured after oligomycin injection. Maximal respiration represents the maximum rate of respiration that cells can achieve and, it is calculated after FCCP addition. Non-mitochondrial respiration is the oxygen consumption after the injection of rotenone and antimycin A and, it is due to a subset of other cellular enzymes. Proton leak represents the basal respiration not coupled to ATP production and it is calculated as the difference between the maximal and the non-mitochondrial respiration. Spare respiratory capacity is the capability of the cells to respond to a sudden increased energetic demand and it is calculated as the difference between the maximal and the basal respiration. **B** Schematic representation of the electron transport chain (ETC) with detailed description of drugs target: rotenone inhibits complex I, antimycin A complex III, oligomycin complex V, while FCCP is a membrane uncoupler.

Plates were normalized post-assay by CyQUANT Cell Proliferation Assays (Thermo Fisher Scientific, MA, USA) based on DNA content and analyzed using Seahorse Bioscience Report

Generators. The mean+SEM values of at least three independent experiments are represented. Statistical comparison of the data sets was performed using Student's t-test. The differences are presented with the corresponding statistical significance.

3.2.2.4 Reactive oxygen species measurement

For the evaluation of intracellular ROS production, a dichloroflouorescein diacetate (DCFDA) cellular ROS detection assay kit (Abcam, Cambridge, UK) was used. Fibroblasts or SH-SY5Y cells were labeled with 25 μM 2,7-DCFDA for 45 min at 37°C and then cultured an additional hour with or without 150 µM tert-butyl hydrogen peroxide (TBHP), a ROS-mimic activity. Cells were then analyzed on a fluorescent plate reader (SpectraMax® ID3, Molecular Devices LLC, San Jose, CA) at a wavelengths Ex/Em: 485 nm/535 nm and the difference in ROS levels between treated and untreated condition were expressed as relative fluorescent units (RFU) after background subtraction. For each well DCFDA signal was normalized on Hoechst 33342 intensity.

3.2.2.5 Immunofluorescence stains

The cells adherent on sterile glass coverslips, previously treated with Poly-D-Lysine (Sigma-Aldrich) were fixed in PFA for 15min and permeabilized with 0.1% Triton X-100 in PBS1X for 15 min. According the experiment design controls and patients cells were fixed with any treatment (NT), after the addition of the uncoupling agent FCCP ($20\,\mu$M concentrated, only for control cells), and 2h later FCCP addition. Then, coverslips were washed in PBS1X and incubated in a blocking solution (FBS 20% in PBS1X) for 1 h at room temperature. Overnight incubation in a cold room was performed with the rabbit polyclonal anti-TOM20 (Santa Cruz Biotechnology; dilution 1:100). As secondary anti-rabbit antibody (dilution 1:1000) conjugated with AlexaFluor 555 dye (Cell Signaling Technology Inc., Danvers, MA) was used for 1h at room temperature in a humid chamber. Nuclei were stained with the fluorescent dye 4,6-diamidino-2-phenylindole-dihydrochloride 5 μg/ml (DAPI, Sigma-Aldrich). Stained cells were mounted for microscopy. Images were acquired using a Nikon Ti2-E inverted microscope equipped with a DS-Qi2Mc camera and collected with a Nikon 60 x Plan Apocr λ (NA=1.40) oil immersion objective, using a TRITC and DAPI filter sets. Then mitochondrial network was evaluated measuring mitochondrial shape with Image J following manual instructions (Merrill, Flippo, and Strack 2017).

3.2.2.6 Mitochondrial membrane potential measurement

Fibroblasts were plated on dark lid dishes (WillCo-Dish® glass bottom dish, WillCo Wells BV, NL) and grown in regular medium for 24 hours. Mitochondrial membrane potential ($\Delta\psi$m) was assessed with TMRM (Invitrogen, Carlsbad, CA) to label active mitochondria. TMRM is a cell permeant, positively-charged fluorescent dye, which accumulates in active mitochondria in a potential-dependent manner. Depolarized or inactive mitochondria fail to take up the probe which

remains scattered in the cytosol. The dye was loaded onto cells at 100 nM in Hank's Balanced Salt Solution supplemented with 10 mM HEPES, pH 7.4, at 37 °C for 5 minutes; the cells were then wash in PBS and images were acquired with the Nikon Ti2-E inverted fluorescence microscope described before.

3.3 Trial in patients

Having obtained ethics committee approval from the Tuscany CEP, a registered clinical trial to test safety of increasing doses of *miglustat* in ambulant SPG11 patients was started at the Neurogentic Center, IRCCS Fondazione Stella Maris, Pisa (TreatSPG11, ClinicalTrials.gov Identifier: NCT04768166). With patients' (or caregivers) written informed consent, the study enrolled 13 consecutive SPG11 ambulant patients (with or without walking aids). This is an open label, increasing doses test of miglustat in patients with biallelic variants in the SPG11 gene. The primary outcome was to assess safety as reported as number of severe adverse events (SAE), defined as any untoward medical occurrence that at any dose results in death, in a life-threatening event, requires inpatient hospitalization or causes prolongation of existing hospitalization.

Figure 8 summarizes the main scheme of the TreatSPG11 trial. The clinical design and outcomes of the trial are beyond the scope of this dissertation. We took the opportunity to collect exploratory outcomes by investigating blood from patients in the study at time zero (baseline, T0), after 12 weeks of treatment with *miglustat* (T1) and after 12 weeks in the follow up period free of *miglustat* (T2).

Blood samples of all enrolled patients were collected at times T0, T1 and T2 in the trial, plasma was immediately purified in small aliquots and then stored at -80°C until use.
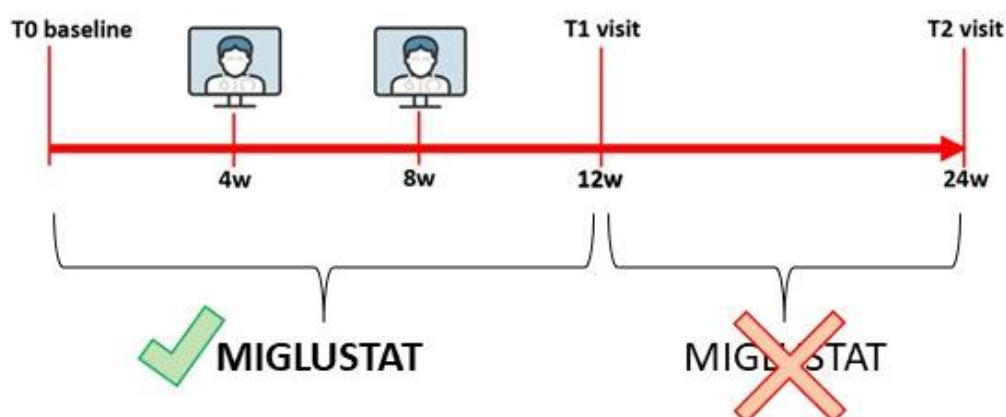
Figure 8. Schematic overview of the TreatSPG11 trial. Patients were samples at T0 (at baseline before the trial started), at T1, and T2, once the drug had been stopped). w: week.

3.4 Multi-omics approaches

3.4.1 Chemicals and materials

Formic acid (5.33002) and the two salts ammonium formate (14266) and ammonium bicarbonate (40867), all eluent additives for liquid chromatography-mass spectrometry (LC-MS), were purchased, respectively, from Merck (Darmstadt, Germany) and Fluka Analytical (Sigma-Aldrich, St. Louis, MO). Methanol (1.06035), 2-propanol (1.02781) and acetonitrile (1.00029), both hypergrade solvents LiChrosolv for LC-MS, were bought from Merck (Darmstadt, Germany), while chloroform (366927, for HPLC), NaCl (S3014), sodium deoxycholate (SDC, D6750), albumin from bovine serum (A7906), Trizma base (T6066) and HCl (258148) from Sigma-Aldrich. Reagent A (23228) and reagent B (1859078) for Pierce BCA (bicinchoninic acid) Protein Assay were purchased from Thermo Scientific (Rockford, IL). Iodoacetamide (IAA, RPN6302V), dithiothreitol (DTT, D1 309.0010), trypsin modified sequencing grade (11418033001) and N,N-dimethylsphingosine (d18:1) (DMS, 860496O) were obtained, respectively, from GE Healthcare (Chicago, IL), Duchefa Biochemie (Haarlem, The Netherlands), Roche (Indianapolis, IN) and Avanti Polar Lipids (Alabaster, USA). Spin columns (M1003) and their filters (M2110) were purchased from Mo Bi Tec (Goettingen, Germany) while their VersaFlash spherical C18 stationary phase from Supelco Analytical (Bellefonte, PA). Milli-Q deionized water was filtered on Millipak filter (0.22 μm, MPGL040001) and purified on a LC-Pak cartridge (C18, LCPAK0001) (all Millipore, Bedford, MA).

3.4.2 Groups analysed

The experimental groups of multi-omics studies were patients untreated (P_NT, n= 6), patients treated with miglustat (P_T, n= 6) and age-matched untreated healthy control donors (C_NT, n= 3).

3.4.3 Proteomic

3.4.3.1 Proteomic on fibroblasts

3.4.3.1.1 Sample processing

The cell pellets were thawed at room temperature, centrifugated at 13000 rpm for 2 min at 4 °C in a Microcentrifuge Heraeus Biofuge Fresco (Thermo Scientific, MA, USA), the supernatant liquid was removed and 100 μl of 1% SDC in Ambic 50 mM solution were added to each sample. After incubation at 80 °C for 10 min at 500 rpm in a ThermoMixer C (Eppendorf AG, Hamburg, Germany) the samples were ultrasonicated and the protein content was evaluated by BCA assay using bovine serum albumin as standard. Protein extracts were reduced and alkylated, respectively, with 10 mM DTT (incubation at 65 °C for 30 min) and 20 mM IAA (incubation at 37 °C for 30 min in the dark) and then digested with trypsin (1:50 w/w) at 37 °C for 16 hours. The

resulting peptide mixtures were treated with 10% TFA to stop the tryptic digestion and precipitate the deoxycholic acid. The supernatants were subsequently purified on C18 spin columns. The eluates were evaporated to dryness under vacuum at 36 °C (Speed Vac Concentrator, Savant Instruments Inc., Farmingdale, NY), resuspended in 50 µl of 5/95 CH3CN/0.1% HCOOH to achieve a final peptide concentration of 2 µg/µl and finally transferred in plastic vials for LC-MS/MS analysis. Moreover, for each of the three conditions (P_T, P_NT, C_NT), sample pools were prepared by mixing equal quantity of the biological replicates.

3.4.3.1.2 Analysis through mass spectrometry

Sample analyses were performed using a micro-HPLC Eksigent Ekspert microLC 200 combined with a Triple TOF 5600 mass spectrometer equipped with a Turbo Ion Spray probe as ion source (all ABSCIEX, Concord, Ontario, Canada). Five µl of each sample/pool, set in an autosampler at 8 °C, were injected onto a C18 Jupiter column (150 mm x 0.3 mm i.d., 4 µm particle size, 90 Å) thermostated at 30 °C and equipped with a micro trap C18 (10 mm x 0.3 mm) (both Phenomenex, Torrance, CA). The flow rate was set at 5 µl/min and the mobile phases A and B were, respectively, H2O and CHCN3, both with 0.1% HCOOH. The elution program was: 0 min, 5% B; 1 min, 5% B; 51 min, 22% B; 51.5 min, 90% B; 53.5 min, 90% B; 54 min, 5% B; 60 min, 5%B. Chromatographic performances and TOF accuracy were evaluated using an intra-run injection (5 µl) of beta-galactosidase 100 fmoli/µl. The mass spectrometer was set in positive ion mode and the operation conditions of the ion source were the following: ion spray voltage floating 5.5 kV, probe temperature 150 °C, curtain gas 25 psi, ion source gas 1 and gas 2 respectively 30 and 20 psi, declustering potential 100 V. N2, as inert gas, was used for MS/MS (tandem mass) experiments.

For ion library generation (protein identification) sample pools were analyzed (double injection) with an information dependent acquisition (IDA) tandem mass spectrometry method based on a MS1 survey scan from which the 20 most abundant precursor ions were selected for subsequent fragmentation (CID = collision induced dissociation). MS1 survey scans were acquired with a maximum resolving power of 30000 in a range of 250-1250 m/z, while MS/MS scans at 25000 of resolving power in a range of 100-1500 m/z in a high sensitivity mode. CID experiments were carried out using a rolling collision energy automatically calculated according to the m/z and the charge state of the candidate ion, with a collision energy spread (CES) of 5 V. Precursor ions with a charge state of 1+ were excluded from data dependent selection. Acquired data were subjected to protein identification using Protein Pilot (ABSCIEX) as probabilistic search tool, using the Homo Sapiens taxon (20381 entries) on UniProtKB/Swiss-Prot database (release March 2021). For database search: trypsin was selected as digestion enzyme and carbamidomethylation of

cysteine residues was selected as fixed modification. In the ion library thus generated 503 proteins were identified with 1% critical false discovery rate (FDR).

For protein quantitation, the SWATH (Sequential Window Acquisition of all THeoretical mass spectra) data independent acquisition (DIA) method was used. The 15 samples (double injection) were cyclically acquired with the same MS1 survey scan used for IDA experiment followed by 50 MS/MS experiments with an m/z sequential variable range (maximum resolving power of 25000, high sensitivity mode, rolling collision energy, CES 5 V).

3.4.3.1.3 Data analysis

SWATH files, jointly with the ion library, were processed using PeakView (version 2.1) and MarkerView (version 1.2.1) software (both ABSCIEX) to extract the peak areas of all the quantifiable peptides and proteins (421 proteins quantified). Protein abundances were normalized on the basis of the media total abundance per sample. To reveal patterns in data an unsupervised multivariate method was first used. Principal Component Analysis (PCA) was performed in order to reduce the variation of the protein dataset to a small number of dimensions. For each protein, fold change (FC) value was calculated as the ratio between the mean of expression in patient and the mean of expression in control (P_T vs C_NT e P_NT vs C_NT). Level of significance between groups was addressed by performing a Student's two-tailed t-test and p-values were corrected using the Benjamini–Hochberg procedure, to minimize any type I errors and thus the occurrence of false positives. The list of the significant (adjusted p value < 0.05) and differentially expressed (FC ≤ 1/1.5 for down-regulation or FC ≥1.5 for up-regulation) was obtained using R software (version 4.1.1).

All differentially expressed proteins were subjected to Gene Ontology (GO) enrichment analysis, using the package ViSEAGO (1.8.0) (Brionne, Juanchich, and Hennequet-Antier 2019) of R software. Enrichment analysis was performed using the Fisher's exact test and the classic algorithm. GO term with a p-value < 0.01 were considered significant for the analysis. The annotation resource used was the human Uniprot-GOA (version: 2021-12-21) and the analysis was conducted with respect to Biological Processes (BPs). To disclose hidden relationships and to better understand the results of BPs analysis, we performed GO annotations and enriched GO terms using Semantic Similarity (SS). The SS between enriched GO terms were calculated using the Wang method, that is based on the topology of GO graph structure. The information content (IC) of a GO term was computed by the negative log probability of the term occurring in GO corpus, so that a rarely used term contains a greater amount of information. Finally, most informative results were filtered so to show only enriched GO terms with IC > 6.

3.4.4 Lipidomic

3.4.4.1 Lipidomic on fibroblasts

3.4.4.1.1 Sample processing

Pellets of cell samples under study (groups as above) were thawed at room temperature and 150 µl of TrisHCl 50 mM pH 8, containing 120 mM NaCl, were added to each sample. After incubation at 80 °C for 10 min at 500 rpm in a ThermoMixer C (Eppendorf AG,) the samples were ultrasonicated and the protein content was evaluated by BCA assay using bovine serum albumin as standard. To 100 µl of each extract, 200 µl of NaCl 150 mM and 1.2 ml of N,N-dimethylsphingosine (d18:1) (DMS) 0.25 µM in CHCl3/MeOH 2/1 (as internal standard) were added, according to a modified Folch protocol for lipid extraction (Folch, Lees, and Stanley 1957). The samples were incubated in Thermomixer at 25 °C for 30 min at 1000 rpm and then centrifugated at 13000 rpm for 5 min at 10 °C. 800 µl of the lower phase were withdrawn, evaporated under vacuum at 36 °C (Speed Vac Concentrator) till dryness, resuspended in 80 µl of CHCl3/MeOH 2/1 and finally transferred in a glass vial for LC-MS/MS analysis.

3.4.4.1.2 Analysis through mass spectrometry

Targeted lipidomics analysis was carried out by liquid chromatography-electrospray ionization-tandem mass spectrometry. LC-MS/MS analyses were performed using a Nexera X2 HPLC system (Shimadzu, Kyoto, Japan) combined with a QTrap 5500 mass spectrometer (SCIEX,) equipped with a Turbo V™ ESI source. Vials were put in a refrigerated autosampler at 5 °C and each sample was double injected (injection volume 0.5 µl). In order to avoid carryover, two needle wash solutions were used: MeOH/i-PrOH 50/50 and MeOH/CHCl3 1/2. Gradient elution, at a flow rate of 0.2 ml/min, was performed on a Kinetex column packed with C8 phase (100 × 2.1 mm, 1.7 µm, 100 Å) by Phenomenex (Torrance, CA). Mobile phase A was MeOH/H2O/i-PrOH 50/45/5 while phase B MeOH/i-PrOH 50/50, both with 5 mM ammonium formate. The gradient elution program was: 0 min, 65% B; 0.5 min, 65% B; 10 min, 100% B; 15 min, 100% B; 15.1 min, 65% B; 20 min, 65% B. The column temperature was 45 °C. The mass spectrometer was set in positive ion mode and the operation conditions were the following: curtain gas 30 psi, ion spray voltage 5 kV, probe temperature 200 °C, ion source gas 1 and gas 2 30 psi, declustering potential 100 V, entrance potential 10 V, collision cell exit potential 19 V, collisional gas N2. A selected reaction monitoring (SRM) acquisition was accomplished using Analyst Software 1.6.3 (SCIEX, Concord, Ontario, Canada) for 182 lipid species belonging to 11 lipid classes (PC, LPC, PE, LPE, TG, DG, CE, SM, Cer, GM2 and GM3), using a fixed dwell time of 5 msec. Previous studies (Michelucci et al. 2021 and unpublished material) had been performed in order to optimized collision energies for each lipid class and to select the appropriate precursor/product ion for each Q1/Q3 transition.

3.4.4.1.3 Data analysis

Lipidomics experimental data were analyzed using Lipidr package (version 2.8.0) (Mohamed, Molendijk, and Hill 2020) of R software. The package implements a series of function to facilitate inspection, analysis and visualization of lipidomics datasets. Data were loaded on Lipidr in an object called LipidomicsExperiment, which included all peak area measurements, lipid annotation data (automatically inferred on the basis of lipid names referring to LIPID MAPS Database) and clinical annotations for the samples. Firstly, lipidomics data were subjected to quality control and visualization, then normalized using Probabilistic Quotient Normalization (PQN) method (Dieterle et al. 2006).

To reveal patterns in data, an unsupervised multivariate method was first used. Principal Component Analysis (PCA) was performed to reduce the variation of the lipid dataset to a small number of dimensions. Differential analysis was conducted comparing lipids expression levels in different groups. Lipids were considered significant and differentially altered with an adjusted p-value < 0.05 and a fold change $FC \leq 1/1.5$ or $FC \geq 1.5$. Finally, all lipids were subjected to lipid set enrichment analysis (LSEA) (Mohamed, Molendijk, and Hill 2020; Subramanian et al. 2005) to detect preferential enrichment of certain lipid classes in patients with respect to controls. Lipid classes were considered significantly enriched with an adjusted p-value lower than 0.05.

3.4.4.2 Lipidomic on plasma

3.4.4.2.1 Sample processing

Plasma samples, stored at -80 °C, were thawed at room temperature and immediately subjected to lipid extraction and analysis. Lipid extraction from an aliquot of plasma was performed according to Folch procedure (Folch, Lees, and Stanley 1957): 50 μl of sample were put in a 1.5 ml microcentrifuge tube and were diluted with 100 μl of 150 mM NaCl aqueous solution and 600 μl of 0.0625 μM DMS (chosen as internal standard, ISTD) in MeOH/CHCl3 1/2. The biphasic solution thus formed was incubated at 25 °C for 30 min at 1000 rpm in a Thermomixer Compact (Eppendorf) and then centrifuged at 13000 rpm for 10 min at 10 °C in a Microcentrifuge Heraeus Biofuge Fresco (Thermo Scientific). From each sample an aliquot of the lower phase was transferred into a glass vial for the subsequent high performance liquid chromatography-tandem mass analysis (LC-MS/MS).

3.4.4.2.2 Analysis through mass spectrometry

The analysis through mass spectrometry was the same as for lipidomic on fibroblasts.

3.4.4.2.3 Data analysis

Data analysis were performed using Lipidr package (version 2.8.0) (Mohamed, Molendijk, and Hill 2020) of R software as in lipidomic analysis on fibroblasts. Nonetheless, in this analysis

normalization was performed on the basis of the media ISTD area per sample. Therefore, differential analysis was conducted comparing lipids expression level in patients at T=1 and at T=0 using paired T-test and controls. Lipids were considered significant and differentially altered with an adjusted p-value < 0.05 and a fold change FC ≤ 1/1.3 or FC ≥1.5.

3.5 Generation of CRISPR/Cas9 cell line

3.5.1 SPG11 CRISPR/Cas9 guide RNA

Single-guide RNA (sgRNA) was chosen from among top targets identified by CHOPCHOP software with NGG PAM and zero off-target following the criteria and the process for guide RNA design and selection of Hsu et al. 2013 and Doench et al. 2016. Forward and reverse primers (**Table S1**) were design for cloning.

3.5.2 Cloning

The expression vector pSpCas9(BB)-2A-Puro (pX459) V2.0 plasmid (Addgene Plasmid #62988) was used for cloning sgRNA (**Figure 9**).
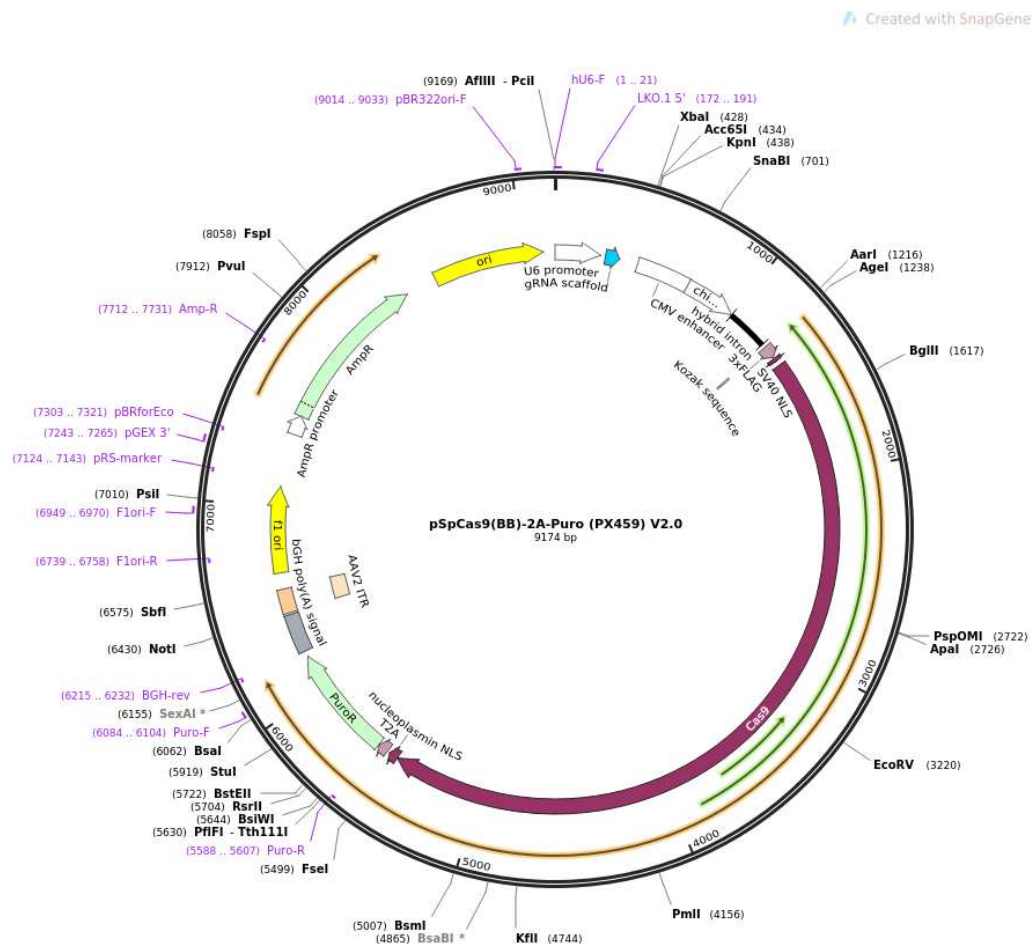
Figure 9. Addgene pSpCas9(BB)-2A-Puro plasmid map (created with SnapGene: http://www.snapgene.com)

29

One μg of vector was digested with 10 units of the enzyme BbsI (Thermo Scientific,) at 37°C for 2 h and then DNA was purified using Gel Extraction kit (QIAGEN). SPG11 sgRNA forward and reverse were dissolved at 100 μM concentration and 1 μl of both were mixed and annealed in the thermal cycler at 37°C for 30 min, 95°C for 5 min followed by cooling down the mixture from 25°C at 5°C/min to 10°C. The ligation was performed mixing oligo duplex with the purified expression vector and T4 DNA ligase (New England BioLabs) at 16°C over-night. Plasmid-Safe™ ATP-Dependent DNase (Epicentre-Illumina) was used to remove the yet linearized DNA fragments from ligation reaction. The plasmid was then transformed into a competent E. coli strain (One Shot Stbl3 Chemically Competent e. coli; Invitrogen). Then cells were plating on a LB agar with 100 μg/mL ampicillin, that makes possible to select only cells containing the plasmid; some colonies were picked to isolate the plasmid DNA (QIAprep® spin miniprep Kit; QIAGEN). To check the correct insertion of the guide construct (annealed forward and reverse strand of sgRNA) plasmid U6 fragment was amplified and sequenced.

3.5.3 Transfection

About $3x10^4$ of SH-SY5Y cells were seeded in a 6-well plate for 24 h and transfected with lipofectamine 3000 (Invitrogen) mixed to pX459-SPG11 sgRNA vector or empty vector as control followed the manufacturer's instructions. The transfected cells will encode for the Cas9 nuclease and use the sgRNA like a template to drive the DSB on genome DNA. One-day post transfection cells were gowned in regular media supplemented with 5 ug/mL puromycin 24 h and then with 3 ug/mL to select cells which had incorporate the exogenous DNA. A parental cell line was treated in puromycin under the same condition in order to drive the treatment time. When 100% of parental cells was dead due to puromycin effect the antibiotic selection was stopped and the survived transfected cells incorporates plasmid. By Tracking of Indels by Decomposition (TIDE) web tool, a simple, quick assay to accurately characterize and quantify the induced mutations, were used to assessed genome editing events. Based on the quantitative sequence trace data from two standard capillary sequencing reactions the TIDE software quantified the editing efficacy and identified the predominant types of insertions and deletions (indels) in the DNA of a targeted cell pool (Brinkman et al. 2014). Furthermore, a western blotting analysis for the target protein were performed to correlate the genotype modifications with protein expression. Once evaluated the overall editing efficiency, the transfection pools is used to isolate single clones by "limiting-dilution technique": cells suspension was diluted and plated at a density of 0.3cell/well (in a 96 multiwell plate) in order to have a statistic guarantee to achieve few wells that contain only one cell.

3.5.4 Verification of the genomic modification of clones

Genotype and phenotype of clones grown in wells under regular conditions (grown time $\cong$ 3 weeks), were verified by standard sequencing methods and Western blotting analyses respectively. Only the identified pure edited clones with a total lack of protein expression were expanded for downstream application. Generated CRISPR KO clones could be considered stable and grown like the parental cell lines.

3.6 Statistical analysis

All experiments were performed at least in triplicate and the means ± SEM were reported. Statistics were performed using GraphPad Prism software, using Student t test, one-way ANOVA depending on the experiments. Significance was set at $P < 0.05$ (*), $P < 0.01$ (**), $P < 0.001$ (***) and $P < 0.0001$ (****). Statistical analysis for lipidomic and proteomics studies was described before.

4. RESULTS

4.1 Molecular studies

We studied 22 SPG11 patients that are genotypically and clinically described in **Table 1**. In the table are also reported gender and age of patients with the age of the onset of HSP symptoms. Most patients underwent a skin biopsy; the difference between the age at onset of symptoms and the age at biopsy was considered as the duration of the disease. However, patients 21 and 22 did not undergo a diagnostic skin biopsy; their disease duration was assessed by the time of PBMC studies.

Table 1. Description of the 22 SPG11 patients. SPG11 mutations were defined on NM_025137.4 Ref Seq. CC: corpus callosum; PNP: peripheral polyneuropathy; SPRS: Spastic Paraplegia Rating Scale; yrs: years; WM: white matter. * points to patients of TreatSPG11 trial.

PATIENT	GENOTYPE	PROTEIN CHANGE	CLINICAL CHARACTERISTICS	GENDER, AGE	AGE AT ONSET (HSP)	AGE OF BIOPSY	DURATION OF DISEASE
1 *	c.3257del / c.4339C>T	p.Ala1086ValfsTer23 / p.Gln1447Ter	Spastic gait requiring the use of a walker; bradykinesia, dysarthria, mild cognitive impairment and mood disorders, urge incontinence, CC atrophy, mild PNP. Latest SPRS score (21 yrs): 27/52	M, 21	14	18	4
2 *	c.5986dup / [c.6175C>T; c.6331dup]	p.Cys1196LeufsTer4 / [p.Arg2059Trp; p.Glu2111GlyfsTer38]	Spastic paraplegia, uses a wheelchair in most daily activities, walks few steps with two crutches, dysarthria, mild cognitive impairment, urge incontinence, mild dysphagia for liquids, periventricular WM hyperintensities and CC atrophy. Latest SPRS score (27 yrs): 34/52	M, 27	16	25	9
3 *	c.6754+2_6754+3dup / c.6739_6742del	p.Glu2247LeufsTer14	Spastic paraparesis; he uses the wheelchair outdoors and double canes in the home environment; dysarthria, mild cognitive impairment, urge incontinence, periventricular WM hyperintensities and CC atrophy, mild PNP. Latest SPRS score (19 yrs): 26/52	M, 19	13	17	4
4	c.4416del / c.7000-3_7000-2insGGA	p.Leu1473TrpfsTer56	Spastic gait requiring the use of a walker; mild cognitive impairment, urge incontinence, PNP. Latest SPRS score (47 yrs): 29/52	M, 50	30	46	16
5 *	c.4307_4308del / c.662G>A	p.Gln1436ArgfsTer7 / p.Trp221Ter	Spastic paraparesis; he uses the wheelchair outdoors and double canes in the home environment; dysarthria, mild cognitive impairment, urinary urgency, CC atrophy. Latest SPRS score (31 yrs): 26/52	M, 31	19	22	3
6	c.5014G>T /	p.Glu1672Ter /	Spastic gait; mild dysarthria, mild cognitive	F, 24	15	19	4

PATIENT	GENOTYPE	PROTEIN CHANGE	CLINICAL CHARACTERISTICS	GENDER, AGE	AGE AT ONSET (HSP)	AGE OF BIOPSY	DURATION OF DISEASE
	c.6856C>T	p.Arg2286Ter	impairment, urinary urgency, WM hyperintensities and CC atrophy, PNP. Latest SPRS score (19 yrs): 17/52				
7 *	c.4307_4308del / c.4307_4308del	p.Gln1436ArgfsTer7 / p.Gln1436ArgfsTer7	Spastic paraplegia, uses a wheelchair in most daily activities, walks few steps with a walker, mild cognitive impairment, urge incontinence, periventricular WM hyperintensities and CC atrophy. Latest SPRS score (29 yrs): 30/52	F, 29	19	23	4
8	c.1323G>A / c.1951C>T	p.Trp441Ter / p.Arg651Ter	Spastic gait requiring the use of a walker; dysarthria, mild cognitive impairment, urinary urgency, CC atrophy. Latest SPRS score (25 yrs): 28.5/52	F, 25	14	22	8
9	c.3122_3124del / c.5014G>T	p.Arg1041del / p.Glu1672Ter	Spastic gait requiring the use of a cane; mild dysarthria, mild dysphagia for liquids, mild cognitive impairment, urinary urgency, periventricular WM hyperintensities. Latest SPRS score (28 yrs): 19.5/52	F, 28	17	26	9
10	c.3122_3124del / c.5014G>T	p.Arg1041del / p.Glu1672Ter	Spastic gait requiring the use of double crutches; mild dysarthria, mild cognitive impairment, urinary urgency. Latest SPRS score (30 yrs): 23/52	F, 30	24	28	4
11	c.2849dup / c.1602+1G>A	p.Leu950PhefsTer4	Spastic paraplegia, wheelchair-bound, dysarthria, mild cognitive impairment, urge incontinence, mild dysphagia. Latest SPRS score (42 yrs): 40.5/52	M, 43	23	42	19
12	c.4604dup / c.5989_5992del	p.Leu1536SerfsTer10 / p.Leu1997MetfsTer60	Spastic paraplegia, wheelchair-bound, dysarthria, mild cognitive impairment, urge incontinence, mild dysphagia, CC atrophy. Latest SPRS score (34 yrs): 40/52	F, 34	21	32	11
13 *	c.2301del / c.6739_6742del	p.Asn767LysTer10 / p.Glu2247LeufsTer14	Spastic gait requiring the use of a cane; mild dysarthria, urinary urgency, periventricular WM hyperintensities and CC atrophy, PNP. Latest SPRS score (20 yrs): 21/52	F, 20	14	19	6
14 *	c.1203del / c.4307_4308del	p.Asp402IlefsTer14 / p.Gln1436ArgfsTer7	Spastic gait requiring the use of a walker; mild cognitive impairment, WM hyperintensities and CC atrophy. Latest SPRS score (23 yrs): 23/52	F, 23	11	22	12
15 *	c.5623C>T / c.5623C>T	p.Gln1875Ter / p.Gln1875Ter	Spastic paraparesis; mild cognitive impairment and mood disorders, rare urinary urgency, WM hyperintensities and CC atrophy. Latest SPRS score (16 yrs): 13.5/52	M, 16	14	15	1
16 *	c.6331dup / c.6331dup	p.Glu2111GlyfsTer38 / p.Glu2111GlyfsTer38	Spastic gait requiring the use of a walker, dysarthria, mild cognitive impairment, mood disorders, urge incontinence, WM hyperintensities and CC atrophy, PNP. Latest	M, 24	14	24	10

PATIENT	GENOTYPE	PROTEIN CHANGE	CLINICAL CHARACTERISTICS	GENDER, AGE	AGE AT ONSET (HSP)	AGE OF BIOPSY	DURATION OF DISEASE
			SPRS score (24 yrs): 22/52				
17 *	c.5014G>T / c.5757_5758del	p.Glu1672Ter / p.Glu1921SerfsTer2	Spastic gait requiring the use of double crutches; mild dysarthria, urinary urgency, mild cognitive impairment, periventricular WM hyperintensities. Latest SPRS score (38 yrs): 23.5/52	M, 38	30	38	8
18 *	c.1735+3_1735+6del / c.1735+3_1735+6del	Skipping exon 8	Spastic gait; mild dysarthria, mild cognitive impairment, urinary urgency, periventricular WM hyperintensities. Latest SPRS score (22 yrs): 17/52	M, 22	12	21	9
19	c.1735+3_1735+6del / c.1735+3_1735+6del	Skipping exon 8	Mild spasticity and mild cognitive impairment, urinary urgency. Latest SPRS score (15 yrs): 6/52	F, 15	14	15	1
20 *	c.3662_3665del / c.6196del	p.Ile1221ArgfsTer8 / p.Gln2066ArgfsTer210	Spastic gait; mild dysarthria, mild cognitive impairment. Latest SPRS score (27 yrs): 15/52	M, 27	23	26	3
21 *	c.6898_6899del	p.Leu2300AlafsTer39	Spastic gait requiring the use of a walker; mild cognitive impairment, dysarthria, WM hyperintensities and CC atrophy. Latest SPRS score (24 yrs): 25/52	F, 24	15	-	9
22	c.6754+2_6754+3dup / c.6739_6742del	p.Glu2247LeufsTer14	Mild spastic gait; borderline intellectual functioning and mood disorders, mild dysphagia, urinary urgency, WM hyperintensities and CC atrophy. Latest SPRS score (16 yrs): 11/52	F,16	13	-	7

We also studied PBMC from some of the carrier parents of the *SPG11* patients (**Table 2**).

Table 2. Description of the genotype with relative protein change of some parents of the *SPG11* patients.

PARENT	GENOTYPE	PROTEIN CHANGE
Carrier-Pt2 ♂	wt / [c.6175C>T; c.6331dup]	wt / [p.Arg2059Trp; p.Glu2111GlyfsTer38]
Carrier-Pt2 ♀	wt / c.5986dup	wt / p.Cys1196LeufsTer4
Carrier-Pt9&10 ♀	wt / c.3122_3124del	wt / p.Arg1041del
Carrier-Pt13 ♂	wt / c.2301del	wt / p.Asn767LysTer10
Carrier-Pt13 ♀	wt / c.6739_6742del	wt / p.Glu2247LeufsTer14
Carrier-Pt15 ♂	wt / c.5623C>T	wt / p.Gln1875Ter

PARENT	GENOTYPE	PROTEIN CHANGE
Carrier-Pt15 ♀	wt / c.5623C>T	wt / p.Gln1875Ter
Carrier-Pt20 ♂	wt / c.3662_3665del	wt / p.Ile1221ArgfsTer8
Carrier-Pt20 ♀	wt / c.6196del	wt / p.Gln2066ArgfsTer21
Carrier-Pt21 ♀	wt / c.6898_6899del	wt / p.Leu2300AlafsTer39

The 22 *SPG11* patients are grouped in 19 families described in the pedigrees of **Figure 10**.
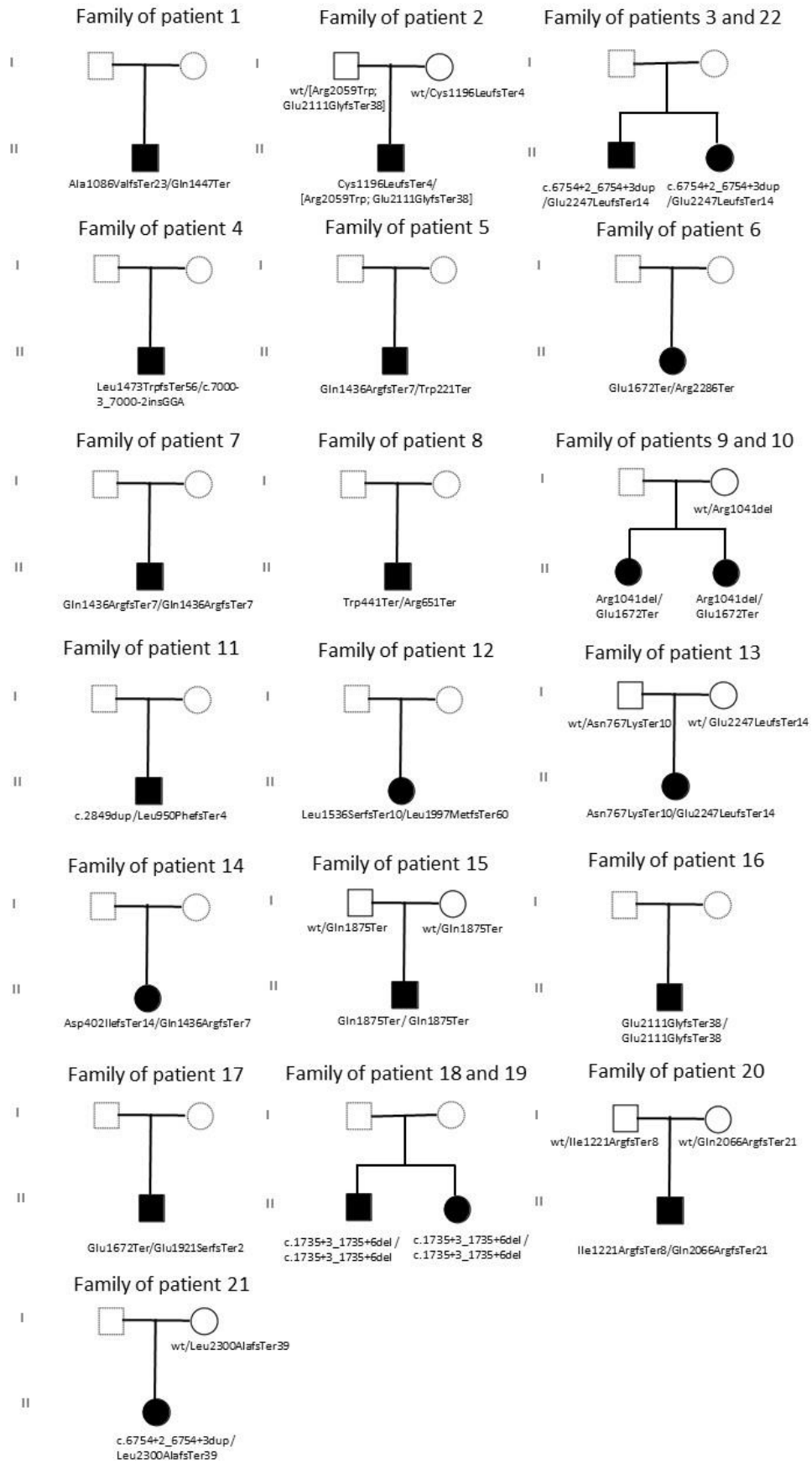
Figure 10. Pedigrees of the 22 SPG11 patients.

The analysis of mutations in *SPG11* patients showed an altered protein in 92.86% of cases, whose 53.57% are frameshift, 25% nonsense and 14.29% splice mutations. Seven % of the mutations were in-frame and missense mutations in combination (**Figure 11**).
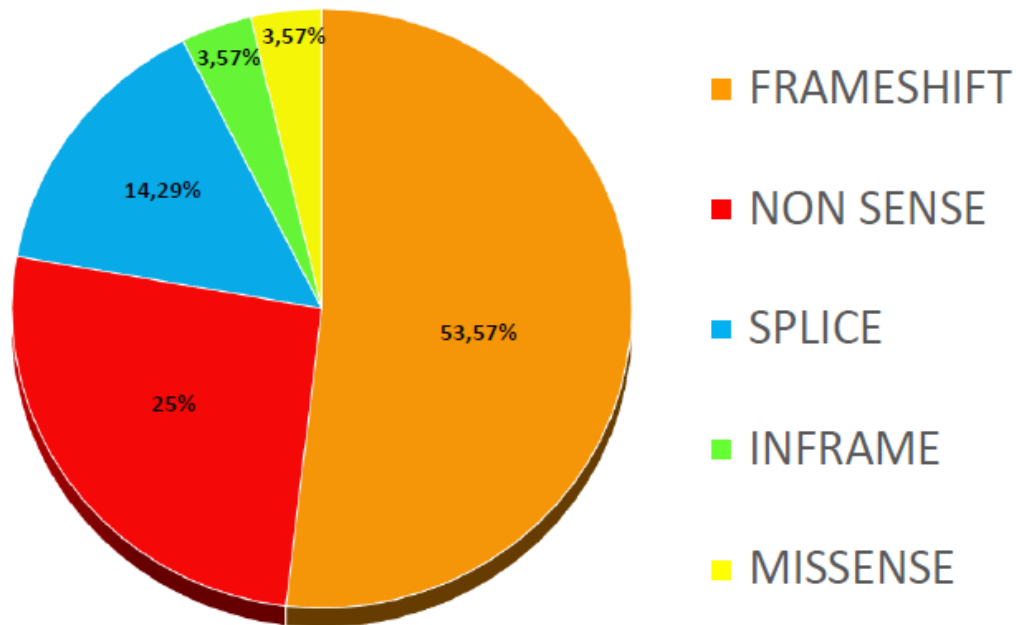
Figure 11. Classifications of mutations (%) in *SPG11* patients.

Although the genetic heterogeneity was high, *SPG11* mRNA was reduced in all patients (**Figure 12A-B**). Immunoblot analysis of SPATACSIN showed an undetectable protein in all patients compared to controls (**Figure 12C**), while its interacting proteins, SPASTIZIN and AP5Z1 showed invariable and reduced levels respectively (**Figure 12D-E**).
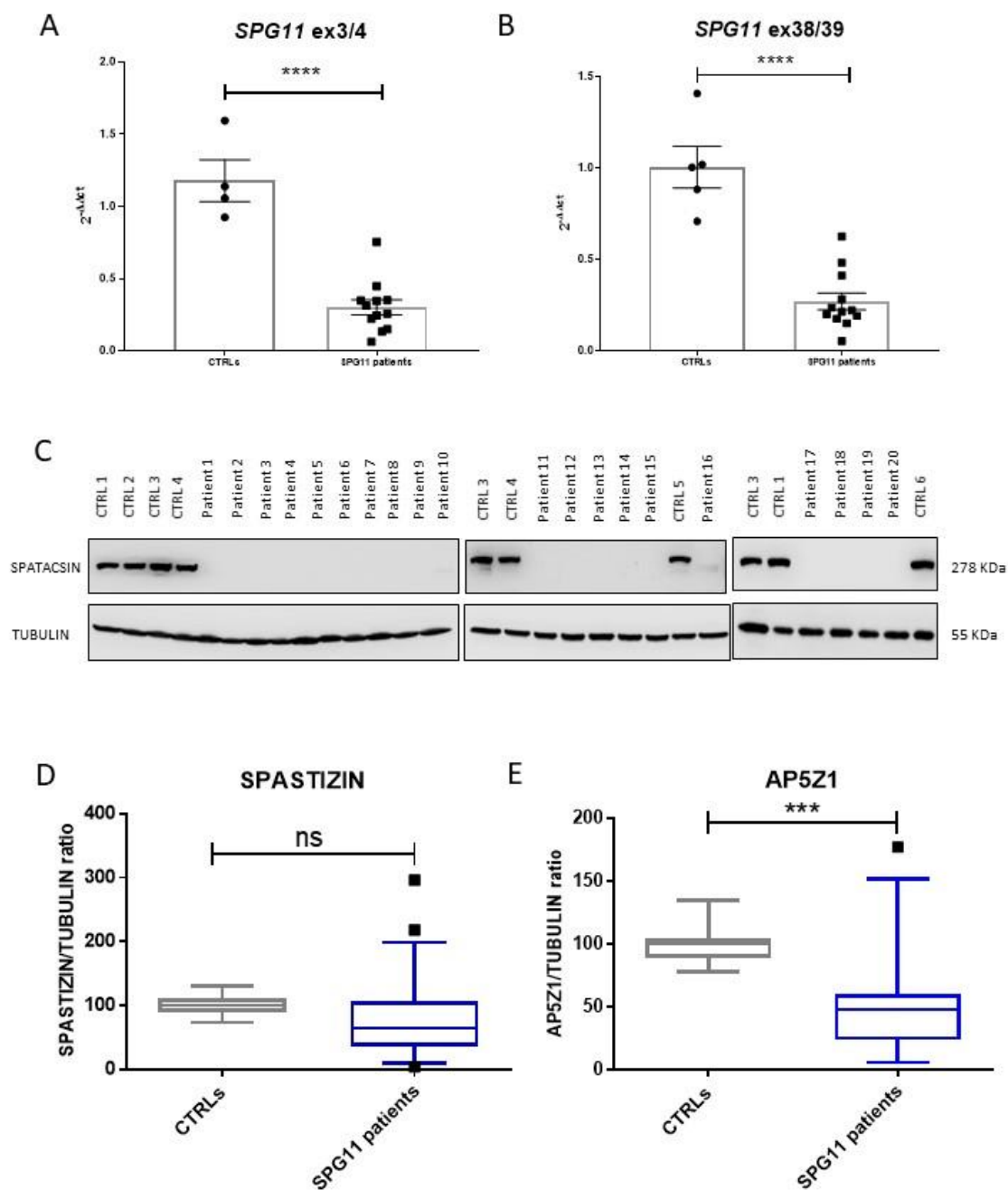
Figure 12. A-B *SPG11* mRNA quantification through qRT-PCR showed a reduced expression in patients skin fibroblasts. mRNA levels were measured with two couple of primers binding the beginning (exons 3/4) or the end of the transcript (exons 38/39). **C-D-E** Immunoblot analysis of SPATACSIN and its interacting proteins (SPASTIZIN and AP5Z1) in skin fibroblasts from patients and control individuals. SPATACSIN protein results undetectable in all patients (**C**), while SPASTIZIN and AP5Z1 showed invariable (**D**) and reduced (**E**) level proteins respectively considering SPG11 patients together compared to controls.

The availability of the blood samples of patients and of their parents permitted us to test SPATACSIN antibody in PBMC. The protein was undetectable in patients compared to controls, whereas carrier parents showed an overall decreased amount level (**Figure 13**).
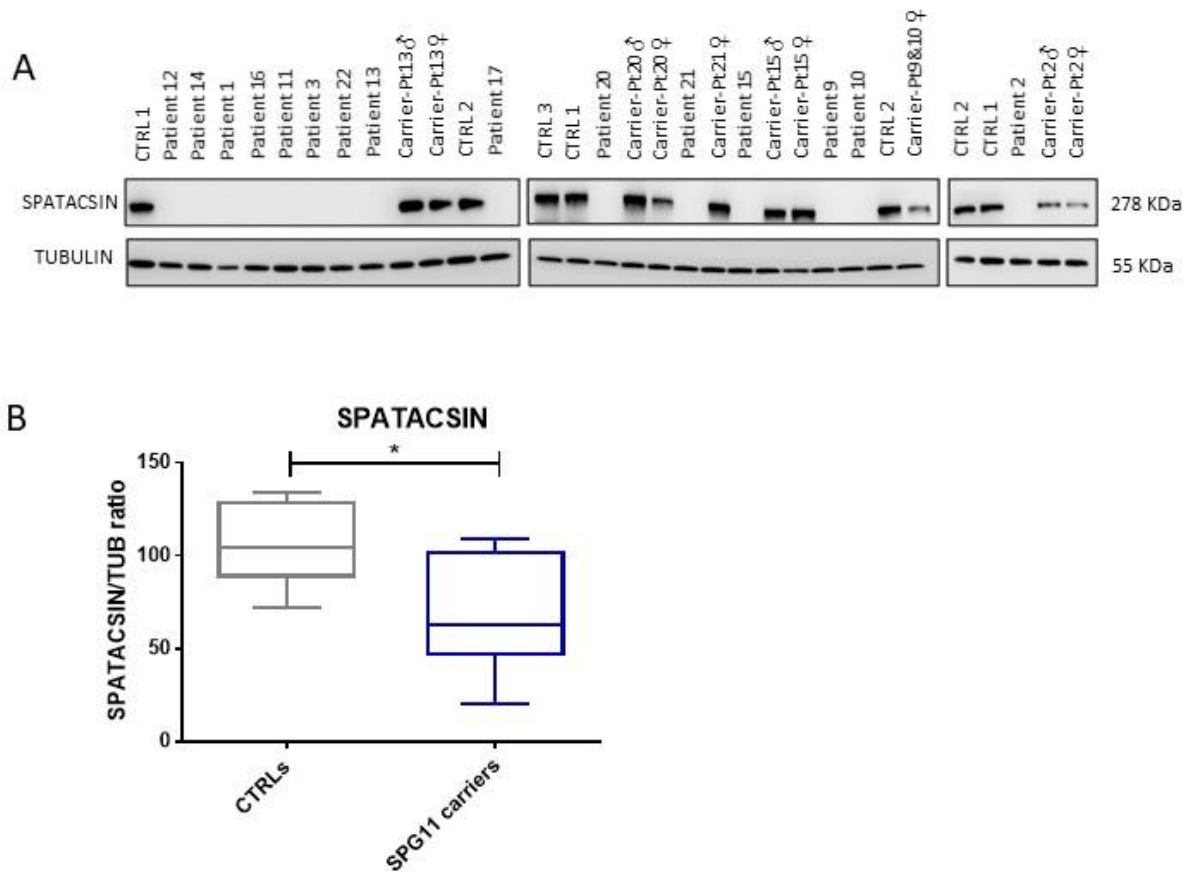
Figure 13. Immunoblot analysis of SPATACSIN on PBMC of SPG11 patients and their parents. **A** SPATACSIN level is undetectable in subjects with two mutations in *SPG11* gene while protein is detected in controls and parents who are carriers of none or one mutation respectively. ♂ and ♀ denote the father and the mother respectively of the patients. **B** Quantification of SPATACSIN level in carriers showed an overall protein reduction.

4.2 Study of oxidative metabolism

The study of the role of SPATACSIN in oxidative metabolism through micro-oxygraphy analysis showed an impaired oxygen consumption rates (OCRs) with a common reduced maximal respiration, spare respiratory capacity (SRC) and proton leak in SPG11 patients compared to controls (**Figure 14**).
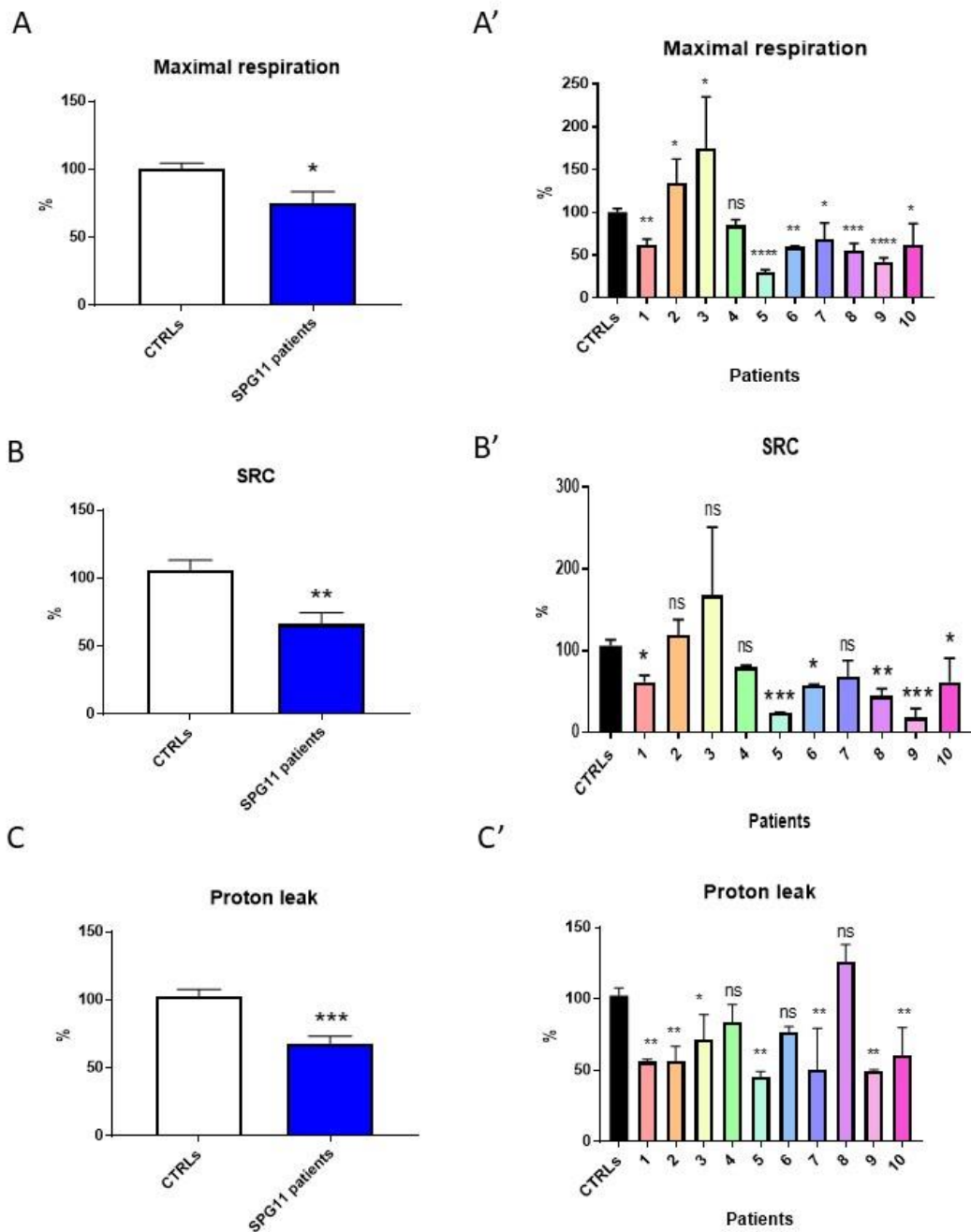
Figure 14. Oxygen consumption rates (OCRs) measured using a Seahorse XF analysed of 10 SPG11 patients compared to controls. Measurements of basal respiration, SRC and proton leak showed a total reduced levels analysing patients together **A-B-C**; and separately **A'-B'-C'**.

An abnormal OCR suggest the presence of mitochondrial dysfunction; hence we investigated the oxidative metabolism in patients' fibroblasts more in detail. We measured ROS levels and we found an increased production in SPG11 patients compared to controls (**Figure 15A-A'**). Therefore, we investigated the mRNA level of the master regulator of anti-oxidative responses *NRF2* and of its regulator *TFEB* and we observed not altered levels in SPG11 patients (data not

showed). To assess a possible post-transcriptional regulation of NRF2, we measured NRF2 protein level through western blot and we notified a global stable concentration of protein in SPG11 patients with a trend toward reduction (**Figure 15B**). Single patient analysis, indeed, showed a decreased NRF2 protein level in some patients compared to controls (**Figure 15B'**).
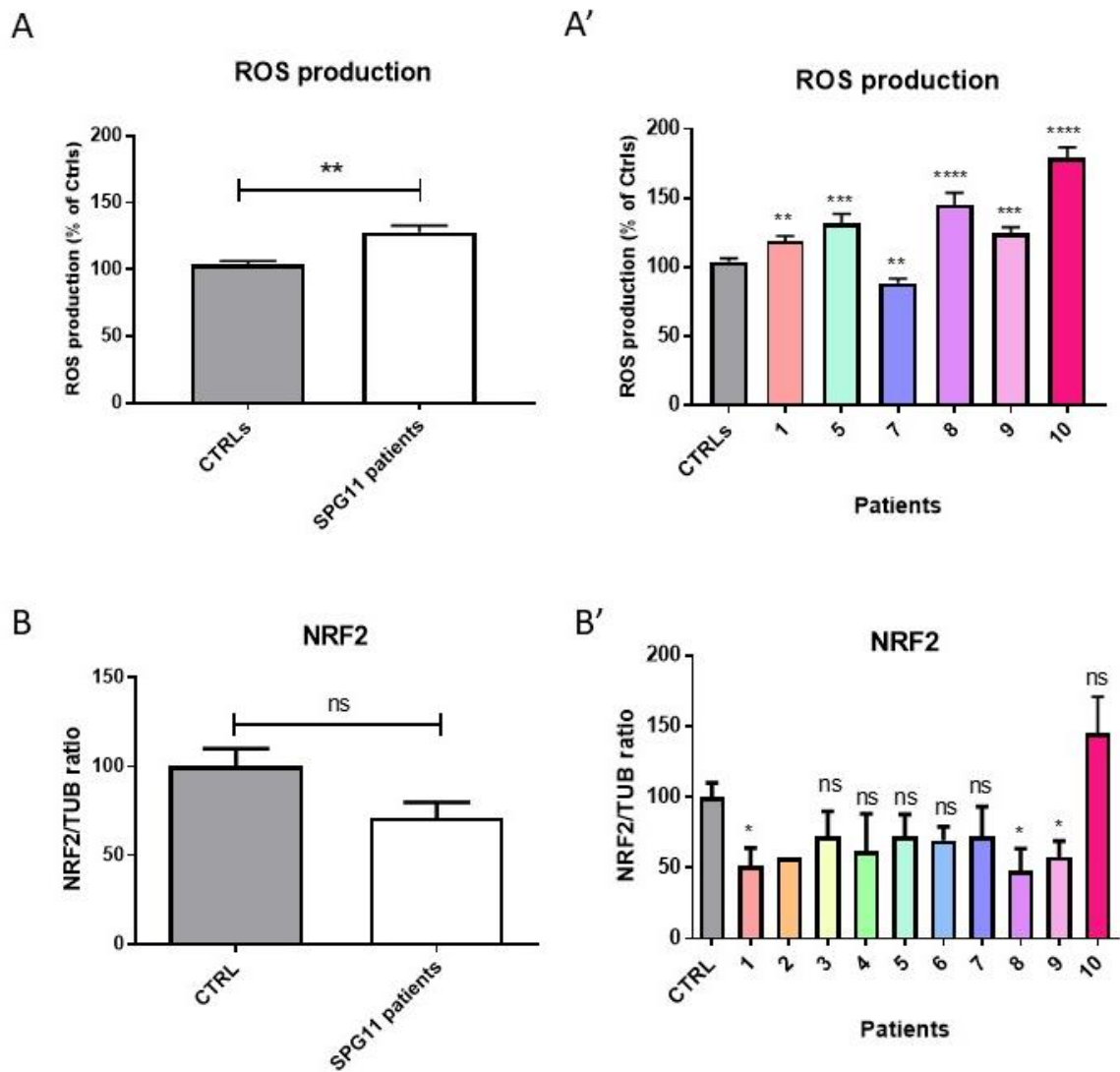
Figure 15. Study of oxidative metabolism in patients skin fibroblasts. **A-A'** Reactive oxygen species (ROS) measurements showed an increased production in SPG11 patients compared to controls. **B-B'** Immunoblot analysis of NRF2 protein showed regular levels in SPG11 patients with a trend toward reduction; while patients' single analysis showed variable level of NRF2 with a reduced NRF2 protein in some of them.

To investigate how impaired cellular respiration related to SPATACSIN deficiency impacts on mitochondrial structure, we investigate mitochondrial network through immunofluorescence of the translocase of outer mitochondrial membrane 20 (TOM20) (**Figure 16A**). The quantification of mitochondrial shape revealed an impaired network of mitochondria in SPG11 patient with a

more fragmented reticulum in basal condition (NT) (**Figure 16B**) whereas no differences were noted after 2 h of recover from the uncoupler FCCP treatment (FCCP-2h-RE).
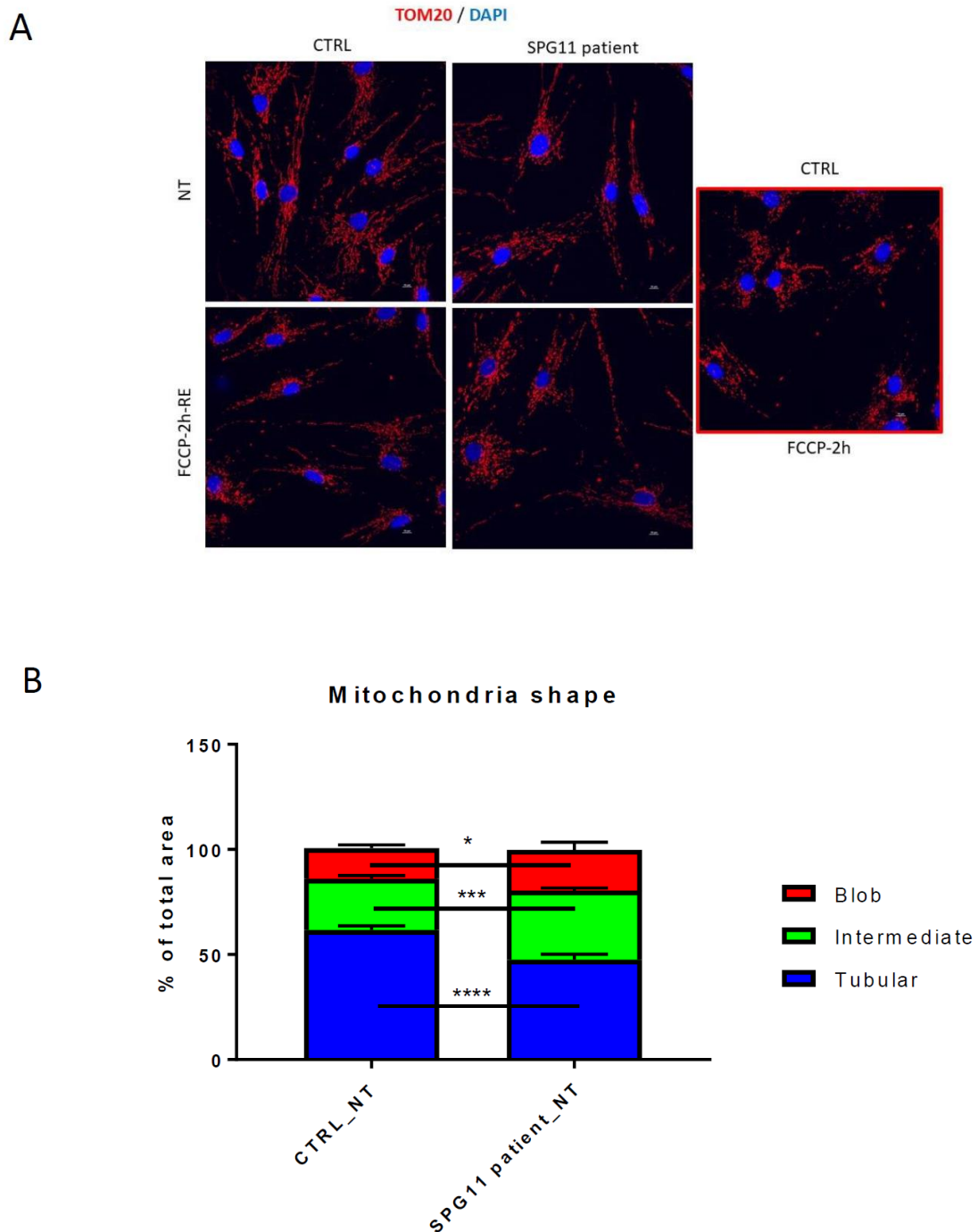
Figure 16. Mitochondrial network organization in SPG11 fibroblasts and control (CTRL). **A** Immunofluorescence staining of TOM20 (red) in basal condition (NT) and after 2 hours of recovery from FCCP treatment. DAPI (blue) labelled nuclei. **B** Mitochondria shape quantification in basal condition showed a more fragmented mitochondrial network in SPG11 patients.

4.3 Multi-omics analysis

4.3.1 Proteomic

A total of 503 proteins were identified by using the spectral library generated and excluding FDR >1%. Among the 421 quantified proteins (**Table S2**), 56 were significant (adj. p-value < 0.05) and differentially expressed (FC ≤ 1/1.5 or FC ≥1.5) when comparing P_NT with C_NT. Of the 56 proteins, 44 were down-regulated and 11 up-regulated in skin fibroblasts (**Figure 17;** listed in **Table 3)**.
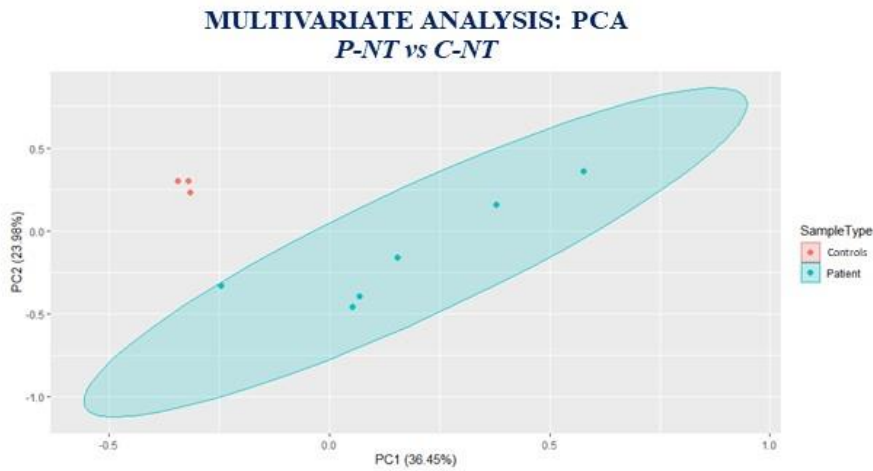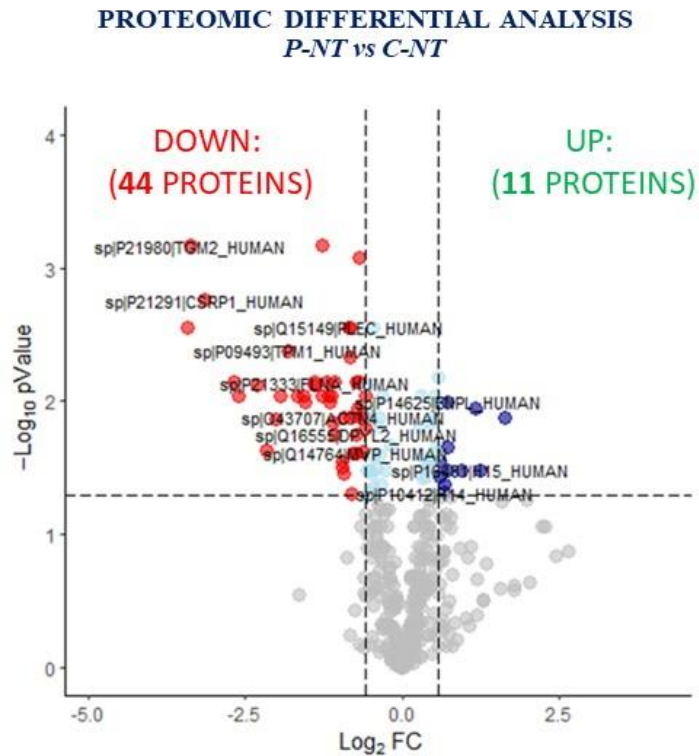
Figure 17. Proteomic analysis in SPG11 patients' fibroblasts compared to controls **A** PCA showed a clear separation between SPG11 patients (light blue) and controls (red). **B** Volcano plot of proteome profile in SPG11 patients fibroblasts for the contrast P_NT vs C_NT. Significant and differentially expressed proteins (thresholds: adj. p-value < 0.05, FC ≤ 1/1.5 or FC ≥1.5) are coloured in blue (up-regulated) and red (down-regulated). Proteins with adj. p-value < 0.05 but not differentially expressed (1/1.5 < FC < 1.5) are in light blue while not significant proteins (p-value ≥ 0.05) in grey.

Table 3. List of the significant and differentially expressed proteins (thresholds: adj. *p*-value < 0.05, FC ≤ 1/1.5 or FC ≥1.5) in the contrast P_NT vs C_NT.

	DOWN (45) Gene ID	UniProtKB/Swiss-Prot code	UP (11) Gene ID	UniProtKB/Swiss-Prot code
1	FLNA	P21333	RCN3	Q96D15
2	MYH9	P35579	ENPL	P14625
3	PLEC	Q15149	AMPN	P15144
4	ACTN1	P12814	H14	P10412
5	VINC	P18206	H32	Q71DI3
6	ACTN4	O43707	H15	P16401
7	CALD1	Q05682	CO6A2	P12110
8	TAGL	Q01995	PGRC1	O00264
9	MYOF	Q9NZM1	CO6A1	P12109
10	GELS	P06396	COTL1	Q14019
11	TPM1	P09493	XRCC5	P13010
12	DPYL2	Q16555		
13	MVP	Q14764		
14	PRDX6	P30041		
15	HSPB1	P04792		
16	ACTA	P62736		
17	WDR1	O75083		
18	STAT1	P42224		
19	MYL6	P60660		
20	TGM2	P21980		
21	S10AB	P31949		
22	PDLI7	Q9NR12		
23	ML12A	P19105		
24	CAP1	Q01518		
25	CSRP1	P21291		

	DOWN (45) Gene ID	UniProtKB/Swiss-Prot code	UP (11) Gene ID	UniProtKB/Swiss-Prot code
26	GARS	P41250		
27	SERC	Q9Y617		
28	LASP1	Q14847		
29	THY1	P04216		
30	DEST	P60981		
31	ZYX	Q15942		
32	MYLK	Q15746		
33	MAP1B	P46821		
34	TBB2A	Q13885		
35	MYL9	P24844		
36	GBG12	Q9UBI6		
37	SYEP	P07814		
38	CNN1	P51911		
39	SRC8	Q14247		
40	SPRC	P09486		
41	KAD1	P00568		
42	CLCB	P09497		
43	MFGM	Q08431		
44	ITIH3	Q06033		
45	KCY	P30085		

Functional analysis through ViSEAGO revealed the following dysregulated pathways: cell-junction organization, blood coagulation and response to wounding, cell muscle components morphogenesis and muscle contraction and actin filament based movement and actin cytoskeleton organization.

4.3.2 Lipidomic

Targeted lipidomic analysis through SRM method permitted to detect 4 categories of lipids sub-divided in different classes and subclasses with a total of 201 transition revealed (**Table 4**).

Table 4. List of categories with classes/subclasses and transitions analyzed through targeted MS/MS (SRM) analysis.

Categories	Classes/Subclasses	Transitions
Glycerolipids (GL)	Diacylglycerols (DG)	22
	Triacylglycerols (TG)	37
Glycerophospholipids (GP)	Phosphatidylcholines (PC)	23
	Lysophosphatidylcholines (LPC)	12
	Phosphatidylethanolamines (PE)	23
	Lysophosphatidylethanolamines (LPE)	6
Sphingolipids (SP)	Ceramides (Cer)	15
	Sphingomyelins (SM)	24
	Gangliosides (GM2, GM3)	16
Sterol lipids (ST)	Cholesteryl esters (CE)	23

TOT = 201

Lipidr analysis allowed to identify 137 lipid species (**Table S3**). Comparing SPG11 fibroblasts with healthy controls showed a set of differentially expressed lipids (**Figure 18A**); 16 lipids resulted down-regulated and 27 up-regulated in patients (**Figure 18B**; **Table 5)**. We observed overall up-regulation of DG and LPC, whereas GM3 resulted down-regulated (**Figure 18C**).

A

MULTIVARIATE ANALYSIS: PCA
P-NT vs C-NT
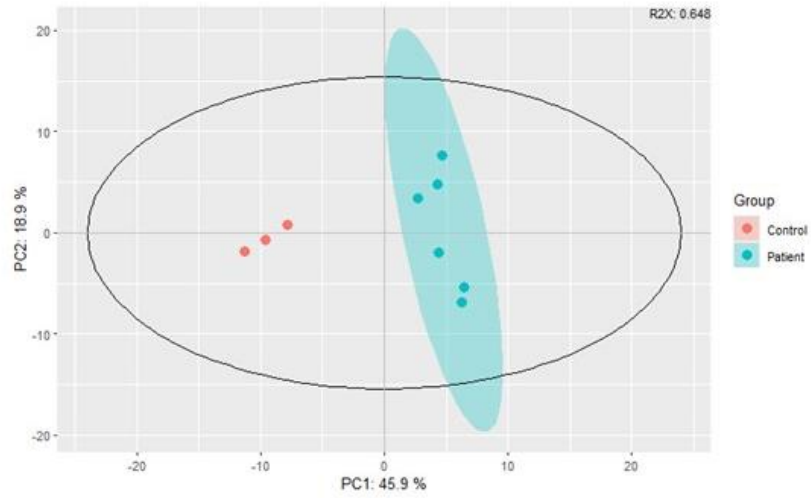
B

LIPIDOMICS DIFFERENTIAL ANALYSIS
P-NT vs C-NT

C
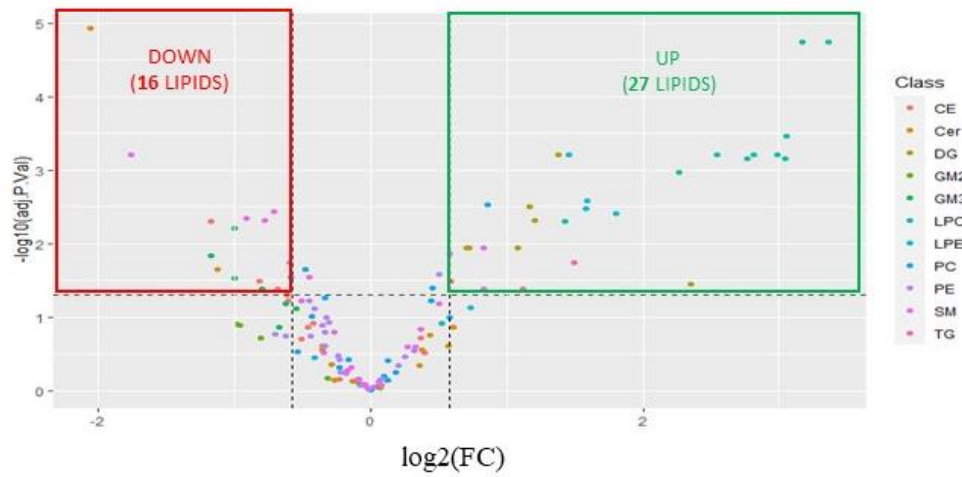
LIPID SET ENRICHMENT ANALYSIS
P-NT vs C-NT

47
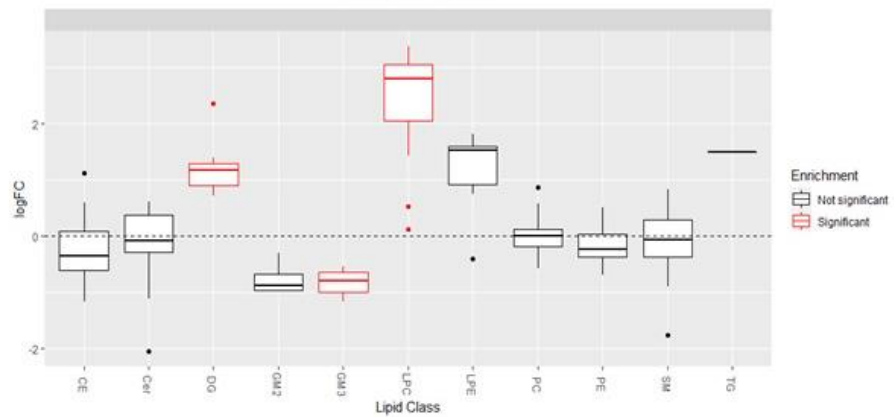
Figure 18. Lipidomic analysis in SPG11 fibroblasts compared to controls (P-NT vs C-NT). **A** PCA showed a clear separation between patients (light blue) and controls (red). **B** Volcano plot showed a pattern of dysregulated lipids in SPG11 fibroblasts. **C** Lipid set enrichment analysis showed the overall status of lipid classes.

Table 5. List of the significant and differentially altered lipid species (thresholds: adj. p-value < 0.05, FC ≤ 1/1.5 or FC ≥1.5) comparing P_NT and C_NT.

	P-NT vs C-NT	
	UP (27)	**DOWN (16)**
1	CE(20:2)	CE(16:0)
2	CE(22:4)	CE(16:2)
3	DG(34:1)	CE(18:2)
4	DG(36:0)	CE(18:3)
5	DG(36:1)	Cer(d18:2/22:0)
6	DG(38:5)	Cer(d18:2/23:1)
7	DG(38:6)	GM3(d18:1/16:0)
8	DG(40:6)	GM3(d18:1/18:0)
9	DG(40:7)	GM3(d18:1/24:0)
10	LPC(16:0)	GM3(d18:1/26:0)
11	LPC(16:0e)	PC(34:3)
12	LPC(16:1)	PE(36:3)
13	LPC(18:0e)	SM(32:2)
14	LPC(18:1)	SM(36:2)
15	LPC(18:2)	SM(36:3)
16	LPC(20:3)	SM(38:3)
17	LPC(20:4)	
18	LPC(22:5)	
19	LPC(22:6)	
20	LPE(16:0)	
21	LPE(18:0)	
22	LPE(18:1)	
23	LPE(18:2)	
24	PC(40:2)	
25	SM(43:1)	
26	SM(43:2)	

	P-NT vs C-NT	
	UP (27)	DOWN (16)
27	TG(56:6)	

4.4 Drugs studies

The therapy in HSP patients is symptomatic but palliative care cannot prevent progressive CNS deterioration. Hence, with the idea to find efficient drugs to ameliorate SPG11 disease progression, we "repositioned" two drugs already used in others neurodegenerative diseases: *ataluren* and *miglustat*.

4.4.1 Ataluren

In a patient harboring mutations in *SPG11* leading to stop codon (and presenting the two best termination codons recognized by ataluren, namely UGA and UAG), we measured mRNA levels in the following conditions: (i) baseline, ((ii) in the presence of 10 mM of caffeine, (iii) in the presence of 40 μM of *ataluren*, and (iv) combination of caffeine and *ataluren* (**Figure 19**). We did not observe a significant effect of the drug, either alone or in combination.
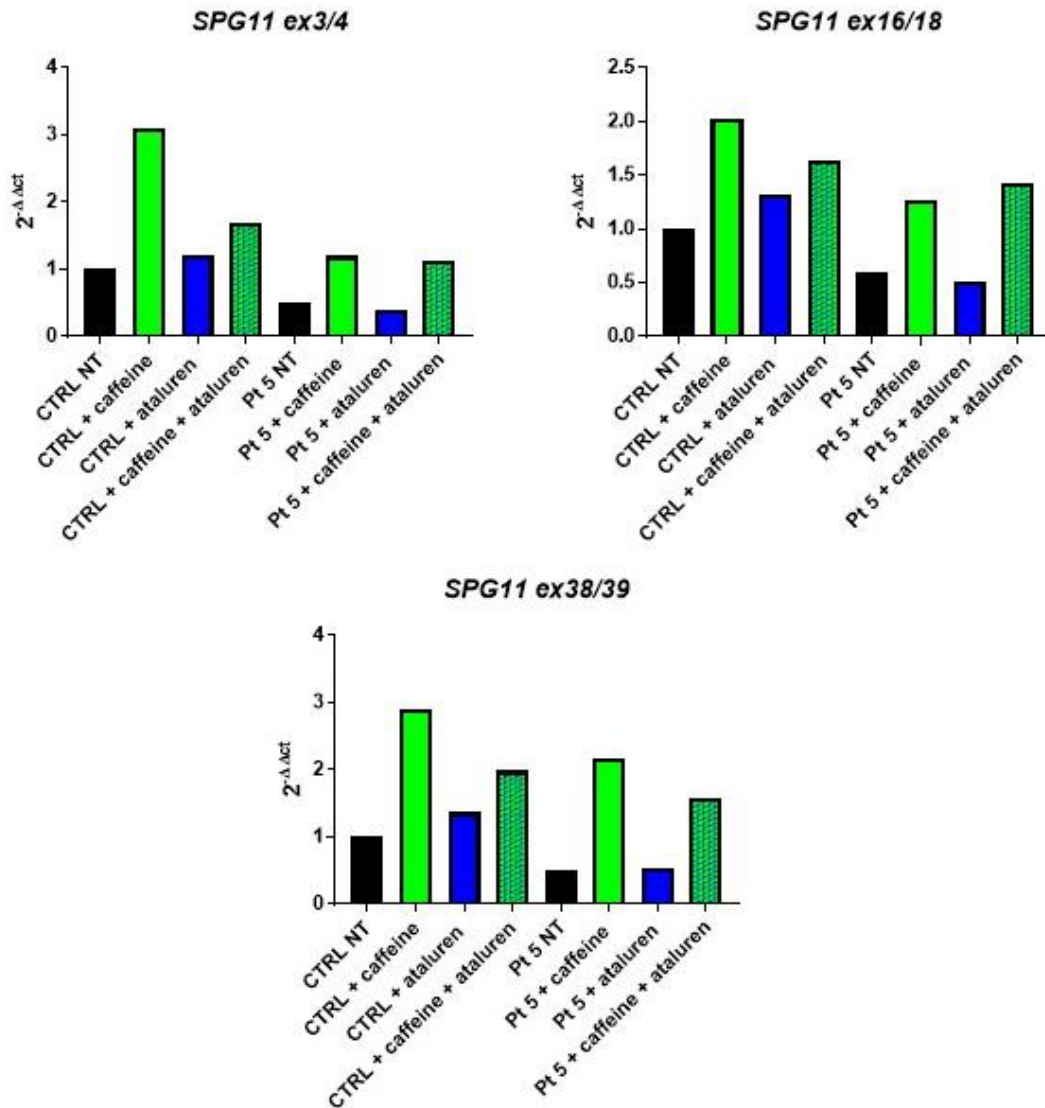
Figure 19. Quantitative Real Time PCR of SPG11 patient and control treated with caffeine 10mM, ataluren 40 μM and with combination of caffeine and ataluren. *SPG11* mRNA level were measured with 3 pairs of primers (ex3/4, ex16/18 and ex38/39) to analyze the full length of mRNA composed by 40 exons.

4.4.2 Miglustat

The pharmacological treatment with *miglustat* in SPG11 has been studied on several grounds. In skin fibroblasts, *miglustat* did not have impact on SPATACSIN mRNA and protein levels (preliminary data, not shown).

4.4.2.1 Study of oxidative stress

Miglustat did not improve the oxidative metabolism in SPG11 fibroblasts with ROS overproduction and mitochondrial network being unmodified as well as the steady state levels of NRF2 protein (**Figure 20**).
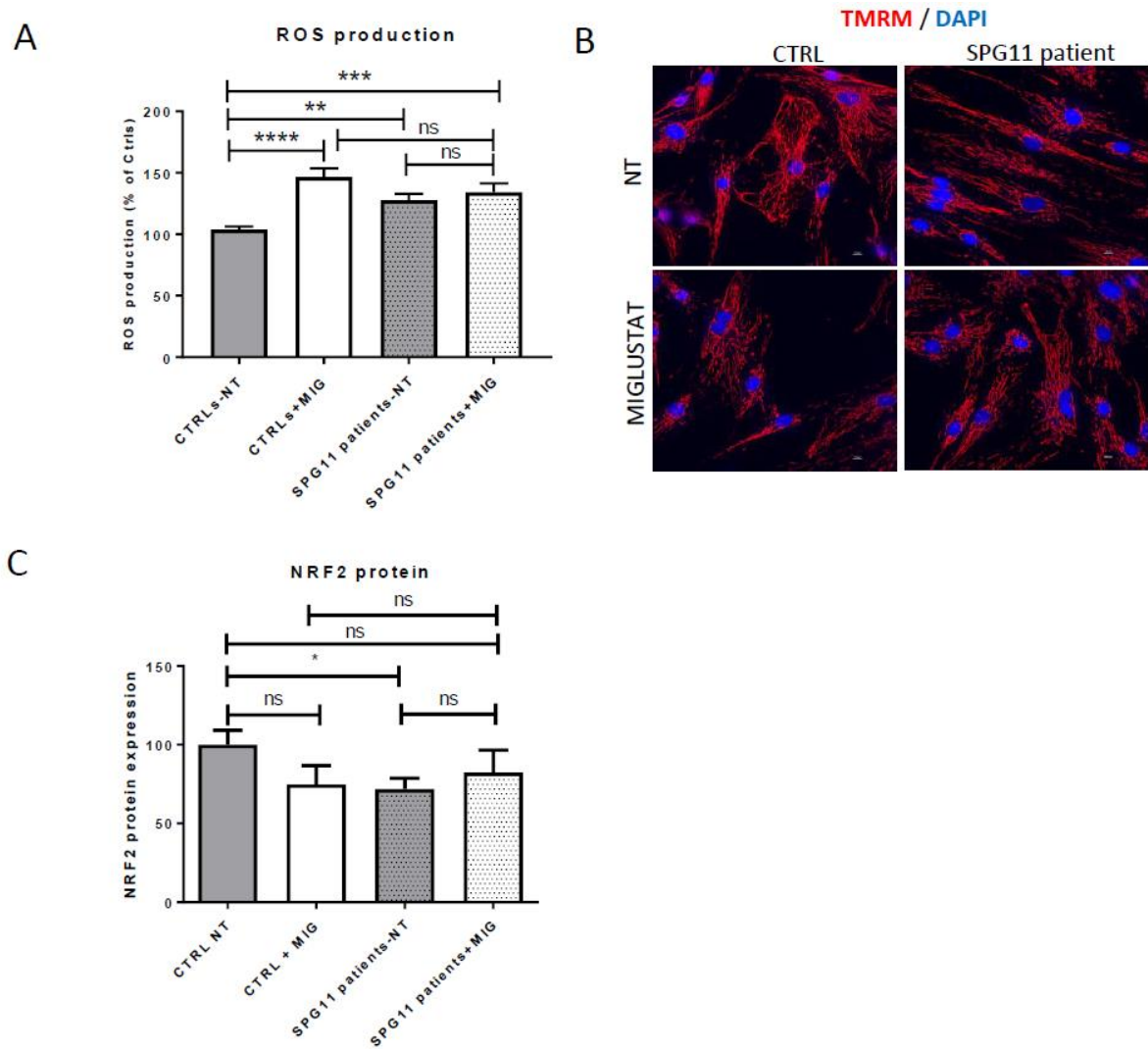
Figure 20. Study of the effect of *miglustat* on oxidative metabolism. **A** ROS production in SPG11 patients was not modified by *miglustat* treatment. **B** Immunofluorescence analysis of mitochondrial network through TMRM probe showed that *miglustat* did not influence mitochondrial composition. **C** Immunoblot of NRF2 showed no differences between fibroblasts of SPG11 patients-NT (untreated) and of SPG11 patients treated with *miglustat*.

4.4.2.2 Multi-omics analysis

4.4.2.2.1 Proteomic

Proteomic analysis on fibroblasts treated with *miglustat* showed 77 proteins differentially expressed comparing P_T with C_NT. Of these, 57 were down-regulated and 20 up-regulated (see **Table 6**).

Table 6. List of the significant and differentially expressed proteins (thresholds: adj. *p*-value < 0.05, FC ≤ 1/1.5 or FC ≥1.5) in the contrast P_T vs C_NT.

	DOWN (57) Gene ID	UniProtKB/Swiss-Prot code	UP (20) Gene ID	UniProtKB/Swiss-Prot code
1	CSRP1	P21291	ROAA	Q99729
2	CNN1	P51911	HNRPD	Q14103
3	TGM2	P21980	H32	Q71DI3
4	ACTA	P62736	STMN1	P16949
5	TAGL	Q01995	HNRPU	Q00839
6	MYLK	Q15746	PDIA4	P13667
7	MFGM	Q08431	BIP	P11021
8	MYL9	P24844	RCN3	Q96D15
9	HSPB1	P04792	PDIA6	Q15084
10	CALD1	Q05682	CO6A2	P12110
11	PDLI7	Q9NR12	COTL1	Q14019
12	TPM1	P09493	PDIA3	P30101
13	STAT1	P42224	H14	P10412
14	FLNA	P21333	VASN	Q6EMK4
15	GELS	P06396	PGRC1	O00264
16	LMCD1	Q9NZU5	ENPL	P14625
17	MYH9	P35579	CALR	P27797
18	SERC	Q9Y617	H15	P16401
19	MYL6	P60660	AMPN	P15144
20	ACTN1	P12814	HBA	P69905
21	TBB2A	Q13885		
22	SRC8	Q14247		
23	ML12A	P19105		
24	DEST	P60981		
25	MYOF	Q9NZM1		
26	LASP1	Q14847		
27	ACTN4	O43707		
28	PLEC	Q15149		
29	VINC	P18206		
30	SPRC	P09486		
31	PRDX6	P30041		
32	GBG12	Q9UBI6		
33	MVP	Q14764		

	DOWN (57) Gene ID	UniProtKB/Swiss-Prot code	UP (20) Gene ID	UniProtKB/Swiss-Prot code
34	ZYX	Q15942		
35	SH3L1	O75368		
36	HLAA	P04439		
37	G6PI	P06744		
38	DPYL2	Q16555		
39	FLNC	Q14315		
40	CLCB	P09497		
41	WDR1	O75083		
42	KCY	P30085		
43	MAP1B	P46821		
44	TPM4	P67936		
45	KAD1	P00568		
46	S10AB	P31949		
47	CAP1	Q01518		
48	PFKAP	Q01813		
49	APT	P07741		
50	NIBA2	Q96TA1		
51	SEPT9	Q9UHD8		
52	TLN1	Q9Y490		
53	ARPC5	O15511		
54	LAMP1	P11279		
55	SEPT2	Q15019		
56	PROF1	P07737		
57	GARS	P41250		

Using ViSEAGO, the 77 dysregulated proteins were grouped in 16 clusters, some specifically dysregulated only in untreated or treated group, others dysregulated in both groups and some others differentially modulated among groups (**Figure 21**).
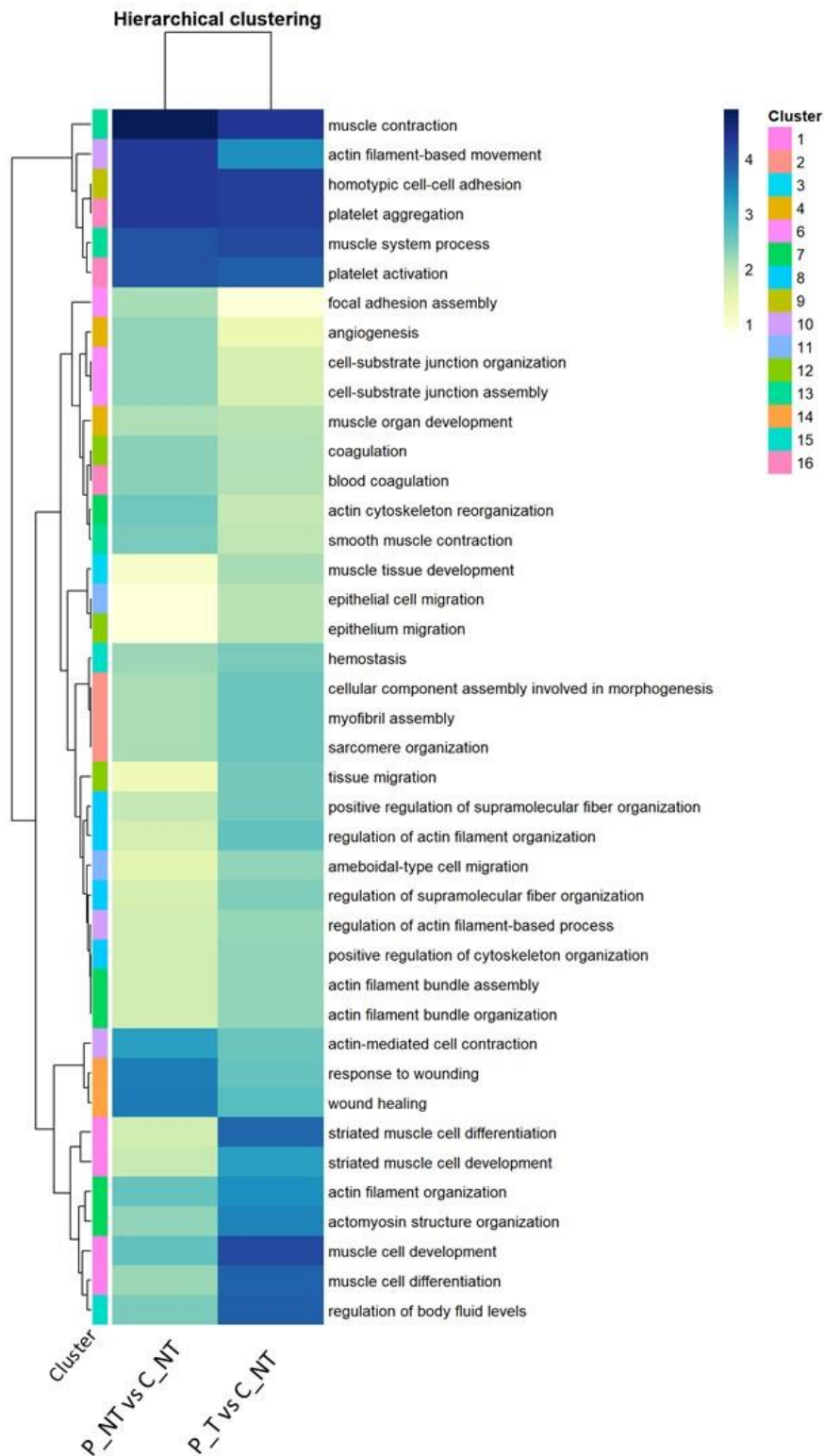
Figure 21. Heatmap of the functional analysis through ViSEAGO showed the difference of dysregulated pathways comparing P_T and P_NT with C_NT. On the right are listed the 16 clusters highlighted and on the left the level of dysregulation is showed through colors range from white to blue as showed in the key.

It is of note that *miglustat* had impact on pathways related to muscle contraction, actin filament-based movement and action cytoskeleton organization, and the response to wounding.

4.4.2.2.2 Lipidomic

The effect of the *miglustat* was also evaluated on the lipidome of patients and controls fibroblasts, and a modulation of GM3 lipid species was observed in patients as in controls (**Figure 22A**). Lipidomic differential analysis of P-T compared to C-NT showed 17 lipids down-regulated and 36 up-regulated (**Figure 22B**), listed in **Table 7**. Regarding lipid classes, we observed that LPC were up-regulated, whereas GM2 and GM3 down-regulated (**Figure 22C**).
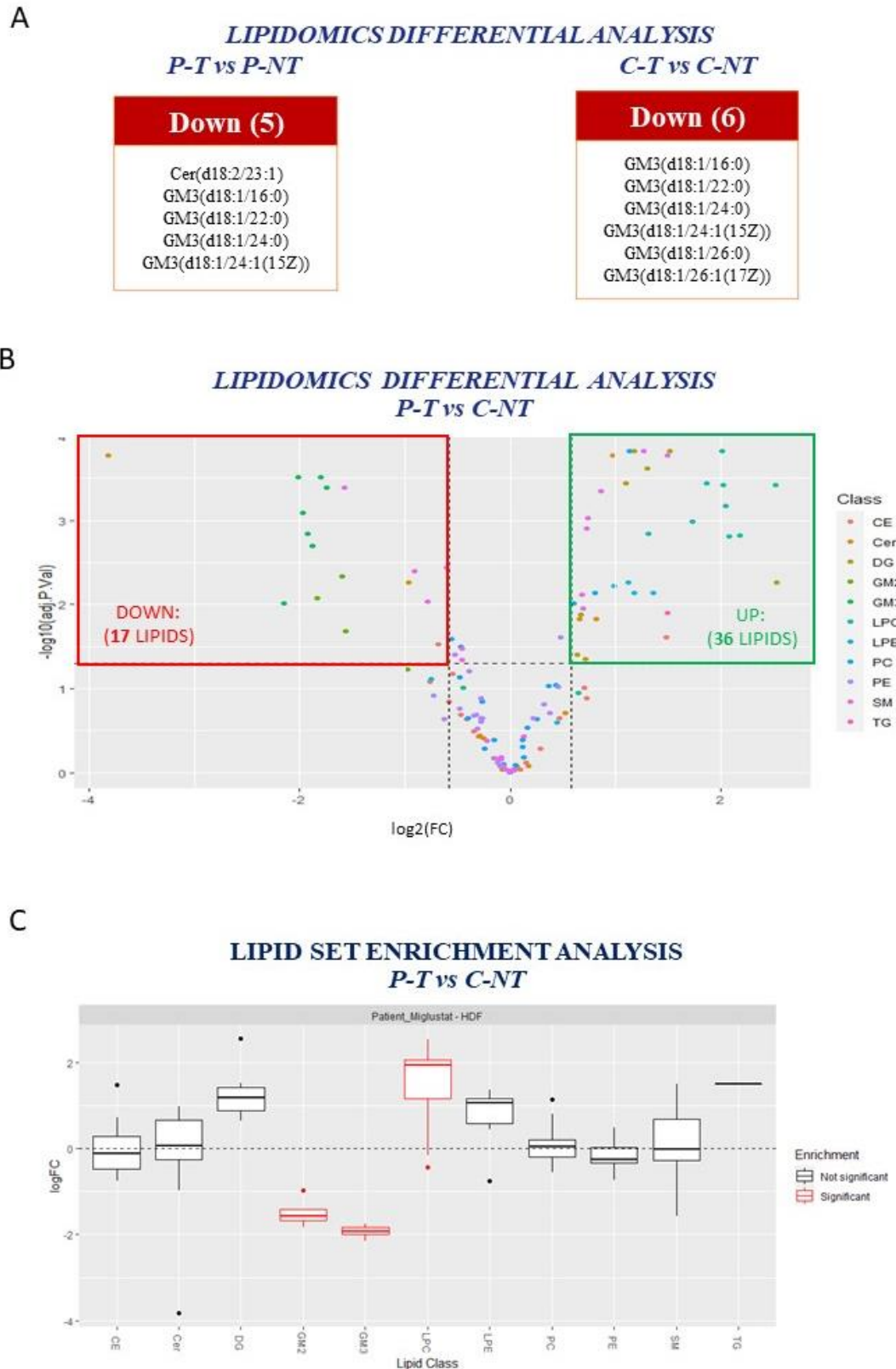
Figure 22. Lipidomic analysis of fibroblasts treated with miglustat. **A** Impact of miglustat on patients and controls fibroblasts. **B** Volcano plot of P-T vs C-NT showed the dysregulated lipids. **C** Lipid set enrichment analysis showed the overall status of lipid classes.

Table 7. List of the significant and differentially altered lipid species (thresholds: adj. p-value < 0.05, FC ≤ 1/1.5 or FC ≥1.5) in contrast P_T vs C_NT.

	P_T vs C_NT	
	UP (36)	**DOWN (17)**
1	CE(22:4)	CE(16:0)
2	Cer(d18:1/22:0)	Cer(d18:2/22:0)
3	Cer(d18:1/23:0)	Cer(d18:2/23:1)
4	Cer(d18:1/24:1)	GM2(d18:1/22:0)
5	Cer(d18:1/25:0)	GM2(d18:1/24:0)
6	DG(34:1)	GM2(d18:1/24:1(15Z))
7	DG(36:0)	GM3(d18:1/16:0)
8	DG(36:1)	GM3(d18:1/18:0)
9	DG(38:5)	GM3(d18:1/22:0)
10	DG(38:6)	GM3(d18:1/24:0)
11	DG(40:6)	GM3(d18:1/24:1(15Z))
12	DG(40:7)	GM3(d18:1/26:0)
13	LPC(16:0)	GM3(d18:1/26:1(17Z))
14	LPC(16:0e)	SM(32:2)
15	LPC(16:1)	SM(36:2)
16	LPC(18:1)	SM(36:3)
17	LPC(18:2)	SM(38:3)
18	LPC(20:3)	
19	LPC(20:4)	
20	LPC(22:5)	
21	LPC(22:6)	
22	LPE(16:0)	
23	LPE(18:0)	
24	LPE(18:1)	
25	LPE(18:2)	
26	PC(38:2)	
27	PC(40:2)	
28	PC(40:4)	
29	SM(41:1)	
30	SM(41:2)	
31	SM(42:1)	
32	SM(42:2)	
33	SM(43:1)	
34	SM(43:2)	
35	SM(43:3)	
36	TG(56:6)	

Moreover, using the opportunity of blood sampling during the TreatSPG11 clinical trial, we observed that differential lipidomic analysis with *miglustat* treatment comparing baseline with T1, showed 4 lipid species differentially expressed, namely, DG(34:0), DG(34:4), DG(36:0) and GM3(d18:1/26:1(17Z)) (**Figure 23**).
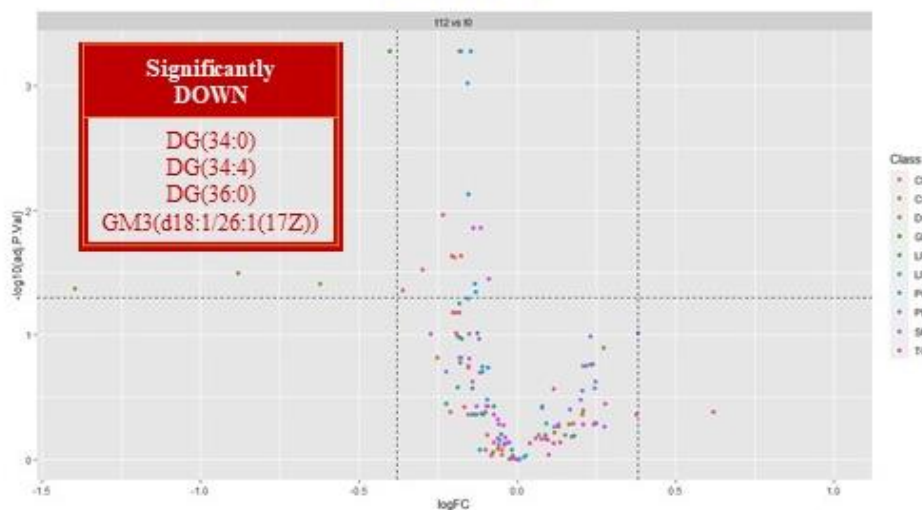
Figure 23. Volcano plot of lipidomic differential analysis in plasma of patients analyzed at T=0 and after 12 weeks of miglustat intake (T=1). In the red box were reported the lipids differentially expressed.

4.5 SPG11 knock-out cell line

The primarily affected cell type in SPG11 are neuronal cells, that mainly express SPATACIN protein. We therefore turned to study the effect of *SPG11* mutations in a neuronal cell model and thus through CRISPR/Cas9 technology we obtain a pool of mutations in exon 1 of *SPG11* gene in SH-SY5Y cell line. The efficiency of the process was of 71,5% and the impact on the protein was evaluated with immunoblot analysis. SPATACSIN protein was reduced to 34% in cells transfected with SPG11 sgRNA 1 (pool 1-SPG11) compared to controls: untrasfected cells (WT) and cells transfected with px459 empty vector (px459 empty) (**Figure 24**).
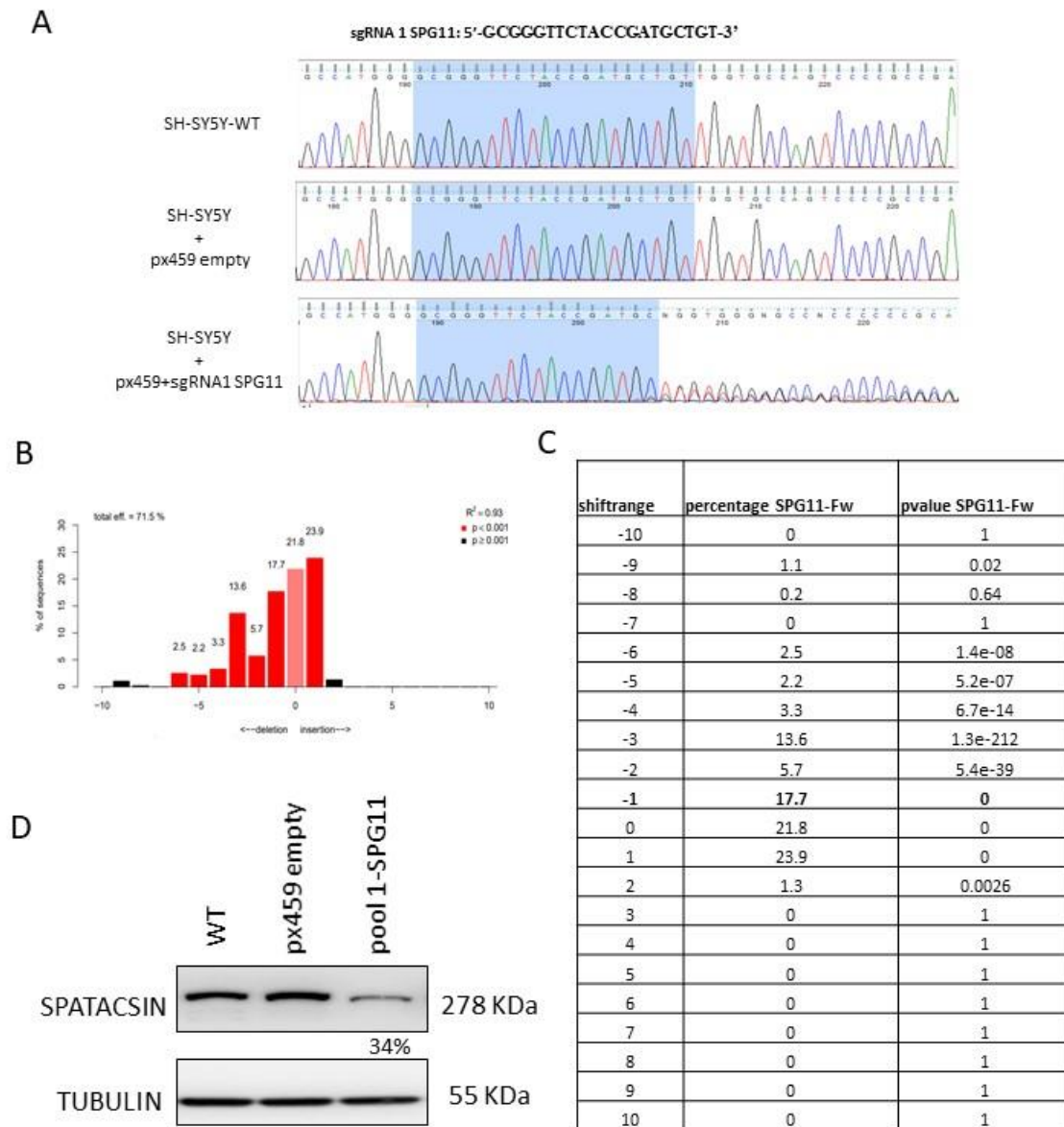
Figure 24. SPG11 knock-out (KO) in SH-SY5Y cell line. **A** gDNA electropherograms showed the consequence of gene editing strategy at DNA level of untrasfected SH-SY5Y cells (WT), cells transfected with empty vector (px459 empty) and cells transfected with px459 with sgRNA1 SPG11 (pool 1-SPG11). **B-C** Efficacy of gene editing with the percentages of insertions and deletions present in pool 1–SPG11 calculated with TIDE tool. **D** Immunoblot analysis of SPATACSIN showed a reduced level protein in pool 1-SPG11.

Then, pool 1-SPG11 has been screen to find a clone with a single mutation in *SPG11* gene causing a knock-out protein. We selected a clone with a deletion of base (T) at -3 from PAM sequence (**Figure 25A**). The clone KO-SPG11 carried the mutation c.86del resulting in a premature termination codon in the first protein amminoacids (p.Leu29ArgfsTer29) (**Figure 25B**). Immunoblot analysis of clone KO-SPG11 revealed an undetectable SPATACSIN and

SPASTIZIN proteins, while AP5Z1 was reduced to 74% compared to WT and px459 empty cells (**Figure 25C**).
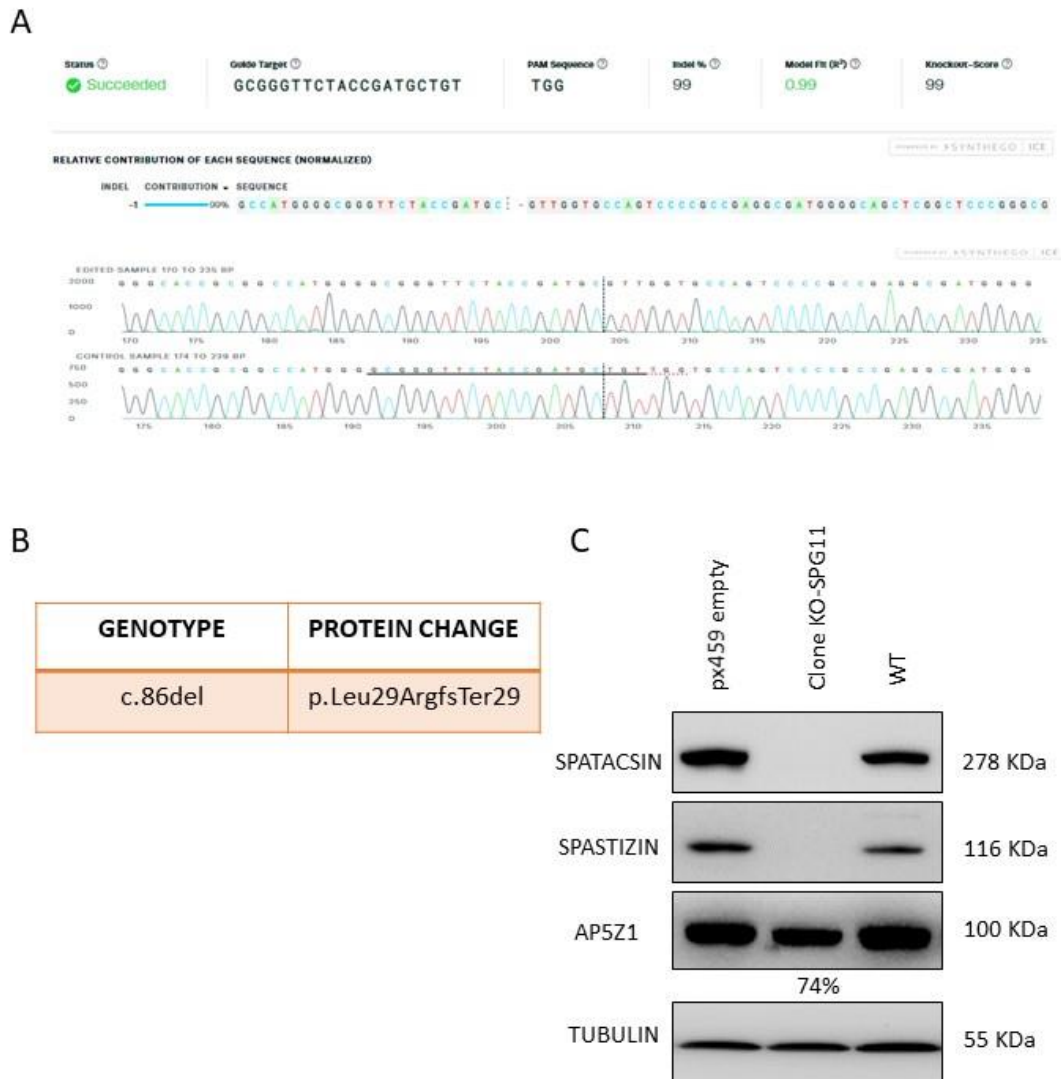
Figure 25. SPG11 KO clone generating with CRISPR/Cas9 technology. **A** gDNA electropherogram of SPG11 KO clone showed a deletion of a nucleotide at -3 for PAM sequence. The analysis is performed with SYNTHEGO ICE tool. **B** Genotype and protein change prediction of clone KO-SPG11. **C** Immunoblot of SPATACSIN and its interacting proteins (SPASTIZIN and AP5Z1) of clone KO-SPG11.

Studies of oxidative metabolism in a KO clone showed ROS overproduction and impaired OCR with reduced basal and maximal respiration, ATP production and proton leak (**Figure 26**).
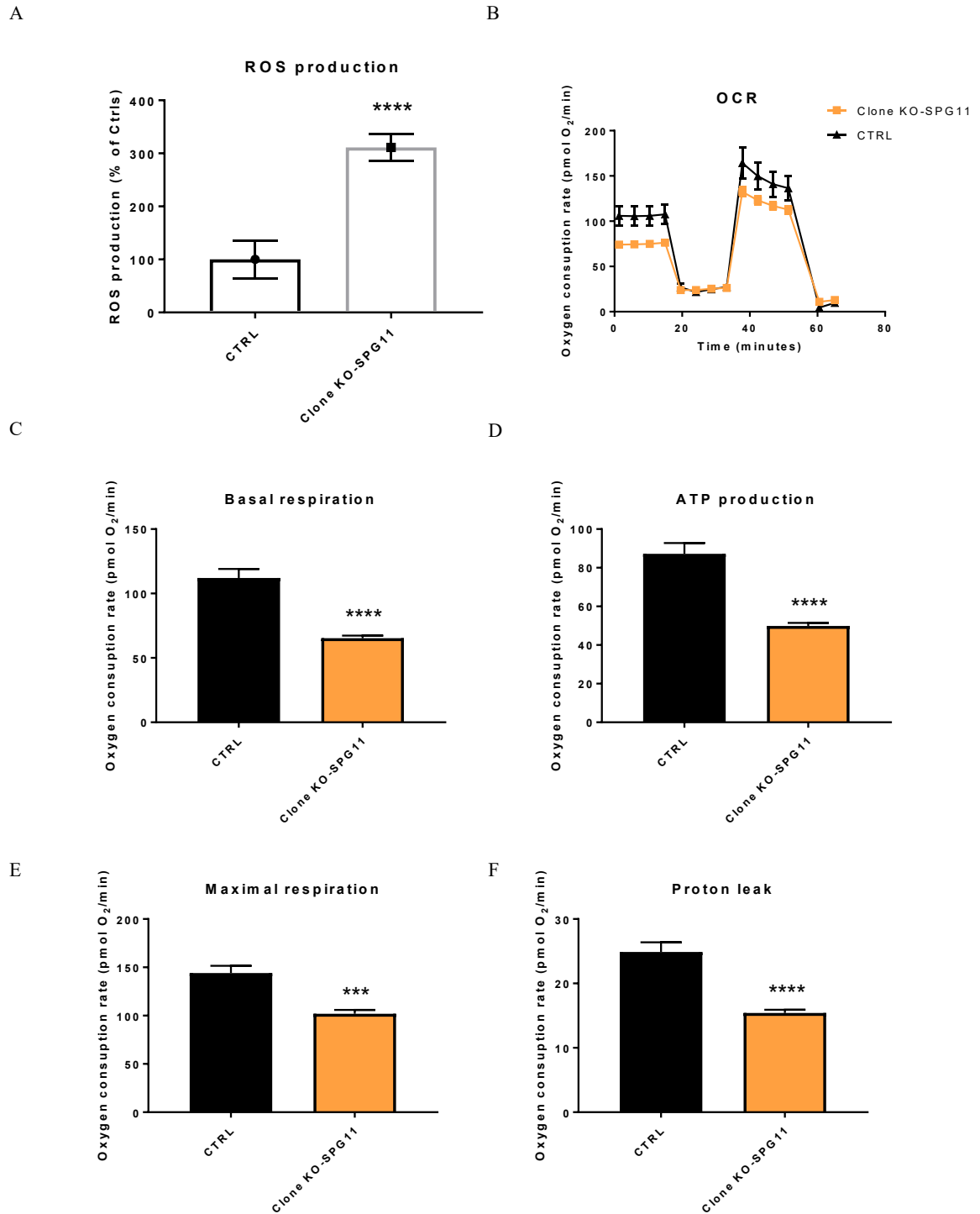
Figure 26. Oxidative analysis of the clone KO-SPG11. **A** ROS measurement showed an increased ROS production in clone KO-SPG11 compared to control (CTRL). **B** OCR plot showed an altered micro-oxygraphy of clone KO-SPG11 with a decreased basal respiration (**C**), ATP production (**D**), maximal respiration (**E**) and proton leak (**F**). The CTRL cells are SH-SY5Y transfected with px459 empty.

5. DISCUSSION

Many HSPs are currently without any therapeutic option. The unmet need to identify successful treatments in HSPs other than palliative care is challenged by the still limited information on the pathogenetic mechanisms. It is important to restraint the phenotypic variability of HSPs to avoid "noise" in the analysis. To circumvent this issue our strategy is to validate therapeutic strategy in a molecularly homogeneous form of HSP and then to extend potential treatments to rarer forms of HSP that share common physiopathological mechanisms. In this work we studied the SPG11-HSP, one of the most common autosomal recessive complex form of HSP. We focused on biological material from 22 patients and demonstrated an undetectable SPATACIN protein in all of their skin fibroblasts, compatible with a loss of function mechanism. The result was corroborated by a decreased *SPG11* mRNA level, likely due to *SPG11* mutations that destabilized the mRNA leading toward an increased degradation. Considering age at onset, disease duration, clinical characteristics, and disability scores, assessed with the SPRS rating scale (Schule et al. 2006), we did not disclose clear genotype-phenotype correlation in AR-SPG11 patients (Pozner et al. 2020). This is a common feature of neurodegenerative diseases (Longo et al. 2021). It is known that SPATACSIN works in a complex with SPASTIZIN/ZFYVE26 and AP5Z1 (Hirst et al. 2013; 2018), two proteins encoded by the *SPG15* and *SPG48* genes, respectively. Hence, we studied the levels of SPATACSIN interacting proteins in patients skin fibroblasts and we observed a decreased AP5Z1 levels. This means that *SPG11* mutations do not affect ZFYVE26 expression levels (Vantaggiato et al. 2019), while influence AP5Z1. A similar finding was observed in SPG11-KO neuronal cells where SPASTIZIN was also undetectable. The latter finding might relate to the earlier mutation (c.86del; p.Leu29ArgfsTer29) we defined in mutant SH-SY5Y cells, a potential explanation of the difference between cell lines (Wagner et al. 2019). An immediate consequence of these findings is two-fold: (i) SPATACSIN levels in PBMC or even in a slightly more invasive punch biopsy can assist a more rapid detection of the genetic aetiology in complex forms of HSP defining a possible SPG11 case; (ii) modulation of AP5Z1 levels might be considered to influence SPATACSIN expression.

In our study, we also observed that impaired SPATACSIN leads to altered mitochondrial respiration in terms of maximal respiration, SRC and proton leak that revealed a stressed cellular status with impaired mitochondrial network resulting in ROS overproduction (Ahmad et al. 2013) with an impact on NRF2 protein levels (Kasai et al. 2020) suggesting that some patients should benefit from antioxidant therapy (Voets et al. 2012). Evidences demonstrated that NRF2 activity is repressed in diabetes patients, due to high glucose concentrations (Cheng et al. 2013; Rabbani et al. 2019). It is worth noting that there is a high rate of obesity among SPG11 patients, a potential risk factor for diabetes (de Bot et al. 2013; Cardozo-Hernández, Rezende, and França

2020). This observation suggests that NRF2 should be considered as potential target for therapies in SPG11. We also observed that $SPG11^{-/-}$ neuroblastoma cell lines showed increased ROS production with impaired mitochondrial respiration considering basal and maximal respiration, ATP production and proton leak. Hence, data obtained in fibroblasts and confirmed in SH-SY5Y cells should be considered when approaching therapies in SPG11-HSP (Ebrahimi-Fakhari et al. 2021).

Furthermore, the novel information of this study was the multi-omic characterization of biological material derived from SPG11 patients. Proteomic and lipidomic analyses unraveled a set of proteins and lipids capable to distinguish SPG11 patients from healthy controls. The dysregulated pathways highlighted through functional analysis of proteomic results concerned cells organization surmising defects in actin filament and cytoskeleton organization that impact also in muscle contractions and blood coagulation in wounding response. Indeed, actin filaments are fundamental for sarcomere contraction (Cooper 2000) and fribin-clots structure (Janmey et al. 1992). These data are in concordance with the already known role of SPTACSIN in neurites plasticity through cytoskeleton stability (Pérez-Brangulí et al. 2014), but further studies to clarify this issue should be warranted. Moreover, a proteomic analysis of $SPG11^{-/-}$ neuroblastoma cell line will better elucidate the putative pathways involved in the disease comparing them to the data obtain in proteomic patients fibroblast as happened in ARSACS (Morani et al. 2021). Lipidomic studies pointed out a set of dysregulated lipid classes in SPG11 patients, namely, DG, LPC and GM3. Strikingly, we observed that GM3 resulted down-regulated in skin fibroblasts, opposed to what has been described in isolated lysosomal fraction of cerebral cortex of 8 month-old $SPG11^{-/-}$ mice, and in cortical neurons derived from patients fibroblasts, (Boutry et al. 2018). However, SPG11-HSP categorized as LSDs (lysosomal storage disorders) shows defects in the metabolic pathways in the degradation of glycoshingolipids (GLSs). In LSDs depending on the type of GLS dysregulated there are different clinical phenotypes and there is a differential distribution of the various GLSs in different tissues related to the disease. In Fabry disease, globotriaosylceramide (Gb3) storage occurs in many cell types (vascular endothelium, kidney, heart) whereas glucosylceramide accumulates in many cell types in Gaucher disease, including neurons (Lachmann 2009). The present study suggests that skin fibroblasts are a easy to use cell model of SPG11 disease but cannot sufficiently to draw conclusions on what happens to the brain of SPG11 patients. Although our data suggest involvement of SPTACSIN in GLSs and lysophospholipides pathways, it remains unclear the molecular mechanisms leading to changes in lipid classes in the context of SPG11 patients. Having the possibility to monitor lipidome profiles in real clinical setting might circumvent this issue. We explored the latter possibility with a subset of patients undergoing a pharmacological clinical trial. We observed that lipidic species dysregulated at baseline were some DG and GM3. Plasma diacylglycerol composition is considered a biomarker of metabolic defects (Polewski et al. 2015). Treatment with *miglustat* did

not appear to significantly modify this lipid signature and further studies should be performed. To this point, it is important our observation that in skin cells *miglustat* acts on muscle contraction and response to wounding, perhaps as a response to global recovery of actin filament and cytoskeleton organization, as well as impacts on hexosylceramides, the precursors of gangliosides, as suggested in an animal model of Niemann-Pick disease type C (Hoque et al. 2020). Moreover, miglustat up-regulates some PC and SM, such as PC(38:2), PC(40:4), PC(34:3), SM(41:1), SM(41:2), SM(42:1), SM(42:2) and SM(43:3) and a similar accumulation of SM and PC has recently reported in colon rectal cancer cells treated with miglustat (Jennemann et al. 2021). Furthermore, the involvement of this drug in sphingolipids metabolism is corroborated by the up regulation of some ceramides, like Cer(d18:1/22:0), Cer(d18:1/23:0), Cer(d18:1/24:1) and Cer(d18:1/25:0). Lastly miglustat treatment even though does not modify the total content of CE, in particular balances some CE levels, such as CE(20:2), CE(16:2), CE(18:2) and CE(18:3) (**Table 8**). Taken together, our attempt to use *miglustat* highlights new lipid classes in SPG11 but it does not appear to "correct" the biological processes in SPG11. A similar scenario was faced by piloting *ataluren* to improve transcription of SPATACSIN.

Table 8. Comparison between the significant and differentially altered lipid species of contrast P_NT vs C_NT and P_T vs C_NT. In bold are highlighted le lipid species in common between the 2 contrasts.

	P-NT vs C-NT		P-T vs C-NT	
	UP (27)	**DOWN (16)**	**UP (36)**	**DOWN (17)**
1	CE(20:2)	**CE(16:0)**	**CE(22:4)**	**CE(16:0)**
2	**CE(22:4)**	CE(16:2)	Cer(d18:1/22:0)	**Cer(d18:2/22:0)**
3	**DG(34:1)**	CE(18:2)	Cer(d18:1/23:0)	**Cer(d18:2/23:1)**
4	**DG(36:0)**	CE(18:3)	Cer(d18:1/24:1)	GM2(d18:1/22:0)
5	**DG(36:1)**	**Cer(d18:2/22:0)**	Cer(d18:1/25:0)	GM2(d18:1/24:0)
6	**DG(38:5)**	**Cer(d18:2/23:1)**	**DG(34:1)**	GM2(d18:1/24:1(15Z))
7	**DG(38:6)**	**GM3(d18:1/16:0)**	**DG(36:0)**	**GM3(d18:1/16:0)**
8	**DG(40:6)**	**GM3(d18:1/18:0)**	**DG(36:1)**	**GM3(d18:1/18:0)**
9	**DG(40:7)**	**GM3(d18:1/24:0)**	**DG(38:5)**	GM3(d18:1/22:0)
10	**LPC(16:0)**	**GM3(d18:1/26:0)**	**DG(38:6)**	**GM3(d18:1/24:0)**
11	**LPC(16:0e)**	PC(34:3)	**DG(40:6)**	GM3(d18:1/24:1(15Z))
12	**LPC(16:1)**	PE(36:3)	**DG(40:7)**	**GM3(d18:1/26:0)**
13	LPC(18:0e)	**SM(32:2)**	**LPC(16:0)**	GM3(d18:1/26:1(17Z))
14	**LPC(18:1)**	**SM(36:2)**	**LPC(16:0e)**	**SM(32:2)**
15	**LPC(18:2)**	**SM(36:3)**	**LPC(16:1)**	**SM(36:2)**
16	**LPC(20:3)**	**SM(38:3)**	**LPC(18:1)**	**SM(36:3)**

	P-NT vs C-NT		P-T vs C-NT	
	UP (27)	DOWN (16)	UP (36)	DOWN (17)
17	LPC(20:4)		LPC(18:2)	SM(38:3)
18	LPC(22:5)		LPC(20:3)	
19	LPC(22:6)		LPC(20:4)	
20	LPE(16:0)		LPC(22:5)	
21	LPE(18:0)		LPC(22:6)	
22	LPE(18:1)		LPE(16:0)	
23	LPE(18:2)		LPE(18:0)	
24	PC(40:2)		LPE(18:1)	
25	SM(43:1)		LPE(18:2)	
26	SM(43:2)		PC(38:2)	
27	TG(56:6)		PC(40:2)	
28			PC(40:4)	
29			SM(41:1)	
30			SM(41:2)	
31			SM(42:1)	
32			SM(42:2)	
33			SM(43:1)	
34			SM(43:2)	
35			SM(43:3)	
36			TG(56:6)	

6. CONCLUSIONS AND FUTURE PERSPECTIVES

In the context of HSPs we focused on SPG11-HSP, the most frequent form of autosomal recessive HSP. This is a neurodegenerative disease with no cure requiring new insights on the mechanisms to find new opportunity to therapy. In this study the recruited 22 SPG11 patients, a relatively large number of patients in a rare condition. The study of SPG11 cell lines linked altered cellular status and mitochondrial dysfunction to the disease process. Moreover, a multi-omics approach in SPG11 skin fibroblasts offered a new outlook at the level of proteins and lipids. The new information will serve for improved knowledge of patients' relevant biomarkers and potential targets to therapy. Such an approached has been shown in this PhD research program with a proof-of-principle approach.

The future perspectives of this work are the extension of molecular and oxidative metabolism studies on all SPG11 patients; multi-omics approach on $SPG11^{-/-}$ neuroblastoma cell line; the validation of the results of proteomic on skin fibroblasts through western blot and immunofluorescence experiments; with integration with a more complete metabolomic outlook.

7. CONTRIBUTIONS AND ACKNOLEDGEMENTS

8. REFERENCES

Ahmad, T., K. Aggarwal, B. Pattnaik, S. Mukherjee, T. Sethi, B. K. Tiwari, M. Kumar, et al. 2013. "Computational Classification of Mitochondrial Shapes Reflects Stress and Redox State." *Cell Death & Disease* 4 (1): e461–e461. https://doi.org/10.1038/cddis.2012.213.

Ahmed, Zeeshan. 2020. "Practicing Precision Medicine with Intelligently Integrative Clinical and Multi-Omics Data Analysis." *Human Genomics* 14 (1): 1–5. https://doi.org/10.1186/s40246-020-00287-z.

Aslam, Bilal, Madiha Basit, Muhammad Atif Nisar, Mohsin Khurshid, and Muhammad Hidayat Rasool. 2017. "Proteomics: Technologies and Their Applications." *Journal of Chromatographic Science* 55 (2): 182–96. https://doi.org/10.1093/chromsci/bmw167.

Bak, Rasmus O., Natalia Gomez-Ospina, and Matthew H. Porteus. 2018. "Gene Editing on Center Stage." *Trends in Genetics* 34 (8): 600–611. https://doi.org/10.1016/j.tig.2018.05.004.

Balaban, Robert S., Shino Nemoto, and Toren Finkel. 2005. "Mitochondria, Oxidants, and Aging." *Cell* 120 (4): 483–95. https://doi.org/10.1016/j.cell.2005.02.001.

Benard, Giovanni, Nadège Bellance, and Caroline Jose. 2011. *Mitochondrial Dynamics and Neurodegeneration*. Edited by Bingwei Lu. *Mitochondrial Dynamics and Neurodegeneration*. Dordrecht: Springer Netherlands. https://doi.org/10.1007/978-94-007-1291-1.

Bertoni, Carmen, and John Namgoong. 2016. "Clinical Potential of Ataluren in the Treatment of Duchenne Muscular Dystrophy." *Degenerative Neurological and Neuromuscular Disease*, May, 37. https://doi.org/10.2147/DNND.S71808.

Blackstone, Craig. 2012. "Cellular Pathways of Hereditary Spastic Paraplegia." *Annual Review of Neuroscience* 35 (1): 25–47. https://doi.org/10.1146/annurev-neuro-062111-150400.

Bot, Susanne T de, Rogier C Burggraaff, Johanna C Herkert, Helenius J Schelhaas, Bart Post, Adinda Diekstra, Reinout O van Vliet, et al. 2013. "Rapidly Deteriorating Course in Dutch Hereditary Spastic Paraplegia Type 11 Patients." *European Journal of Human Genetics* 21 (11): 1312–15. https://doi.org/10.1038/ejhg.2013.27.

Boutry, Maxime, Julien Branchu, Céline Lustremant, Claire Pujol, Julie Pernelle, Raphaël Matusiak, Alexandre Seyer, et al. 2018. "Inhibition of Lysosome Membrane Recycling Causes Accumulation of Gangliosides That Contribute to Neurodegeneration." *Cell Reports* 23 (13): 3813–26. https://doi.org/10.1016/j.celrep.2018.05.098.

Boutry, Maxime, Alexandre Pierga, Raphaël Matusiak, Julien Branchu, Marc Houllegatte, Yoan Ibrahim, Elise Balse, et al. 2019a. "Loss of Spatacsin Impairs Cholesterol Trafficking and Calcium Homeostasis." *Communications Biology* 2 (1): 380. https://doi.org/10.1038/s42003-019-0615-z.

———. 2019b. "Loss of Spatacsin Impairs Cholesterol Trafficking and Calcium Homeostasis." *Communications Biology* 2 (1): 380. https://doi.org/10.1038/s42003-019-0615-z.

Branchu, Julien, Maxime Boutry, Laura Sourd, Marine Depp, Céline Leone, Alexandrine Corriger, Maeva Vallucci, et al. 2017. "Loss of Spatacsin Function Alters Lysosomal Lipid Clearance Leading to Upper and Lower Motor Neuron Degeneration." *Neurobiology of Disease* 102 (June): 21–37. https://doi.org/10.1016/j.nbd.2017.02.007.

Braschinsky, Mark, Siiri-Merike Lüüs, Katrin Gross-Paju, and Sulev Haldre. 2009. "The Prevalence of Hereditary Spastic Paraplegia and the Occurrence of SPG4 Mutations in Estonia." *Neuroepidemiology* 32 (2): 89–93. https://doi.org/10.1159/000177033.

Brinkman, Eva K., Tao Chen, Mario Amendola, and Bas van Steensel. 2014. "Easy Quantitative Assessment of Genome Editing by Sequence Trace Decomposition." *Nucleic Acids Research* 42 (22): e168–e168. https://doi.org/10.1093/nar/gku936.

Brionne, Aurélien, Amélie Juanchich, and Christelle Hennequet-Antier. 2019. "ViSEAGO: A Bioconductor Package for Clustering Biological Functions Using Gene Ontology and Semantic Similarity." *BioData Mining* 12 (1): 16. https://doi.org/10.1186/s13040-019-0204-1.

Cardozo-Hernández, Ana Luisa de Carvalho, Thiago Junqueira Ribeiro Rezende, and Marcondes Cavalcante França. 2020. "Hereditary Spastic Paraplegia Type 11 (SPG11) Is Associated with Obesity and Hypothalamic Damage." *Journal of the Neurological Sciences* 416 (September): 116982. https://doi.org/10.1016/j.jns.2020.116982.

Castellanos, Daniel Báez, Cynthia A. Martín-Jiménez, Felipe Rojas-Rodríguez, George E. Barreto, and Janneth González. 2021. "Brain Lipidomics as a Rising Field in Neurodegenerative Contexts: Perspectives with Machine Learning Approaches." *Frontiers in Neuroendocrinology* 61 (April): 100899. https://doi.org/10.1016/j.yfrne.2021.100899.

Chang, Jaerak, Seongju Lee, and Craig Blackstone. 2014. "Spastic Paraplegia Proteins Spastizin and Spatacsin Mediate Autophagic Lysosome Reformation." *Journal of Clinical Investigation* 124 (12): 5249–62. https://doi.org/10.1172/JCI77598.

Cheng, Xinghua, Sarah J. Chapple, Bijal Patel, William Puszyk, David Sugden, Xiaoke Yin, Manuel Mayr, Richard C.M. Siow, and Giovanni E. Mann. 2013. "Gestational Diabetes Mellitus Impairs Nrf2-Mediated Adaptive Antioxidant Defenses and Redox Signaling in Fetal Endothelial Cells

In Utero." *Diabetes* 62 (12): 4088–97. https://doi.org/10.2337/db13-0169.

Cooper. 2000. *The Cell: A Molecular Approach. 2nd Edition.* Sinauer As. Sunderland (MA).
   https://www.ncbi.nlm.nih.gov/books/NBK9961/.

Darios, Frédéric, Fanny Mochel, and Giovanni Stevanin. 2020. "Lipids in the Physiopathology of
   Hereditary Spastic Paraplegias." *Frontiers in Neuroscience* 14 (February): 1–19.
   https://doi.org/10.3389/fnins.2020.00074.

Dieterle, Frank, Alfred Ross, Götz Schlotterbeck, and Hans Senn. 2006. "Probabilistic Quotient
   Normalization as Robust Method to Account for Dilution of Complex Biological Mixtures.
   Application in 1 H NMR Metabonomics." *Analytical Chemistry* 78 (13): 4281–90.
   https://doi.org/10.1021/ac051632c.

Doench, John G, Nicolo Fusi, Meagan Sullender, Mudra Hegde, Emma W Vaimberg, Katherine F
   Donovan, Ian Smith, et al. 2016. "Optimized SgRNA Design to Maximize Activity and
   Minimize Off-Target Effects of CRISPR-Cas9." *Nature Biotechnology* 34 (2): 184–91.
   https://doi.org/10.1038/nbt.3437.

Ebrahimi-Fakhari, Darius. 2018. "Congenital Disorders of Autophagy: What a Pediatric Neurologist
   Should Know." *Neuropediatrics* 49 (01): 018–025. https://doi.org/10.1055/s-0037-1608652.

Ebrahimi-Fakhari, Darius, Julian E Alecu, Barbara Brechmann, Marvin Ziegler, Kathrin Eberhardt,
   Hellen Jumo, Angelica D'Amore, et al. 2021. "High-Throughput Imaging of ATG9A
   Distribution as a Diagnostic Functional Assay for Adaptor Protein Complex 4-Associated
   Hereditary Spastic Paraplegia." *Brain Communications* 3 (4).
   https://doi.org/10.1093/braincomms/fcab221.

Ebrahimi-Fakhari, Darius, Afshin Saffari, Lara Wahlster, Jenny Lu, Susan Byrne, Georg F.
   Hoffmann, Heinz Jungbluth, and Mustafa Sahin. 2016. "Congenital Disorders of Autophagy: An
   Emerging Novel Class of Inborn Errors of Neuro-Metabolism." *Brain* 139 (2): 317–37.
   https://doi.org/10.1093/brain/awv371.

Fahy, Eoin, Shankar Subramaniam, Robert C. Murphy, Masahiro Nishijima, Christian R.H. Raetz,
   Takao Shimizu, Friedrich Spener, Gerrit van Meer, Michael J.O. Wakelam, and Edward A.
   Dennis. 2009. "Update of the LIPID MAPS Comprehensive Classification System for Lipids."
   Journal of Lipid Research 50 (SUPPL.): S9–14. https://doi.org/10.1194/jlr.R800095-JLR200.

Ficicioglu, Can. 2008. "Review of Miglustat for Clinical Management in Gaucher Disease Type 1."
   Therapeutics and Clinical Risk Management Volume 4 (2): 425–31.
   https://doi.org/10.2147/TCRM.S6865.

Folch, Jordi, M. Lees, and G.H. Sloane Stanley. 1957. "A SIMPLE METHOD FOR THE ISOLATION AND PURIFICATION OF TOTAL LIPIDES FROM ANIMAL TISSUES." *Journal of Biological Chemistry* 226 (1): 497–509. https://doi.org/10.1016/S0021-9258(18)64849-5.

Geraghty, R J, A Capes-Davis, J M Davis, J Downward, R I Freshney, I Knezevic, R Lovell-Badge, et al. 2014. "Guidelines for the Use of Cell Lines in Biomedical Research." *British Journal of Cancer* 111 (6): 1021–46. https://doi.org/10.1038/bjc.2014.166.

Giudice, Temistocle Lo, Federica Lombardi, Filippo Maria Santorelli, Toshitaka Kawarai, and Antonio Orlacchio. 2014. "Hereditary Spastic Paraplegia: Clinical-Genetic Characteristics and Evolving Molecular Mechanisms." *Experimental Neurology* 261 (November): 518–39. https://doi.org/10.1016/j.expneurol.2014.06.011.

Güner, Fabian, Tatyana Pozner, Florian Krach, Iryna Prots, Sandra Loskarn, Ursula Schlötzer-Schrehardt, Jürgen Winkler, Beate Winner, and Martin Regensburger. 2021. "Axon-Specific Mitochondrial Pathology in SPG11 Alpha Motor Neurons." *Frontiers in Neuroscience* 15 (July): 1–14. https://doi.org/10.3389/fnins.2021.680572.

Gupta, Sanjeev K., and Pratyoosh Shukla. 2017. "Gene Editing for Cell Engineering: Trends and Applications." *Critical Reviews in Biotechnology* 37 (5): 672–84. https://doi.org/10.1080/07388551.2016.1214557.

Harding, A.E. 1983. "CLASSIFICATION OF THE HEREDITARY ATAXIAS AND PARAPLEGIAS." *The Lancet* 321 (8334): 1151–55. https://doi.org/10.1016/S0140-6736(83)92879-9.

Hasin, Yehudit, Marcus Seldin, and Aldons Lusis. 2017. "Multi-Omics Approaches to Disease." *Genome Biology* 18 (1): 83. https://doi.org/10.1186/s13059-017-1215-1.

Hedera. n.d. "Hereditary Spastic Paraplegia Overview." *GeneReviews® [Internet].* Seattle (WA): University of Washington, Seattle. https://www.ncbi.nlm.nih.gov/sites/books/NBK1509/.

Hirst, Jennifer, Georg H. H. Borner, James Edgar, Marco Y. Hein, Matthias Mann, Frank Buchholz, Robin Antrobus, and Margaret S. Robinson. 2013. "Interaction between AP-5 and the Hereditary Spastic Paraplegia Proteins SPG11 and SPG15." Edited by Anne Spang. *Molecular Biology of the Cell* 24 (16): 2558–69. https://doi.org/10.1091/mbc.e13-03-0170.

Hirst, Jennifer, Daniel N. Itzhak, Robin Antrobus, Georg H. H. Borner, and Margaret S. Robinson. 2018. "Role of the AP-5 Adaptor Protein Complex in Late Endosome-to-Golgi Retrieval." Edited by Sandra Schmid. *PLOS Biology* 16 (1): e2004411. https://doi.org/10.1371/journal.pbio.2004411.

Hoque, Sanzana, Yuki Kondo, Nodoka Sakata, Yusei Yamada, Madoka Fukaura, Taishi Higashi, Keiichi Motoyama, et al. 2020. "Differential Effects of 2-Hydroxypropyl-Cyclodextrins on Lipid Accumulation in Npc1-Null Cells." *International Journal of Molecular Sciences* 21 (3): 898. https://doi.org/10.3390/ijms21030898.

Hsu, Patrick D., David A. Scott, Joshua A. Weinstein, F. Ann Ran, Silvana Konermann, Vineeta Agarwala, Yinqing Li, et al. 2013. "DNA Targeting Specificity of RNA-Guided Cas9 Nucleases." *Nature Biotechnology* 31 (9): 827–32. https://doi.org/10.1038/nbt.2647.

Huang, Zhao, Linguang Ma, Canhua Huang, Qifu Li, and Edouard C. Nice. 2017. "Proteomic Profiling of Human Plasma for Cancer Biomarker Discovery." *PROTEOMICS* 17 (6): 1600240. https://doi.org/10.1002/pmic.201600240.

Janmey, PA, JA Lamb, RM Ezzell, S Hvidt, and SE Lind. 1992. "Effects of Actin Filaments on Fibrin Clot Structure and Lysis." *Blood* 80 (4): 928–36. https://doi.org/10.1182/blood.V80.4.928.928.

Jennemann, Richard, Martina Volz, Felix Bestvater, Claudia Schmidt, Karsten Richter, Sylvia Kaden, Johannes Müthing, Hermann-Josef Gröne, and Roger Sandhoff. 2021. "Blockade of Glycosphingolipid Synthesis Inhibits Cell Cycle and Spheroid Growth of Colon Cancer Cells In Vitro and Experimental Colon Cancer Incidence In Vivo." *International Journal of Molecular Sciences* 22 (19): 10539. https://doi.org/10.3390/ijms221910539.

Jeyakumar, Mylvaganam, Terry D. Butters, Mario Cortina-Borja, Victoria Hunnam, Richard L. Proia, V. Hugh Perry, Raymond A. Dwek, and Frances M. Platt. 1999. "Delayed Symptom Onset and Increased Life Expectancy in Sandhoff Disease Mice Treated with N-Butyldeoxynojirimycin." *Proceedings of the National Academy of Sciences* 96 (11): 6388–93. https://doi.org/10.1073/pnas.96.11.6388.

Kasai, Shuya, Sunao Shimizu, Yota Tatara, Junsei Mimura, and Ken Itoh. 2020. "Regulation of Nrf2 by Mitochondrial Reactive Oxygen Species in Physiology and Pathology." *Biomolecules* 10 (2): 320. https://doi.org/10.3390/biom10020320.

Klebe, S., G. Stevanin, and C. Depienne. 2015. "Clinical and Genetic Heterogeneity in Hereditary Spastic Paraplegias: From SPG1 to SPG72 and Still Counting." *Revue Neurologique* 171 (6–7): 505–30. https://doi.org/10.1016/j.neurol.2015.02.017.

Kovac, Stjepana, Plamena R. Angelova, Kira M. Holmström, Ying Zhang, Albena T. Dinkova-Kostova, and Andrey Y. Abramov. 2015. "Nrf2 Regulates ROS Production by Mitochondria and NADPH Oxidase." *Biochimica et Biophysica Acta (BBA) - General Subjects* 1850 (4): 794–801. https://doi.org/10.1016/j.bbagen.2014.11.021.

Lachmann, Robin H. 2009. "Substrate-Reduction Therapy with Miglustat for Glycosphingolipid

Storage Disorders Affecting the Brain." *Expert Review of Endocrinology & Metabolism* 4 (3): 217–24. https://doi.org/10.1586/eem.09.8.

Lentini, Laura, Raffaella Melfi, Patrizia Cancemi, Ivana Pibiri, and Aldo Di Leonardo. 2019. "Caffeine Boosts Ataluren's Readthrough Activity." *Heliyon* 5 (6): e01963. https://doi.org/10.1016/j.heliyon.2019.e01963.

Lightbody, Gaye, Valeriia Haberland, Fiona Browne, Laura Taggart, Huiru Zheng, Eileen Parkes, and Jaine K. Blayney. 2019. "Review of Applications of High-Throughput Sequencing in Personalized Medicine: Barriers and Facilitators of Future Progress in Research and Clinical Application." *Briefings in Bioinformatics* 20 (5): 1795–1811. https://doi.org/10.1093/bib/bby051.

Longo, Fabiana, Daniele De Ritis, Annarita Miluzio, Davide Fraticelli, Jonathan Baets, Marina Scarlato, Filippo M. Santorelli, Stefano Biffo, and Francesca Maltecca. 2021. "Assessment of Sacsin Turnover in Patients With ARSACS." *Neurology* 97 (23): e2315–27. https://doi.org/10.1212/WNL.0000000000012962.

Loughran, Gary, Ming-Yuan Chou, Ivaylo P. Ivanov, Irwin Jungreis, Manolis Kellis, Anmol M. Kiran, Pavel V. Baranov, and John F. Atkins. 2014. "Evidence of Efficient Stop Codon Readthrough in Four Mammalian Genes." *Nucleic Acids Research* 42 (14): 8928–38. https://doi.org/10.1093/nar/gku608.

Lyseng-Williamson, Katherine A. 2014. "Miglustat: A Review of Its Use in Niemann-Pick Disease Type C." *Drugs* 74 (1): 61–74. https://doi.org/10.1007/s40265-013-0164-6.

Marraffini, Luciano A. 2015. "CRISPR-Cas Immunity in Prokaryotes." *Nature* 526 (7571): 55–61. https://doi.org/10.1038/nature15386.

Martin, Elodie, Constantin Yanicostas, Agnès Rastetter, Seyedeh Maryam Alavi Naini, Alissia Maouedj, Edor Kabashi, Sophie Rivaud-Péchoux, Alexis Brice, Giovanni Stevanin, and Nadia Soussi-Yanicostas. 2012. "Spatacsin and Spastizin Act in the Same Pathway Required for Proper Spinal Motor Neuron Axon Outgrowth in Zebrafish." *Neurobiology of Disease* 48 (3): 299–308. https://doi.org/10.1016/j.nbd.2012.07.003.

McCormack, Paul L, and Karen L Goa. 2003. "Miglustat." *Drugs* 63 (22): 2427–34. https://doi.org/10.2165/00003495-200363220-00006.

McDermott, C. 2000. "Hereditary Spastic Paraparesis: A Review of New Developments." *Journal of Neurology, Neurosurgery & Psychiatry* 69 (2): 150–60. https://doi.org/10.1136/jnnp.69.2.150.

Merrill, Ronald A., Kyle H. Flippo, and Stefan Strack. 2017. "Measuring Mitochondrial Shape with

ImageJ." In , 31–48. https://doi.org/10.1007/978-1-4939-6890-9_2.

Michelucci, Elena, Nicoletta Di Giorgi, Francesco Finamore, Jeff M. Smit, Arthur J. H. A. Scholte, Giovanni Signore, and Silvia Rocchiccioli. 2021. "Lipid Biomarkers in Statin Users with Coronary Artery Disease Annotated by Coronary Computed Tomography Angiography." *Scientific Reports* 11 (1): 12899. https://doi.org/10.1038/s41598-021-92339-0.

Mishra, Himanshu K., Iryna Prots, Steven Havlicek, Zacharias Kohl, Francesc Perez-Branguli, Tom Boerstler, Lukas Anneser, et al. 2016. "GSK3ß-dependent Dysregulation of Neurodevelopment in SPG11-patient Induced Pluripotent Stem Cell Model." *Annals of Neurology* 79 (5): 826–40. https://doi.org/10.1002/ana.24633.

Mohamed, Ahmed, Jeffrey Molendijk, and Michelle M. Hill. 2020. "Lipidr: A Software Tool for Data Mining and Analysis of Lipidomics Datasets." *Journal of Proteome Research* 19 (7): 2890–97. https://doi.org/10.1021/acs.jproteome.0c00082.

Moosajee, Mariya, Dhani Tracey-White, Matthew Smart, Marla Weetall, Simona Torriano, Vasiliki Kalatzis, Lyndon da Cruz, Peter Coffey, Andrew R. Webster, and Ellen Welch. 2016. "Functional Rescue of REP1 Following Treatment with PTC124 and Novel Derivative PTC-414 in Human Choroideremia Fibroblasts and the Nonsense-Mediated Zebrafish Model." *Human Molecular Genetics* 25 (16): 3416–31. https://doi.org/10.1093/hmg/ddw184.

Morani, Federica, Stefano Doccini, Giovanna Chiorino, Fabiana Fattori, Daniele Galatolo, Elisa Sciarrillo, Federica Gemignani, Stephan Züchner, Enrico Silvio Bertini, and Filippo Maria Santorelli. 2021. "Functional Network Profiles in ARSACS Disclosed by Aptamer-Based Proteomic Technology." *Frontiers in Neurology* 11 (January). https://doi.org/10.3389/fneur.2020.603774.

Morgan, Neil V, Bryndis Yngvadottir, Mary O'Driscoll, Graeme R Clark, Diana Walsh, Ezequiel Martin, Louise Tee, Evan Reid, Hannah L Titheradge, and Eamonn R Maher. 2021. "Evidence That Autosomal Recessive Spastic Cerebral Palsy-1 (CPSQ1) Is Caused by a Missense Variant in HPDL." *Brain Communications* 3 (1): 1–10. https://doi.org/10.1093/braincomms/fcab002.

Murala, Sireesha, Elanagan Nagarajan, and Pradeep C. Bollu. 2021. "Hereditary Spastic Paraplegia." *Neurological Sciences* 42 (3): 883–94. https://doi.org/10.1007/s10072-020-04981-7.

Park, Jee-Yun, Sunhyo Kim, Hee Young Sohn, Young Ho Koh, and Chulman Jo. 2019. "TFEB Activates Nrf2 by Repressing Its E3 Ubiquitin Ligase DCAF11 and Promoting Phosphorylation of P62." *Scientific Reports* 9 (1): 14354. https://doi.org/10.1038/s41598-019-50877-8.

Pascual, B., S. T. De Bot, M. R. Daniels, M. C. França, C. Toro, M. Riverol, P. Hedera, et al. 2019. "'Ears of the Lynx' MRI Sign Is Associated with SPG11 and SPG15 Hereditary Spastic

Paraplegia." *American Journal of Neuroradiology* 40 (1): 199–203. https://doi.org/10.3174/ajnr.A5935.

Peng, Liyuan, David I. Cantor, Canhua Huang, Kui Wang, Mark S. Baker, and Edouard C. Nice. 2018. "Tissue and Plasma Proteomics for Early Stage Cancer Detection." *Molecular Omics* 14 (6): 405–23. https://doi.org/10.1039/C8MO00126J.

Pensato, Viviana, Barbara Castellotti, Cinzia Gellera, Davide Pareyson, Claudia Ciano, Lorenzo Nanetti, Ettore Salsano, et al. 2014. "Overlapping Phenotypes in Complex Spastic Paraplegias SPG11, SPG15, SPG35 and SPG48." *Brain* 137 (7): 1907–20. https://doi.org/10.1093/brain/awu121.

Pérez-Brangulí, Francesc, Himanshu K. Mishra, Iryna Prots, Steven Havlicek, Zacharias Kohl, Domenica Saul, Christine Rummel, et al. 2014. "Dysfunction of Spatacsin Leads to Axonal Pathology in SPG11-Linked Hereditary Spastic Paraplegia." *Human Molecular Genetics* 23 (18): 4859–74. https://doi.org/10.1093/hmg/ddu200.

Platt, Frances M., and Mylvaganam Jeyakumar. 2008. "Substrate Reduction Therapy." *Acta Paediatrica* 97 (s457): 88–93. https://doi.org/10.1111/j.1651-2227.2008.00656.x.

Polewski, Michael A., Maggie S. Burhans, Minghui Zhao, Ricki J. Colman, Dhanansayan Shanmuganayagam, Mary J. Lindstrom, James M. Ntambi, and Rozalyn M. Anderson. 2015. "Plasma Diacylglycerol Composition Is a Biomarker of Metabolic Syndrome Onset in Rhesus Monkeys." *Journal of Lipid Research* 56 (8): 1461–70. https://doi.org/10.1194/jlr.M057562.

Pozner, Tatyana, Martin Regensburger, Tobias Engelhorn, Jürgen Winkler, and Beate Winner. 2020. "Janus-Faced Spatacsin (SPG11): Involvement in Neurodevelopment and Multisystem Neurodegeneration." *Brain* 143 (8): 2369–79. https://doi.org/10.1093/brain/awaa099.

Pozner, Tatyana, Annika Schray, Martin Regensburger, Dieter Chichung Lie, Ursula Schlötzer-Schrehardt, Jürgen Winkler, Soeren Turan, and Beate Winner. 2018. "Tideglusib Rescues Neurite Pathology of SPG11 IPSC Derived Cortical Neurons." *Frontiers in Neuroscience* 12 (December): 1–10. https://doi.org/10.3389/fnins.2018.00914.

Puranik, Nidhi, Dhananjay Yadav, Shiv Kumar Yadav, Vishal K. Chavda, and Jun-O Jin. 2020. "Proteomics and Neurodegenerative Disorders: Advancements in the Diagnostic Analysis." *Current Protein & Peptide Science* 21 (12): 1174–83. https://doi.org/10.2174/1389203721666200511094222.

Rabbani, Piul S., Marc A. Soares, Sophia G. Hameedi, Rohini L. Kadle, Adnan Mubasher, Maria Kowzun, and Daniel J. Ceradini. 2019. "Dysregulation of Nrf2/Keap1 Redox Pathway in Diabetes Affects Multipotency of Stromal Cells." *Diabetes* 68 (1): 141–55.

https://doi.org/10.2337/db18-0232.

Razzaq, Asad, and Ardas Masood. 2018. "CRISPR/Cas9 System: A Breakthrough in Genome
Editing." *Molecular Biology* 07 (02). https://doi.org/10.4172/2168-9547.100021.

Ribas, Graziela S., Ricardo Pires, Janice Carneiro Coelho, Daiane Rodrigues, Caroline Paula Mescka,
Camila S. Vanzin, Giovana B. Biancini, et al. 2012. "Oxidative Stress in Niemann-Pick Type C
Patients: A Protective Role of N-butyl-deoxynojirimycin Therapy." *International Journal of
Developmental Neuroscience* 30 (6): 439–44. https://doi.org/10.1016/j.ijdevneu.2012.07.002.

Rowe, Steven M, and John P Clancy. 2009. "Pharmaceuticals Targeting Nonsense Mutations in
Genetic Diseases." *BioDrugs* 23 (3): 165–74. https://doi.org/10.2165/00063030-200923030-
00003.

Salinas, Sara, Christos Proukakis, Andrew Crosby, and Thomas T. Warner. 2008. "Hereditary Spastic
Paraplegia: Clinical Features and Pathogenetic Mechanisms." *The Lancet Neurology* 7 (12):
1127–38. https://doi.org/10.1016/S1474-4422(08)70258-8.

Sarkar, Hajrah, Andreas Mitsios, Matthew Smart, Jane Skinner, Ailsa A. Welch, Vasiliki Kalatzis,
Peter J. Coffey, Adam M. Dubis, Andrew R. Webster, and Mariya Moosajee. 2019. "Nonsense-
Mediated MRNA Decay Efficiency Varies in Choroideremia Providing a Target to Boost Small
Molecule Therapeutics." *Human Molecular Genetics* 28 (11): 1865–71.
https://doi.org/10.1093/hmg/ddz028.

Saxena, Uday. 2012. "Bioenergetics Failure in Neurodegenerative Diseases: Back to the Future."
Expert Opinion on Therapeutic Targets 16 (4): 351–54.
https://doi.org/10.1517/14728222.2012.664135.

Schule, R., T. Holland-Letz, S. Klimpe, J. Kassubek, T. Klopstock, V. Mall, S. Otto, B. Winner, and
L. Schols. 2006. "The Spastic Paraplegia Rating Scale (SPRS): A Reliable and Valid Measure of
Disease Severity." *Neurology* 67 (3): 430–34.
https://doi.org/10.1212/01.wnl.0000228242.53336.90.

Schüle, Rebecca, and Ludger Schöls. 2011. "Genetics of Hereditary Spastic Paraplegias." *Seminars in
Neurology* 31 (05): 484–93. https://doi.org/10.1055/s-0031-1299787.

Seaman, Matthew N. J. 2019. "Back From the Brink: Retrieval of Membrane Proteins From Terminal
Compartments." *BioEssays* 41 (3): 1800146. https://doi.org/10.1002/bies.201800146.

Siddiqui, Nadeem, and Nahum Sonenberg. 2016. "Proposing a Mechanism of Action for Ataluren."
Proceedings of the National Academy of Sciences 113 (44): 12353–55.
https://doi.org/10.1073/pnas.1615548113.

Sitarska, Dominika, Anna Tylki-Szymańska, and Agnieszka Ługowska. 2021. "Treatment Trials in Niemann-Pick Type C Disease." *Metabolic Brain Disease*, no. Vanier 2013 (October). https://doi.org/10.1007/s11011-021-00842-0.

Southgate, Laura, Dimitra Dafou, Jacqueline Hoyle, Nan Li, Esther Kinning, Peter Critchley, Andrea H. Németh, et al. 2010. "Novel SPG11 Mutations in Asian Kindreds and Disruption of Spatacsin Function in the Zebrafish." *Neurogenetics* 11 (4): 379–89. https://doi.org/10.1007/s10048-010-0243-8.

Stevanin, Giovanni, Filippo M Santorelli, Hamid Azzedine, Paula Coutinho, Jacques Chomilier, Paola S Denora, Elodie Martin, et al. 2007. "Mutations in SPG11, Encoding Spatacsin, Are a Major Cause of Spastic Paraplegia with Thin Corpus Callosum." *Nature Genetics* 39 (3): 366–72. https://doi.org/10.1038/ng1980.

Subramanian, A., P. Tamayo, V. K. Mootha, S. Mukherjee, B. L. Ebert, M. A. Gillette, A. Paulovich, et al. 2005. "Gene Set Enrichment Analysis: A Knowledge-Based Approach for Interpreting Genome-Wide Expression Profiles." *Proceedings of the National Academy of Sciences* 102 (43): 15545–50. https://doi.org/10.1073/pnas.0506580102.

Swerdlow, Russell H. 2016. "Bioenergetics and Metabolism: A Bench to Bedside Perspective." *Journal of Neurochemistry* 139 (October): 126–35. https://doi.org/10.1111/jnc.13509.

Tang, Xi-Dian, Fei Gao, Ming-Jie Liu, Qin-Lei Fan, De-Kun Chen, and Wen-Tao Ma. 2019. "Methods for Enhancing Clustered Regularly Interspaced Short Palindromic Repeats/Cas9-Mediated Homology-Directed Repair Efficiency." *Frontiers in Genetics* 10 (June). https://doi.org/10.3389/fgene.2019.00551.

Tesson, Christelle, Jeanette Koht, and Giovanni Stevanin. 2015. "Delving into the Complexity of Hereditary Spastic Paraplegias: How Unexpected Phenotypes and Inheritance Modes Are Revolutionizing Their Nosology." *Human Genetics* 134 (6): 511–38. https://doi.org/10.1007/s00439-015-1536-7.

Vantaggiato, Chiara, Elena Panzeri, Marianna Castelli, Andrea Citterio, Alessia Arnoldi, Filippo Maria Santorelli, Rocco Liguori, et al. 2019. "ZFYVE26/SPASTIZIN and SPG11/SPATACSIN Mutations in Hereditary Spastic Paraplegia Types AR-SPG15 and AR-SPG11 Have Different Effects on Autophagy and Endocytosis." *Autophagy* 15 (1): 34–57. https://doi.org/10.1080/15548627.2018.1507438.

Varga, Rita-Eva, Mukhran Khundadze, Markus Damme, Sandor Nietzsche, Birgit Hoffmann, Tobias Stauber, Nicole Koch, et al. 2015. "In Vivo Evidence for Lysosome Depletion and Impaired Autophagic Clearance in Hereditary Spastic Paraplegia Type SPG11." Edited by Gregory A.

Cox. *PLOS Genetics* 11 (8): e1005454. https://doi.org/10.1371/journal.pgen.1005454.

Voets, A.M., P.J. Lindsey, S.J. Vanherle, E.D. Timmer, J.J. Esseling, W.J.H. Koopman, P.H.G.M. Willems, et al. 2012. "Patient-Derived Fibroblasts Indicate Oxidative Stress Status and May Justify Antioxidant Therapy in OXPHOS Disorders." *Biochimica et Biophysica Acta (BBA) - Bioenergetics* 1817 (11): 1971–78. https://doi.org/10.1016/j.bbabio.2012.07.001.

Wagner, Matias, Daniel P. S. Osborn, Ina Gehweiler, Maike Nagel, Ulrike Ulmer, Somayeh Bakhtiari, Rim Amouri, et al. 2019. "Bi-Allelic Variants in RNF170 Are Associated with Hereditary Spastic Paraplegia." *Nature Communications* 10 (1): 4790. https://doi.org/10.1038/s41467-019-12620-9.

Zhang, Jing, C. Dirk Keene, Catherine Pan, Kathleen S. Montine, and Thomas J. Montine. 2008. "Proteomics of Human Neurodegenerative Diseases." *Journal of Neuropathology & Experimental Neurology* 67 (10): 923–32. https://doi.org/10.1097/NEN.0b013e318187a832.

9. SUPPLEMENTARY MATERIAL

Table S1. Primers used in the study

Primer name	Sequence (from 5' to 3')	Use
SPG11-3-Fw	GTTTCACACTTCCCTTGCCTGC	qPCR
SPG11-4-Rv	AGAAATCTTGGCTGGCTCCTGT	qPCR
SPG11-16-Fw	GCATCTTCTTTATGTCTACCTTG	qPCR
SPG11-18-Rv	TGGCCTGATTGGTGGGAATC	qPCR
SPG11-38-Fw	AGGCCCAGCACTGTCAGC	qPCR
SPG11-39-Rv	GCCTCAGCCACAATAGAAGCC	qPCR
SPG11 CRISPR guide RNA 1 - forward	CACCGCGGGTTCTACCGATGCTGT	CRISPR/Cas9
SPG11 CRISPR guide RNA 1 - reverse	AAACACAGCATCGGTAGAACCCGC	CRISPR/Cas9

Table S2. List of the 421 proteins quantified through proteomic analysis. In the table are reported the logFC and the adjusted pValue of the contrasts P-NT vs C-NT and P-T vs C-NT.

Molecule	Contrast.x P-NT vs C-NT		Contrast.y P-T vs C-NT	
	logFC.x	adj.P.Val.x	logFC.y	adj.P.Val.y
sp|Q09666|AHNK	-0,30	0,0091	-0,34	0,0052
sp|P21333|FLNA	-1,39	0,0072	-1,59	0,0008
sp|P35579|MYH9	-1,27	0,0091	-1,39	0,0023
sp|P08670|VIME	0,17	0,2040	0,25	0,0549
sp|Q15149|PLEC	-0,86	0,0028	-0,97	0,0008
sp|Q14315|FLNC	-0,47	0,1478	-0,79	0,0177
sp|Q9Y490|TLN1	-0,49	0,0351	-0,62	0,0141
sp|P02545|LMNA	-0,18	0,1722	-0,16	0,2231
sp|P12814|ACTN1	-1,12	0,0091	-1,27	0,0014
sp|P11021|BIP	0,31	0,0091	0,73	0,0018
sp|P14618|KPYM	-0,35	0,0132	-0,43	0,0053
sp|P07237|PDIA1	0,43	0,0869	0,44	0,0071
sp|P07355|ANXA2	0,12	0,2029	0,13	0,3242
sp|O75369|FLNB	-0,16	0,8683	-0,33	0,7286
sp|P67936|TPM4	-0,54	0,0124	-0,69	0,0054
sp|Q00610|CLH1	-0,22	0,0650	-0,23	0,0053
sp|P02751|FINC	0,84	0,4515	-0,05	0,8815

	Contrast.x P-NT vs C-NT		Contrast.y P-T vs C-NT	
Molecule	**logFC.x**	**adj.P.Val.x**	**logFC.y**	**adj.P.Val.y**
sp|Q07065|CKAP4	0,25	0,1225	0,20	0,1444
sp|P08238|HS90B	0,40	0,2560	0,41	0,1977
sp|P18206|VINC	-0,73	0,0071	-0,91	0,0008
sp|P11142|HSP7C	-0,03	0,8748	-0,14	0,2651
sp|P07437|TBB5	-0,05	0,6132	-0,12	0,2561
sp|P04083|ANXA1	0,34	0,2070	0,32	0,1197
sp|P04406|G3P	-0,13	0,2390	-0,25	0,1702
sp|P06733|ENOA	0,19	0,2029	0,11	0,6120
sp|P04075|ALDOA	-0,09	0,7992	-0,26	0,4770
sp|P08758|ANXA5	0,53	0,1484	0,48	0,2851
sp|P30101|PDIA3	0,58	0,0101	0,88	0,0018
sp|P08133|ANXA6	-0,33	0,1484	-0,36	0,1143
sp|O43707|ACTN4	-0,93	0,0132	-1,00	0,0048
sp|P27797|CALR	0,58	0,0066	1,09	0,0002
sp|Q05682|CALD1	-1,67	0,0091	-2,08	0,0013
sp|P68104|EF1A1	-0,26	0,0650	-0,34	0,0130
sp|Q01995|TAGL	-2,30	0,0076	-2,62	0,0010
sp|P13639|EF2	0,10	0,5083	0,01	0,9684
sp|P00338|LDHA	0,31	0,3508	0,08	0,8239
sp|Q13813|SPTN1	-0,22	0,1793	-0,25	0,1452
sp|P55072|TERA	0,03	0,8030	0,08	0,5565
sp|P00558|PGK1	0,07	0,9115	-0,24	0,6714
sp|P60174|TPIS	0,14	0,7034	0,07	0,8678
sp|P14625|ENPL	0,72	0,0101	0,98	0,0018
sp|P62937|PPIA	-0,18	0,0215	-0,32	0,0130
sp|P26038|MOES	-0,18	0,2070	-0,26	0,0455
sp|Q9NZM1|MYOF	-1,07	0,0072	-1,15	0,0008
sp|P06396|GELS	-1,40	0,0076	-1,55	0,0011
sp|P50454|SERPH	-0,27	0,4913	-0,47	0,1997
sp|P09493|TPM1	-1,80	0,0042	-1,89	0,0008
sp|P63104|1433Z	0,59	0,2775	0,76	0,1252
sp|P13489|RINI	-0,10	0,3514	-0,21	0,0583
sp|P23284|PPIB	0,44	0,0869	0,49	0,0372
sp|P25705|ATPA	0,28	0,0745	0,28	0,0112
sp|O00299|CLIC1	-0,06	0,9526	0,19	0,8421
sp|Q16555|DPYL2	-0,72	0,0178	-0,79	0,0085
sp|P15144|AMPN	1,63	0,0134	1,67	0,0141
sp|P22314|UBA1	-0,01	0,9292	-0,01	0,9399
sp|Q14764|MVP	-0,73	0,0244	-0,83	0,0130
sp|P05556|ITB1	-0,36	0,1827	-0,18	0,4358

Molecule	Contrast.x P-NT vs C-NT		Contrast.y P-T vs C-NT	
	logFC.x	adj.P.Val.x	logFC.y	adj.P.Val.y
sp|P10809|CH60	0,69	0,1334	0,59	0,1397
sp|P30041|PRDX6	-0,83	0,0046	-0,85	0,0008
sp|Q15084|PDIA6	0,48	0,0134	0,75	0,0014
sp|P06576|ATPB	0,34	0,0378	0,31	0,0053
sp|P04792|HSPB1	-2,17	0,0233	-2,16	0,0163
sp|P02452|CO1A1	0,43	0,5659	-0,15	0,8308
sp|Q14697|GANAB	0,63	0,1377	0,42	0,2642
sp|P19338|NUCL	0,46	0,2227	0,25	0,1974
sp|P18669|PGAM1	0,28	0,2159	0,08	0,8678
sp|Q01082|SPTB2	-0,44	0,0262	-0,56	0,0023
sp|P62736|ACTA	-2,67	0,0072	-3,01	0,0008
sp|O43852|CALU	-0,36	0,0650	-0,26	0,0372
sp|P23396|RS3	0,16	0,4716	0,08	0,7355
sp|P23528|COF1	-0,27	0,0326	-0,44	0,0061
sp|P07737|PROF1	-0,55	0,0326	-0,59	0,0210
sp|P09382|LEG1	-0,09	0,3042	-0,10	0,2717
sp|Q06830|PRDX1	0,02	0,8837	-0,24	0,2582
sp|P62805|H4	0,50	0,0496	0,47	0,0359
sp|O60701|UGDH	-0,44	0,0714	-0,44	0,0353
sp|P26641|EF1G	0,03	0,8784	-0,09	0,5174
sp|P61978|HNRPK	0,36	0,0874	0,29	0,0827
sp|Q9P2E9|RRBP1	0,28	0,0251	0,19	0,0955
sp|Q9ULV4|COR1C	-0,45	0,0028	-0,52	0,0028
sp|P63244|RACK1	0,11	0,6981	-0,03	0,9257
sp|O75083|WDR1	-0,68	0,0072	-0,74	0,0014
sp|Q99877|H2B1N	1,20	0,2165	1,23	0,2007
sp|P07900|HS90A	0,02	0,9027	-0,13	0,3791
sp|P09211|GSTP1	-0,24	0,4780	-0,31	0,3863
sp|P42224|STAT1	-1,56	0,0091	-1,72	0,0045
sp|P0DMV9|HS71B	0,22	0,0869	0,13	0,3161
sp|P07602|SAP	0,06	0,8774	0,05	0,8815
sp|P10412|H14	0,67	0,0481	0,90	0,0090
sp|P27824|CALX	0,38	0,0366	0,44	0,0164
sp|P37802|TAGL2	-0,42	0,1007	-0,50	0,1355
sp|P62424|RL7A	0,02	0,8493	-0,07	0,6576
sp|P21589|5NTD	0,55	0,1012	0,57	0,0556
sp|P51149|RAB7A	0,12	0,5944	0,02	0,9191
sp|O60664|PLIN3	-0,01	0,9662	0,01	0,9509
sp|P27348|1433T	0,24	0,4162	0,17	0,3862
sp|Q71DI3|H32	0,60	0,0283	0,60	0,0188

	Contrast.x P-NT vs C-NT		Contrast.y P-T vs C-NT	
Molecule	logFC.x	adj.P.Val.x	logFC.y	adj.P.Val.y
sp|P05387|RLA2	0,14	0,2159	0,03	0,8526
sp|Q96AG4|LRC59	0,48	0,0145	0,44	0,0300
sp|P60660|MYL6	-1,10	0,0143	-1,28	0,0071
sp|Q99497|PARK7	-0,12	0,3042	-0,28	0,0583
sp|P16152|CBR1	-0,35	0,0154	-0,34	0,0141
sp|P30050|RL12	0,14	0,4544	-0,04	0,5933
sp|P29401|TKT	0,04	0,8690	-0,08	0,8012
sp|P22626|ROA2	0,28	0,3163	0,40	0,0378
sp|P21980|TGM2	-3,37	0,0007	-3,20	0,0001
sp|P31949|S10AB	-0,69	0,0008	-0,68	0,0001
sp|P29692|EF1D	-0,01	0,9275	-0,06	0,4071
sp|P08865|RSSA	0,24	0,3482	0,20	0,2183
sp|P07195|LDHB	0,19	0,4753	0,10	0,7813
sp|P13674|P4HA1	0,42	0,4544	0,01	0,9826
sp|Q8NHW5|RLA0L	0,06	0,7690	-0,01	0,9509
sp|Q16658|FSCN1	0,06	0,8784	0,04	0,9416
sp|P12956|XRCC6	0,23	0,2464	0,20	0,5036
sp|P21796|VDAC1	0,44	0,0553	0,23	0,1665
sp|P62269|RS18	0,43	0,1509	0,34	0,2240
sp|P40926|MDHM	0,28	0,1986	0,29	0,0393
sp|P46940|IQGA1	-0,36	0,0251	-0,39	0,0068
sp|O00159|MYO1C	-0,51	0,2526	-0,50	0,2085
sp|P17931|LEG3	0,31	0,4389	-0,02	0,9687
sp|P61158|ARP3	-0,30	0,1612	-0,45	0,0724
sp|Q9NR12|PDLI7	-1,53	0,0101	-1,91	0,0001
sp|P16401|H15	1,24	0,0326	1,34	0,0071
sp|P19105|ML12A	-1,14	0,0101	-1,23	0,0045
sp|P61604|CH10	0,66	0,1562	0,54	0,1274
sp|P04843|RPN1	0,28	0,0154	0,21	0,0353
sp|P16070|CD44	0,69	0,0707	0,66	0,0676
sp|P62826|RAN	0,49	0,1116	0,40	0,0703
sp|P16104|H2AX	0,50	0,2122	0,43	0,2642
sp|Q15365|PCBP1	0,14	0,4863	0,13	0,5295
sp|P39019|RS19	0,15	0,3461	0,04	0,7813
sp|P13667|PDIA4	0,53	0,0091	0,71	0,0008
sp|P30086|PEBP1	0,06	0,5610	-0,09	0,4142
sp|Q99439|CNN2	-0,49	0,2688	-0,56	0,2318
sp|P62241|RS8	-0,47	0,5733	-0,58	0,5310
sp|Q01518|CAP1	-0,59	0,0091	-0,67	0,0008
sp|Q02878|RL6	0,29	0,2070	0,45	0,3242

	Contrast.x P-NT vs C-NT		Contrast.y P-T vs C-NT	
Molecule	logFC.x	adj.P.Val.x	logFC.y	adj.P.Val.y
sp|P07339|CATD	-0,55	0,0984	-0,73	0,0583
sp|P50395|GDIB	-0,12	0,1583	-0,04	0,6348
sp|P35232|PHB	0,38	0,1282	0,46	0,0280
sp|P60842|IF4A1	0,11	0,6171	0,03	0,9166
sp|Q9BUF5|TBB6	-0,47	0,0887	-0,57	0,0514
sp|P07858|CATB	-0,19	0,7968	-0,36	0,6360
sp|P31943|HNRH1	0,29	0,3132	0,31	0,2642
sp|P22392|NDKB	0,07	0,6969	0,07	0,6827
sp|P08123|CO1A2	0,18	0,7690	-0,02	0,9683
sp|P08134|RHOC	-0,24	0,3099	-0,28	0,1374
sp|P02768|ALBU	0,70	0,6802	0,51	0,7006
sp|P45880|VDAC2	-0,17	0,2269	-0,17	0,1259
sp|P36578|RL4	0,21	0,3132	0,10	0,3461
sp|P62249|RS16	0,10	0,6733	-0,03	0,9191
sp|Q96AY3|FKB10	0,20	0,6674	0,25	0,4384
sp|P09651|ROA1	0,59	0,1570	0,54	0,1978
sp|P62328|TYB4	0,03	0,8866	0,05	0,8982
sp|P06748|NPM	0,17	0,3986	0,23	0,2549
sp|O43175|SERA	-0,20	0,5189	-0,33	0,3863
sp|P15880|RS2	0,38	0,0308	0,08	0,6256
sp|Q9UHD8|SEPT9	-0,52	0,0132	-0,62	0,0014
sp|Q14103|HNRPD	0,62	0,0525	0,60	0,0264
sp|P00387|NB5R3	-0,42	0,0869	-0,51	0,0247
sp|P27816|MAP4	-0,38	0,0595	-0,35	0,0059
sp|P00441|SODC	-0,35	0,6774	-0,35	0,6878
sp|O15460|P4HA2	0,04	0,9115	-0,14	0,5310
sp|P62987|RL40	0,14	0,7437	0,38	0,4257
sp|P01023|A2MG	-0,04	0,9526	-0,04	0,9399
sp|Q9NVA2|SEP11	-0,25	0,2253	-0,38	0,0549
sp|P50990|TCPQ	0,37	0,1008	0,17	0,3345
sp|Q07020|RL18	0,06	0,8866	-0,23	0,6892
sp|Q8NBS9|TXND5	0,45	0,0276	0,42	0,0107
sp|P21291|CSRP1	-3,16	0,0017	-4,24	0,0000
sp|P13987|CD59	0,23	0,2656	-0,23	0,2642
sp|P25398|RS12	0,07	0,6802	0,00	0,9933
sp|Q6NZI2|CAVN1	-0,22	0,4863	-0,30	0,1595
sp|P62851|RS25	-0,19	0,3744	-0,07	0,8005
sp|Q7KZF4|SND1	-0,05	0,8553	-0,17	0,5598
sp|P62820|RAB1A	0,28	0,1852	0,33	0,1967
sp|P49368|TCPG	0,28	0,2259	0,21	0,2050

	Contrast.x P-NT vs C-NT		Contrast.y P-T vs C-NT	
Molecule	logFC.x	adj.P.Val.x	logFC.y	adj.P.Val.y
sp|P09936|UCHL1	-0,27	0,4996	-0,16	0,7118
sp|P0DP25|CALM3	-0,32	0,0419	-0,35	0,0061
sp|Q99584|S10AD	0,74	0,3163	-0,14	0,9013
sp|P40925|MDHC	0,18	0,0869	0,11	0,1792
sp|P26447|S10A4	-0,30	0,5137	-0,39	0,4132
sp|Q00839|HNRPU	0,56	0,0215	0,70	0,0363
sp|O60506|HNRPQ	0,05	0,9115	0,05	0,9131
sp|P55084|ECHB	0,44	0,2455	0,37	0,3304
sp|P09496|CLCA	1,09	0,1236	0,88	0,1962
sp|P12110|CO6A2	0,72	0,0219	0,80	0,0228
sp|P16615|AT2A2	0,61	0,2316	0,51	0,4047
sp|Q00341|VIGLN	0,00	0,9998	-0,16	0,6706
sp|P68371|TBB4B	-0,29	0,1276	-0,36	0,0353
sp|P46782|RS5	0,06	0,6620	-0,01	0,9683
sp|P30044|PRDX5	-0,39	0,1236	-0,39	0,1185
sp|P41250|GARS	-0,77	0,0243	-0,59	0,0100
sp|P30048|PRDX3	0,65	0,1357	0,61	0,0785
sp|P62244|RS15A	0,05	0,8482	-0,13	0,6567
sp|O00264|PGRC1	1,17	0,0113	0,97	0,0248
sp|P13797|PLST	0,07	0,8863	0,19	0,1974
sp|P50502|F10A1	-0,02	0,7515	-0,13	0,0431
sp|O00410|IPO5	-0,07	0,3201	-0,10	0,4357
sp|P12109|CO6A1	0,60	0,0366	0,41	0,0407
sp|P26373|RL13	-0,11	0,5580	-0,12	0,5933
sp|P18085|ARF4	-0,09	0,2903	0,00	0,9826
sp|Q9Y617|SERC	-1,08	0,0180	-1,39	0,0108
sp|P10599|THIO	-0,12	0,5914	-0,08	0,6769
sp|Q14974|IMB1	0,48	0,7697	0,11	0,9509
sp|Q99715|COCA1	2,29	0,0869	2,04	0,1931
sp|Q9NZN4|EHD2	-0,21	0,3261	-0,36	0,0546
sp|P78417|GSTO1	-0,05	0,8772	-0,04	0,8815
sp|P17987|TCPA	-0,52	0,6549	-0,81	0,5395
sp|P06744|G6PI	-0,44	0,2071	-0,79	0,0456
sp|P18124|RL7	0,04	0,8953	0,03	0,9257
sp|P60891|PRPS1	1,79	0,2587	1,38	0,4132
sp|Q14847|LASP1	-1,17	0,0091	-1,09	0,0034
sp|P07996|TSP1	-0,16	0,8021	0,09	0,9077
sp|P06703|S10A6	0,12	0,7034	0,08	0,6185
sp|P53396|ACLY	-0,08	0,7975	-0,24	0,1197
sp|P04216|THY1	-0,93	0,0348	-0,91	0,0546

	Contrast.x P-NT vs C-NT		Contrast.y P-T vs C-NT	
Molecule	logFC.x	adj.P.Val.x	logFC.y	adj.P.Val.y
sp|P37837|TALDO	-0,21	0,2119	-0,15	0,2110
sp|Q86VP6|CAND1	0,02	0,8866	-0,15	0,4682
sp|P61247|RS3A	-0,06	0,7427	-0,14	0,4834
sp|P62753|RS6	-0,12	0,5517	-0,20	0,5941
sp|P32969|RL9	0,12	0,6248	0,00	0,9933
sp|P60953|CDC42	-0,28	0,0694	-0,32	0,0175
sp|P60981|DEST	-1,20	0,0071	-1,18	0,0102
sp|Q15942|ZYX	-0,64	0,0126	-0,83	0,0029
sp|Q15366|PCBP2	0,19	0,5862	0,19	0,5087
sp|P78371|TCPB	0,21	0,2609	0,13	0,3454
sp|P31946|1433B	-0,11	0,6814	-0,14	0,5846
sp|P62277|RS13	-0,05	0,8021	-0,15	0,4263
sp|Q9UBG0|MRC2	1,59	0,0567	1,11	0,0583
sp|P24534|EF1B	-0,12	0,7216	-0,14	0,7097
sp|Q9BS26|ERP44	0,14	0,5517	-0,03	0,8815
sp|P50995|ANX11	0,04	0,8333	-0,04	0,7863
sp|P62258|1433E	0,00	0,9794	-0,02	0,9191
sp|Q14204|DYHC1	-0,45	0,2070	-0,28	0,3691
sp|P63241|IF5A1	0,23	0,3461	0,23	0,3573
sp|P38646|GRP75	0,41	0,2614	0,39	0,1868
sp|P39656|OST48	0,18	0,5070	0,06	0,8154
sp|P04632|CPNS1	-0,22	0,1334	-0,29	0,0163
sp|P84098|RL19	1,58	0,2540	-0,16	0,8713
sp|Q96D15|RCN3	0,72	0,0326	0,74	0,0210
sp|P62701|RS4X	0,21	0,2243	0,04	0,8421
sp|P16949|STMN1	0,71	0,0839	0,62	0,0428
sp|P60866|RS20	0,32	0,1259	0,15	0,5598
sp|P07910|HNRPC	0,34	0,2614	0,34	0,3242
sp|P04080|CYTB	-0,04	0,8542	-0,06	0,8073
sp|P38159|RBMX	0,54	0,0248	0,51	0,0134
sp|P62829|RL23	0,13	0,4753	0,06	0,6739
sp|Q15293|RCN1	0,78	0,0735	0,49	0,2582
sp|Q13162|PRDX4	0,42	0,0650	0,31	0,1188
sp|P46781|RS9	0,23	0,4708	-0,14	0,7829
sp|Q13838|DX39B	0,36	0,0869	0,33	0,0556
sp|Q969G5|CAVN3	-0,09	0,7690	-0,11	0,6120
sp|P49327|FAS	0,18	0,6674	0,21	0,6878
sp|O95782|AP2A1	-0,19	0,8748	0,11	0,9336
sp|P62263|RS14	0,04	0,8519	0,12	0,5598
sp|Q8TAA3|PSMA8	0,10	0,6802	0,04	0,8815

	Contrast.x P-NT vs C-NT		Contrast.y P-T vs C-NT	
Molecule	logFC.x	adj.P.Val.x	logFC.y	adj.P.Val.y
sp|P62913|RL11	0,04	0,8562	0,02	0,8678
sp|P17655|CAN2	-0,34	0,1205	-0,34	0,0475
sp|Q9NQC3|RTN4	-0,25	0,4160	-0,48	0,1862
sp|Q03135|CAV1	-0,22	0,3261	-0,25	0,2007
sp|P52565|GDIR1	-0,32	0,0874	-0,38	0,0540
sp|P04264|K2C1	2,04	0,2243	1,33	0,5547
sp|P55145|MANF	2,46	0,1450	2,25	0,2131
sp|P15311|EZRI	-1,64	0,2840	-1,54	0,3052
sp|P49411|EFTU	0,13	0,8021	0,37	0,4451
sp|P61981|1433G	-0,11	0,5113	-0,13	0,2265
sp|P47756|CAPZB	-0,12	0,3607	-0,18	0,1299
sp|Q02952|AKA12	-0,47	0,3393	-0,20	0,6827
sp|P42765|THIM	0,10	0,8737	0,42	0,3343
sp|Q13642|FHL1	1,29	0,3069	0,86	0,3598
sp|Q15019|SEPT2	-0,54	0,0326	-0,59	0,0085
sp|P62917|RL8	-0,16	0,4802	-0,03	0,8678
sp|Q14019|COTL1	0,94	0,0326	0,81	0,0112
sp|P11940|PABP1	0,19	0,4515	0,03	0,9166
sp|Q15746|MYLK	-2,02	0,0135	-2,50	0,0032
sp|P46821|MAP1B	-0,70	0,0113	-0,70	0,0073
sp|P40121|CAPG	0,62	0,0745	0,56	0,0359
sp|P62942|FKB1A	-0,01	0,9678	-0,16	0,4515
sp|P50914|RL14	-0,05	0,8205	-0,19	0,3097
sp|Q9UBR2|CATZ	0,27	0,6345	0,15	0,7863
sp|Q15185|TEBP	0,24	0,4780	0,23	0,6348
sp|P52209|6PGD	0,62	0,0735	0,49	0,0703
sp|Q9NR31|SAR1A	0,42	0,0276	0,45	0,0162
sp|P07741|APT	-0,42	0,0322	-0,65	0,0495
sp|P83731|RL24	-0,11	0,7049	-0,07	0,7097
sp|P68363|TBA1B	-0,10	0,6747	0,01	0,9808
sp|Q13885|TBB2A	-1,27	0,0007	-1,24	0,0008
sp|P12236|ADT3	0,26	0,4863	0,29	0,1997
sp|P24844|MYL9	-1,92	0,0091	-2,22	0,0014
sp|P11279|LAMP1	-0,65	0,0869	-0,60	0,0455
sp|P14174|MIF	-0,05	0,8784	-0,16	0,6878
sp|Q9H299|SH3L3	-0,30	0,2526	-0,17	0,5329
sp|P69905|HBA	2,00	0,0545	1,94	0,0279
sp|P60903|S10AA	1,79	0,2390	1,60	0,3145
sp|P60033|CD81	-0,35	0,7652	-0,51	0,6767
sp|Q9Y281|COF2	-0,16	0,8382	-0,02	0,9826

	Contrast.x P-NT vs C-NT		Contrast.y P-T vs C-NT	
Molecule	logFC.x	adj.P.Val.x	logFC.y	adj.P.Val.y
sp|O60493|SNX3	0,01	0,9700	-0,05	0,6706
sp|Q07955|SRSF1	0,11	0,7049	0,04	0,8678
sp|P53999|TCP4	0,92	0,1276	0,74	0,1009
sp|Q9BTV4|TMM43	0,16	0,3163	0,10	0,6357
sp|P14314|GLU2B	0,05	0,8716	0,05	0,8421
sp|Q00325|MPCP	0,65	0,4395	0,19	0,8815
sp|P22061|PIMT	-0,03	0,9731	-0,28	0,8421
sp|O95302|FKBP9	0,81	0,1986	0,51	0,4060
sp|P23526|SAHH	0,62	0,5402	0,36	0,7654
sp|O15511|ARPC5	-0,54	0,0076	-0,61	0,0045
sp|P0DME0|SETLP	0,18	0,8401	0,24	0,7858
sp|Q15075|EEA1	0,77	0,0901	0,60	0,0890
sp|P61224|RAP1B	0,26	0,2841	0,14	0,5310
sp|P02461|CO3A1	2,22	0,0869	1,37	0,0785
sp|P61353|RL27	0,27	0,2425	0,19	0,2231
sp|P18621|RL17	0,77	0,0513	0,58	0,0665
sp|O15173|PGRC2	-0,15	0,7334	-0,32	0,3625
sp|P61254|RL26	-0,76	0,3647	-0,36	0,6706
sp|P00367|DHE3	0,07	0,6951	0,14	0,3300
sp|P61313|RL15	1,29	0,3112	0,75	0,5092
sp|Q14195|DPYL3	-0,23	0,0869	-0,34	0,0071
sp|P50991|TCPD	0,37	0,1570	0,32	0,1997
sp|O75396|SC22B	0,06	0,7427	-0,06	0,7822
sp|Q8WUM4|PDC6I	-0,32	0,1236	-0,37	0,0387
sp|P20618|PSB1	0,20	0,5974	-0,06	0,9191
sp|Q01813|PFKAP	-0,51	0,0326	-0,66	0,0151
sp|P54577|SYYC	1,01	0,4253	0,89	0,5087
sp|Q15121|PEA15	-0,20	0,6399	-0,45	0,3345
sp|P36871|PGM1	-0,34	0,4713	-0,38	0,3863
sp|P04439|HLAA	-0,42	0,0869	-0,79	0,0016
sp|P40261|NNMT	1,36	0,1625	1,18	0,2596
sp|Q16851|UGPA	-0,17	0,8650	0,30	0,7151
sp|Q9UBI6|GBG12	-0,83	0,0132	-0,84	0,0210
sp|P13693|TCTP	0,26	0,4716	0,18	0,6294
sp|P15559|NQO1	-0,67	0,6620	-1,74	0,4230
sp|Q96TA1|NIBA2	-0,53	0,0126	-0,64	0,0014
sp|P55209|NP1L1	-0,83	0,5610	-0,48	0,7190
sp|Q99536|VAT1	0,18	0,9186	0,77	0,6395
sp|Q969H8|MYDGF	0,31	0,8197	0,36	0,8005
sp|P40227|TCPZ	0,14	0,5157	0,10	0,6706

	Contrast.x P-NT vs C-NT		Contrast.y P-T vs C-NT	
Molecule	logFC.x	adj.P.Val.x	logFC.y	adj.P.Val.y
sp|P05120|PAI2	0,87	0,6106	0,73	0,6714
sp|Q12907|LMAN2	0,28	0,0714	0,30	0,0102
sp|P28066|PSA5	0,04	0,8059	-0,11	0,5506
sp|Q9Y678|COPG1	0,70	0,3571	0,58	0,4539
sp|P35613|BASI	-0,33	0,2925	-0,48	0,0707
sp|O94979|SC31A	-0,56	0,1276	-0,30	0,3052
sp|Q96CW1|AP2M1	-0,12	0,3302	-0,17	0,1093
sp|O94925|GLSK	0,24	0,5645	0,11	0,7935
sp|P30040|ERP29	0,35	0,0714	0,22	0,3055
sp|P14866|HNRPL	0,24	0,4097	0,17	0,2851
sp|P11766|ADHX	2,66	0,1334	2,00	0,1353
sp|P23246|SFPQ	0,42	0,1484	0,37	0,1997
sp|P07814|SYEP	-0,62	0,0241	-0,47	0,0785
sp|P62273|RS29	-0,61	0,2746	0,00	0,9966
sp|P25786|PSA1	-0,30	0,4681	-0,12	0,4325
sp|Q6EMK4|VASN	-0,09	0,8815	0,95	0,0195
sp|P62899|RL31	0,10	0,6620	0,17	0,3863
sp|E9PAV3|NACAM	0,17	0,2929	0,15	0,4152
sp|P46776|RL27A	0,02	0,9588	-0,12	0,6769
sp|P51911|CNN1	-3,41	0,0028	-3,24	0,0008
sp|Q14247|SRC8	-0,94	0,0277	-1,23	0,0188
sp|P28300|LYOX	0,29	0,8021	0,21	0,8662
sp|P04179|SODM	0,51	0,3881	0,62	0,5028
sp|P49591|SYSC	-0,59	0,0707	-0,68	0,2475
sp|P34932|HSP74	-0,16	0,4780	-0,36	0,2085
sp|O43399|TPD54	-0,12	0,3514	-0,08	0,5310
sp|P68402|PA1B2	-0,46	0,0439	-0,36	0,0749
sp|P49257|LMAN1	0,67	0,4928	0,89	0,3363
sp|P62750|RL23A	0,81	0,6802	0,54	0,8239
sp|Q9NZU5|LMCD1	-0,88	0,1484	-1,50	0,0279
sp|P09486|SPRC	-0,95	0,0312	-0,87	0,0009
sp|Q02543|RL18A	0,00	0,9998	-0,05	0,8678
sp|Q9UBY9|HSPB7	-0,57	0,2917	-0,89	0,1454
sp|P13010|XRCC5	0,68	0,0419	0,57	0,0359
sp|P48444|COPD	-0,46	0,2618	0,06	0,6023
sp|O75915|PRAF3	0,35	0,2841	0,24	0,8012
sp|O15143|ARC1B	-0,50	0,0480	-0,57	0,0314
sp|P40939|ECHA	1,19	0,3980	0,23	0,9166
sp|O75347|TBCA	0,00	0,9806	-0,10	0,5933
sp|Q07954|LRP1	0,11	0,6969	-0,01	0,9826

	Contrast.x P-NT vs C-NT		Contrast.y P-T vs C-NT	
Molecule	logFC.x	adj.P.Val.x	logFC.y	adj.P.Val.y
sp|P46783|RS10	0,14	0,4887	0,13	0,6311
sp|Q70UQ0|IKIP	-0,07	0,6171	-0,03	0,8466
sp|P98082|DAB2	1,05	0,1478	-0,25	0,8550
sp|Q92804|RBP56	0,61	0,1583	0,68	0,1197
sp|Q9BVC6|TM109	0,18	0,3443	0,06	0,8112
sp|P54136|SYRC	0,52	0,5611	0,49	0,6048
sp|P62857|RS28	0,06	0,6969	0,00	0,9826
sp|O60888|CUTA	-0,60	0,7034	-1,17	0,5565
sp|Q99729|ROAA	0,53	0,1852	0,59	0,0276
sp|P07093|GDN	-0,25	0,7220	-0,40	0,6706
sp|P02765|FETUA	0,58	0,6750	0,68	0,6120
sp|P61204|ARF3	-0,02	0,9597	0,04	0,9065
sp|Q9BSJ8|ESYT1	-0,44	0,1334	-0,54	0,0214
sp|P62266|RS23	-0,07	0,8519	0,03	0,9460
sp|P51571|SSRD	0,40	0,0998	0,39	0,0713
sp|P61019|RAB2A	0,61	0,4716	0,79	0,3052
sp|P62854|RS26	0,36	0,2227	0,23	0,3862
sp|P26368|U2AF2	0,26	0,1570	0,28	0,1868
sp|O75368|SH3L1	-0,49	0,1259	-0,80	0,0173
sp|Q9BQB6|VKOR1	-0,04	0,8866	-0,10	0,7258
sp|Q6EEV6|SUMO4	0,40	0,0317	0,27	0,0932
sp|P62861|RS30	-0,40	0,2440	-0,06	0,8713
sp|P00568|KAD1	-0,59	0,0161	-0,68	0,0053
sp|Q92973|TNPO1	-0,13	0,2925	-0,13	0,1073
sp|P46779|RL28	0,27	0,2165	0,20	0,3242
sp|Q15436|SC23A	1,07	0,4753	0,57	0,7705
sp|P62837|UB2D2	-0,12	0,7053	0,05	0,8421
sp|P58546|MTPN	0,08	0,6969	-0,12	0,6357
sp|O14773|TPP1	-0,27	0,4716	-0,54	0,1185
sp|P09497|CLCB	-0,83	0,0028	-0,78	0,0008
sp|O00151|PDLI1	-0,62	0,2070	-0,72	0,1009
sp|P55786|PSA	-0,11	0,9490	0,37	0,8185
sp|O95394|AGM1	0,22	0,1484	0,17	0,3363
sp|Q08431|MFGM	-2,61	0,0091	-2,43	0,0071
sp|P11166|GTR1	0,40	0,5610	0,21	0,8239
sp|Q13509|TBB3	0,30	0,1478	0,34	0,3161
sp|P35221|CTNA1	0,08	0,9373	-0,31	0,8102
sp|Q99832|TCPH	0,14	0,5517	0,10	0,6023
sp|Q13555|KCC2G	-0,40	0,1067	-0,57	0,0050
sp|P17661|DESM	0,76	0,5547	-0,23	0,8223

Molecule	Contrast.x P-NT vs C-NT		Contrast.y P-T vs C-NT	
	logFC.x	adj.P.Val.x	logFC.y	adj.P.Val.y
sp|O75718|CRTAP	-0,23	0,7014	0,24	0,4258
sp|Q06033|ITIH3	-0,65	0,0134	-0,23	0,1312
sp|P30085|KCY	-0,79	0,0497	-0,71	0,0141
sp|P62910|RL32	0,00	0,9998	-0,06	0,8154

Table S3. List of the 137 lipid species identified through lipid r analysis. In the table are reported the logFC and the adjusted pValue of the contrasts P-NT vs C-NT and P-T vs C-NT.

Lipid species	Lipid Class	Contrast.x P-NT vs C-NT		Contrast.y P-T vs C-NT	
		logFC.x	adj.P.Val.x	logFC.y	adj.P.Val.y
CE(14:0)	CE	-0,61	0,0595	-0,47	0,2022
CE(16:0)	CE	-0,82	0,0322	-0,69	0,0295
CE(16:2)	CE	-0,62	0,0500	-0,55	0,0664
CE(17:0)	CE	-0,46	0,1374	-0,30	0,3670
CE(17:1)	CE	-0,35	0,2473	-0,12	0,6856
CE(18:0)	CE	-0,51	0,2019	-0,41	0,2311
CE(18:1)	CE	-0,42	0,1217	-0,35	0,3181
CE(18:2)	CE	-0,68	0,0422	-0,58	0,1418
CE(18:3)	CE	-1,18	0,0049	-0,77	0,0816
CE(20:1)	CE	0,37	0,1948	0,47	0,2246
CE(20:2)	CE	0,59	0,0322	0,70	0,0963
CE(20:3)	CE	0,05	0,8841	0,29	0,5150
CE(20:4)	CE	-0,23	0,7041	0,04	0,9409
CE(22:0)	CE	0,05	0,9037	0,09	0,9099
CE(22:4)	CE	1,12	0,0422	1,48	0,0245
CE(22:5)	CE	0,39	0,3059	0,72	0,1283
CE(22:6)	CE	0,07	0,8434	0,15	0,7470
Cer(d18:0/16:0)	Cer	-0,29	0,4361	-0,26	0,3901
Cer(d18:0/24:0)	Cer	-0,09	0,7610	0,06	0,8511
Cer(d18:0/24:1)	Cer	0,38	0,2774	0,52	0,1939
Cer(d18:1/16:0)	Cer	-0,35	0,2751	-0,29	0,3603
Cer(d18:1/18:0)	Cer	-0,27	0,7307	-0,07	0,9239
Cer(d18:1/20:0)	Cer	0,07	0,9308	0,18	0,8405
Cer(d18:1/22:0)	Cer	0,57	0,2482	0,82	0,0149
Cer(d18:1/23:0)	Cer	0,36	0,4592	0,66	0,0149
Cer(d18:1/24:0)	Cer	-0,13	0,7370	0,06	0,8259
Cer(d18:1/24:1)	Cer	0,61	0,1358	0,72	0,0440
Cer(d18:1/25:0)	Cer	0,44	0,1757	0,98	0,0002
Cer(d18:2/22:0)	Cer	-1,13	0,0222	-0,97	0,0054
Cer(d18:2/23:1)	Cer	-2,06	0,0000	-3,82	0,0002

Lipid species	Lipid Class	Contrast.x P-NT vs C-NT		Contrast.y P-T vs C-NT	
		logFC.x	adj.P.Val.x	logFC.y	adj.P.Val.y
DG(34:1)	DG	0,71	0,0113	0,64	0,0393
DG(36:0)	DG	2,35	0,0362	2,54	0,0054
DG(36:1)	DG	0,72	0,0114	0,67	0,0132
DG(38:5)	DG	1,38	0,0006	1,52	0,0001
DG(38:6)	DG	1,17	0,0031	1,18	0,0001
DG(40:6)	DG	1,21	0,0049	1,30	0,0002
DG(40:7)	DG	1,08	0,0113	1,10	0,0004
GM2(d18:1/16:0)	GM2	-0,32	0,6832	-0,98	0,0592
GM2(d18:1/22:0)	GM2	-0,99	0,1268	-1,84	0,0084
GM2(d18:1/24:0)	GM2	-0,96	0,1290	-1,60	0,0047
GM2(d18:1/24:1(15Z))	GM2	-0,81	0,1948	-1,56	0,0208
GM3(d18:1/16:0)	GM3	-0,80	0,0422	-1,97	0,0008
GM3(d18:1/18:0)	GM3	-1,18	0,0148	-1,93	0,0014
GM3(d18:1/22:0)	GM3	-0,63	0,0662	-1,80	0,0003
GM3(d18:1/24:0)	GM3	-1,00	0,0063	-2,01	0,0003
GM3(d18:1/24:1(15Z))	GM3	-0,55	0,0780	-1,75	0,0004
GM3(d18:1/26:0)	GM3	-1,00	0,0293	-1,88	0,0020
GM3(d18:1/26:1(17Z))	GM3	-0,68	0,1358	-2,16	0,0096
LPC(16:0)	LPC	2,26	0,0011	1,32	0,0015
LPC(16:0e)	LPC	2,82	0,0006	1,86	0,0004
LPC(16:0p)	LPC	0,12	0,7173	-0,44	0,0963
LPC(16:1)	LPC	3,05	0,0007	2,01	0,0001
LPC(18:0)	LPC	0,52	0,1215	-0,15	0,6764
LPC(18:0e)	LPC	1,42	0,0050	0,65	0,1117
LPC(18:1)	LPC	2,99	0,0006	2,03	0,0004
LPC(18:2)	LPC	3,05	0,0003	2,08	0,0015
LPC(20:3)	LPC	3,17	0,0000	2,19	0,0015
LPC(20:4)	LPC	3,37	0,0000	2,52	0,0004
LPC(22:5)	LPC	2,77	0,0007	2,05	0,0007
LPC(22:6)	LPC	2,55	0,0006	1,74	0,0010
LPE(16:0)	LPE	1,80	0,0039	1,36	0,0072
LPE(18:0)	LPE	1,46	0,0006	0,99	0,0060
LPE(18:1)	LPE	1,59	0,0026	1,12	0,0054
LPE(18:2)	LPE	1,58	0,0034	1,18	0,0072
LPE(20:4)	LPE	0,74	0,0741	0,44	0,2531
LPE(22:6)	LPE	-0,41	0,3615	-0,75	0,0772
PC(32:0)	PC	0,45	0,0401	0,43	0,0908
PC(32:1)	PC	0,03	0,9037	0,03	0,9239
PC(32:2)	PC	-0,23	0,4872	-0,24	0,5150
PC(34:0)	PC	0,13	0,3860	0,12	0,4034

Lipid species	Lipid Class	Contrast.x P-NT vs C-NT		Contrast.y P-T vs C-NT	
		logFC.x	adj.P.Val.x	logFC.y	adj.P.Val.y
PC(34:1)	PC	0,07	0,8090	0,13	0,6516
PC(34:2)	PC	0,00	0,9981	0,00	0,9930
PC(34:3)	PC	-0,59	0,0286	-0,56	0,0257
PC(36:0)	PC	-0,48	0,0225	-0,46	0,0315
PC(36:1)	PC	-0,34	0,0545	-0,27	0,1418
PC(36:2)	PC	0,09	0,6329	0,11	0,4862
PC(36:3)	PC	-0,06	0,8101	-0,06	0,7893
PC(36:4)	PC	-0,03	0,8472	-0,02	0,9334
PC(36:5)	PC	-0,43	0,0976	-0,48	0,0734
PC(38:2)	PC	0,44	0,0605	0,60	0,0096
PC(38:4)	PC	-0,09	0,7083	0,05	0,8207
PC(38:5)	PC	0,07	0,7307	0,16	0,2885
PC(38:6)	PC	-0,16	0,3813	-0,16	0,4038
PC(40:2)	PC	0,86	0,0030	1,14	0,0001
PC(40:4)	PC	0,58	0,1023	0,81	0,0072
PC(40:5)	PC	0,19	0,5715	0,37	0,0924
PC(40:6)	PC	0,11	0,7307	0,25	0,2304
PC(40:7)	PC	-0,08	0,8364	0,00	0,9861
PC(40:8)	PC	-0,54	0,3010	-0,40	0,2246
PE(34:0)	PE	0,07	0,8090	0,04	0,9093
PE(34:1)	PE	-0,07	0,8364	-0,09	0,8316
PE(34:2)	PE	-0,44	0,1844	-0,48	0,1717
PE(36:0)	PE	-0,31	0,1176	-0,27	0,2246
PE(36:1)	PE	-0,33	0,1010	-0,28	0,2491
PE(36:2)	PE	-0,41	0,0780	-0,35	0,2107
PE(36:3)	PE	-0,60	0,0184	-0,53	0,0393
PE(36:4)	PE	-0,18	0,5922	-0,10	0,8207
PE(36:5)	PE	-0,63	0,1844	-0,63	0,2311
PE(38:1)	PE	-0,34	0,2482	-0,33	0,2022
PE(38:2)	PE	-0,01	0,9559	0,01	0,9655
PE(38:3)	PE	-0,34	0,1610	-0,28	0,1283
PE(38:4)	PE	0,08	0,7041	0,22	0,2246
PE(38:5)	PE	-0,23	0,3816	-0,12	0,7470
PE(38:6)	PE	-0,70	0,1684	-0,73	0,1198
PE(40:1)	PE	0,50	0,0261	0,38	0,1939
PE(40:4)	PE	0,26	0,3442	0,46	0,0955
PE(40:5)	PE	-0,24	0,3349	-0,06	0,8405
PE(40:6)	PE	-0,45	0,0595	-0,39	0,0623
PE(40:7)	PE	-0,35	0,1281	-0,26	0,2246
PE(42:1)	PE	-0,22	0,5675	-0,31	0,3011

Lipid species	Lipid Class	Contrast.x P-NT vs C-NT		Contrast.y P-T vs C-NT	
		logFC.x	adj.P.Val.x	logFC.y	adj.P.Val.y
PE(42:6)	PE	0,20	0,4592	0,32	0,1531
PE(42:7)	PE	0,33	0,2562	0,48	0,0245
SM(32:1)	SM	-0,03	0,8472	0,02	0,9334
SM(32:2)	SM	-0,78	0,0049	-0,91	0,0040
SM(34:1)	SM	-0,05	0,8145	0,02	0,9239
SM(34:2)	SM	-0,45	0,0284	-0,46	0,0454
SM(35:1)	SM	-0,27	0,1615	-0,09	0,6856
SM(36:1)	SM	-0,35	0,3015	-0,22	0,4128
SM(36:2)	SM	-0,71	0,0037	-0,60	0,0037
SM(36:3)	SM	-1,76	0,0006	-1,58	0,0004
SM(37:1)	SM	-0,17	0,5391	-0,14	0,6764
SM(38:1)	SM	-0,04	0,8596	-0,04	0,9114
SM(38:2)	SM	-0,51	0,0595	-0,46	0,0333
SM(38:3)	SM	-0,91	0,0045	-0,79	0,0093
SM(40:1)	SM	0,06	0,7575	0,03	0,9099
SM(40:2)	SM	-0,10	0,7041	-0,09	0,6554
SM(41:1)	SM	0,32	0,2876	0,74	0,0009
SM(41:2)	SM	0,50	0,0650	0,69	0,0111
SM(41:3)	SM	-0,09	0,7041	-0,01	0,9655
SM(42:1)	SM	0,27	0,2555	0,73	0,0012
SM(42:2)	SM	0,37	0,1471	0,68	0,0076
SM(42:3)	SM	-0,14	0,4830	-0,01	0,9334
SM(42:4)	SM	0,02	0,9037	0,13	0,3670
SM(43:1)	SM	0,83	0,0422	1,49	0,0002
SM(43:2)	SM	0,83	0,0114	1,27	0,0001
SM(43:3)	SM	0,58	0,0138	0,87	0,0004
TG(56:6)	TG	1,50	0,0180	1,50	0,0126